INVESTIGATION OF EJECTOR RE-COMPRESSION ABSORPTION REFRIGERATION CYCLE

By Shenyi Wu, BEng, MSc.

Thesis submitted to the University of Nottingham
for the degree of Doctor of Philosophy, May, 1999

CONTENTS i

ABSTRACT iii
ACKNOWLEDGEMENTS iv
LIST OF FIGURES v
LIST OF TABLES ix
NOMENCLATURE x

CHAPTER 1
INTRODUCTION 1

CHAPTER 2
PAST RESEARCH ON ABSORPTION REFRIGERATION 7
2.1 The Absorption Cycles 8
2.2 Hybrid Absorption Cycles 15
2.3 The Working Fluids 21
2.4 Conclusion 22

CHAPTER 3
THEORETICAL STUDY OF THE EJECTOR
RE-COMPRESSION ABSORPTION CYCLE 25
3.1 Lithium Bromide Absorption Cycles 25
3.2 The Ejector Re-compression Absorption Cycle 30
3.3 The Performance Characteristics of Ejector and Its Modelling 36
3.4 Simulation Model of the Novel Cycle 49
3.5 Factors Affecting the Performance of the Novel Cycle and COP Prediction 50
3.6 Conclusion 57

CHAPTER 4
PRELIMINARY EXPERIMENTAL STUDY
OF THE STEAM EJECTOR 59
4.1 The Experimental Apparatus 59
4.2 The Experimental Approach 63

4.3 Ejector Performance Characteristics 63
4.4 Efficient Use of Ejector 70

CHAPTER 5
MANUFACTURE OF A REFRIGERATOR
BASED ON THE NOVEL REFRIGERATION CYCLE 71
5.1 The Steam Generator 72
5.2 The Concentrator 74
5.3 The Absorber 81
5.4 The Evaporator 83
5.5 The Condenser 84
5.6 Measurement and Control System 85
5.7 Commission of the Experimental Rig 86

CHAPTER 6
EXPERIMENTAL STUDIES ON THE REFRIGERATOR 88
6.1 Experimental Methods 88
6.2 Calculation from the Readings 88
6.3 Experimental Results 93
6.4 Conclusion 111

CHAPTER 7

GENERAL DISCUSSION AND CONCLUSION 112

REFERENCE 115

APPENDIX A 124
APPENDIX B 125
APPENDIX C 127

ABSTRACT

This thesis describes a theoretical and experimental investigation of the ejector re-compression lithium bromide absorption refrigeration cycle. In this novel cycle, a steam ejector is used to enhance the concentration process by compressing the vapour to a state that it can be used to re-heat the solution from where it was evolved. Since this cycle recovers the heat otherwise wasted in a conventional absorption cycle, the energy performance of the cycle is improved. The theoretical study shows that the improvement of the efficiency is proportional to the performance of the steam ejector. A COP of 1.013 was achieved from the experiment in this investigation.

The novel cycle does not only improve the energy efficiency but also avoids the corrosion that will happen when high temperature heat sources are used to drive a lithium bromide absorption refrigerator. The steam ejector in the novel cycle acts as an efficient temperature converter in acceptance of different temperature heat sources, which reduces the energy loss when the temperature difference between the solution and the heat source is big. Therefore, the solution temperature can be set to a low level while the heat source temperature is high. This is significant to avoid the corrosion of lithium bromide solution at high temperature. Furthermore, the construction of the machine based on the novel cycle is simpler than that based on the conventional double-effect cycle. This refrigerator will be more reliable and have a lowed initial capital cost.

The cycle was investigated comprehensively in this thesis. In the theoretical study, a mathematical model for this novel cycle was established. The theoretical study reveals the operation characteristics and the factors that affect the energy efficiency of the cycle as well as how to design a refrigerator based on the novel cycle. In the experimental study, an concept-approved refrigerator was manufactured and tested. The part-load performance of the novel cycle was investigated from the experiment. The theoretical results had a good agreement with the experimental ones.

ACKNOWLEDGEMENT

During my study for PhD degree, I received a lot of help from the people in the Department of Architecture and Building Technology, the School of the Built Environment, the University of Nottingham. Without this help, I can not imagine that I could finish the study. My first thanks should go to Dr. Ian W. Fames. I am very grateful for his generous expert advice, understanding and encouragement in my whole period of the study. He created an excellent research surrounding from which I was benefited. I will never forget what I gained from him. I also wish to thank Mr. Mark Worral for his help in the ejector test, Mr. David Oliver for his wonderful skills to build the experimental rig and Mr. Robert Clark for his help in electrical devices, and all the technicians in this department for their great supports.

I wish to thank EPSRC and the University of Nottingham for their financial and facility support on this project.

Finally, I wish to express my thanks to my wife and my family. Their support has been a great encouragement for me to finish this study.

LIST OF FIGURES

Figure 1.1	The novel absorption cycle	4
Figure 1.2	Single-effect lithium bromide absorption cycle	5
Figure 2.1	Cycle schematic for the triple-effect cycle	9
Figure 2.2	Two-stage triple-effect ammonia-water system	10
Figure 2.3	Low pressure triple effect cycle - cooling mode	12
Figure 2.4	Cycle schematic for GAX cycle	13
Figure 2.5	Branched GAX cycle	14
Figure 2.6	Absorption-compression cycle	17
Figure 2.7	An absorption heat pump by Cacciola (1990)	17
Figure 2.8	An absorption refrigeration cycle proposed by Kulenschimidt (1973)	19
Figure 2.9	Ejector absorber cycle	19
Figure 2.10	Combined ejector-absorption cycle	20
Figure 2.11	Two ejectors absorption cycle	20
Figure 3.1	Single-effect lithium bromide-water refrigeration system	26
Figure 3.2	Thermodynamic cycle of single-effect lithium bromide refrigerator	27
Figure 3.3	Double-effect lithium bromide absorption refrigeration cycle	28
Figure 3.4	Thermodynamic cycle of double effect lithium bromide refrigerator	30
Figure 3.5	The novel refrigeration cycle	31
Figure 3.6	Ejector re-compression absorption refrigeration cycle on P-T-C chart	32
Figure 3.7	Ejector re-compression process	32
Figure 3.8	Structure and pressure profile of the concentrator	34
Figure 3.9	Schematic diagram of ejector	37
Figure 3.10	Performance characteristics of ejector	38
Figure 3.11	Schematic drawing of a supersonic ejector showing the nomenclature used in this section	40
Figure 3.12	Convergent-divergent (de-Laval) nozzle	40
Figure 3.13	Detail of the entrainment model	41

Figure 3.14	Enhancement factor variation with the solution states	52
Figure 3.15	The influence of temperature difference to entrainment ratio	53
Figure 3.16	Comparison of COP vs. concentration	56
Figure 3.17	COP variation with the solution concentration	56
Figure 3.18	COP variation with the steam temperature	57
Figure 4.1	Schematic diagram of the experimental rig	60
Figure 4.2	Photograph of the experimental rig	61
Figure 4.3	Schematic diagram of the ejector assembly	62
Figure 4.4	Entraimnent ratio variation with primary and secondary flows	65
Figure 4.5	Entrainment ratio variation with back-pressure and primary pressure	66
Figure 4.6	Measured variation in entrainment ratio with nozzle pressure ratio for different nozzle exit/throat area ratio	68
Figure 4.7	Measured variation in optimum nozzle exit position with secondary pressure ratio	69
Figure 4.8	Measured effect of primary pressure ratio, diffuser throat area and nozzle pressure ratio on critical condenser pressure	70
Figure 4.9	Measured variation in entrainment ratio with diffuser throat area ratio	70
Figure 5.1	Schematic diagram of the experimental rig	72
Figure 5.2	Photograph of the experimental rig	73
Figure 5.3	Diagram of the steam generator	74
Figure 5.4	Schematic structure of the concentrator	75
Figure 5.5	Diagram of the steam ejector	75
Figure 5.6	View of concentrator heat exchanger tube arrangement from 'A' direction in Figure 5.4	77
Figure 5.7	Fin dimension of the copper tube	77
Figure 5.8	Photograph of the steam ejector	78
Figure 5.9	Photograph of the heat exchanger of the concentrator	78
Figure 5.10	The absorber and evaporator system	83
Figure 5.11	Diagram of the measuring and controlling system	86
Figure 6.1	Measured primary flow rate (0 = 1.1 mm)	90

Figure 6.2	Measured primary flow rate (0 = 1.0 mm)	90
Figure 6.3	Back-pressure and pressure lift ratio (15 bar, 1.1mm throat diameter)	94
Figure 6.4	Back-pressure and pressure lift ratio (12.5 bar, 1.1mm throat diameter)	94
Figure 6.5	Back-pressure and pressure lift ratio (10 bar, 1.1 mm throat diameter)	95
Figure 6.6	Back-pressure and pressure lift ratio (15 bar, 1.0mm throat diameter)	95
Figure 6.7	Back-pressure and pressure lift ratio (12.5 bar, 1.0mm throat diameter)	96
Figure 6.8	Back-pressure and pressure lift ratio (10 bar, 1.0mm throat diameter)	96
Figure 6.9	Entrainment ratio variation with back-pressure (15 bar)	98
Figure 6.10	Entraimnent ratio variation with suction pressure	99
Figure 6.11	Entrainment ratio variation with back-pressure (12.5 Bar)	99
Figure 6.12	Mass ratio of the evolved vapour to the motive steam (15 bar)	100
Figure 6.13	Mass ratio of the evolved vapour to motive steam (12.5 bar)	101
Figure 6.14	Temperature difference between the steam and the solution (at 15 bar motive steam)	102
Figure 6.15	Temperature difference between the steam and the solution (at 12.5 bar motive steam)	103
Figure 6.16	COP variation with motive steam pressure	104
Figure 6.17	COP difference between the part-load and the design operations	105
Figure 6.18	Cooling capacity vs. motive steam pressure	106
Figure 6.19	COP variation with solution concentration	107
Figure 6.20	Comparison of the experimental and theoretical COPs at different solution concentration	108
Figure A1		124
Figure B1	Evaporator volume vs. height	125

Figure B2 Measuring vessel volume vs. height 126
Figure B3 Condenser volume vs. height 126

LIST OF TABLES

Table 3.1	Recommended ejector geometrical features taken from ESDU (1986)	48
Table 3.2	Ejector Entrainment Ratio at different solution condition	51
Table 3.3	Enhancement factor varied with the solution condition	51
Table 3.4	COP Comparison between the single-effect and the ejector boost single-effect cycles	55
Table 4.1	Test Nozzle Geometry	67
Table 4.2	Geometries of 3 test diffusers	69
Table 5.1	Flow geometric sizes of the ejector	76
Table 6.1	Ejector primary rates ($g \cdot min^{-1}$) at different steam pressure	89
Table 6.2	Pressure lift ratio of the steam ejector	93
Table 6.3	The pressure loss between the evaporator and absorber	110

NOMENCLATURE

A	area, m^2
A_D	diffuser throat area, m^2
A_{exit}	primary nozzle exit area, m^2
A_i	surface area inside tube, m^2
A_o	surface area outside tube, m^2
A_t	primary nozzle throat area, m^2
AR	AD/A,
A_T	A_{exit}/A_t
C	concentration
C_v	specific heat at constant volume, $J\cdot(kg\cdot K)^{-1}$
C_p	specific heat at constant pressure, $J\cdot(kg\cdot K)^{-1}$
D	diameter, m
D_{th}	diffuser throat diameter, m
D_{AB}	molecular diffusivity, $m^2\cdot s^{-1}$
COP	Coefficient of Performance
g	gravity accelerate, $m\cdot s^{-2}$
P	pressure, bar or Pa
P_a	atmosphere pressure, bar
h	specific enthalpy, $kJ\cdot(kg\cdot K)^{-1}$
h_{fg}	latent heat of condensation, $kJ\cdot kg^{-1}$
h,	total or stagnation enthalpy, $kJ\cdot kg^{-1}$
$\bar{h}$	mean heat transfer coefficient, $W\cdot(m^2\cdot°C)^{-1}$
k	thermal conductivity, $W\cdot(m\cdot°C)^{-1}$
K_m	mixing section momentum loss coefficient
M_n	Mach Number
rh	mass flow rate, $kg\cdot s^{-1}$
N_n	ratio of total primary to secondary pressures
N_p	ratio of primary to back-pressures
N_s	ratio of back to secondary pressures
$N_{s'}$	critical condenser pressure ratio
$\overline{Nu}$	average Nusselt number

NXP	nozzle exit position, m
Pr	Prandtl number
P,	total or stagnation pressure, Pa or bar
$\dot{q}$	heat flux, $kW \cdot m^{-2}$
$\dot{Q}$	heat flow rate, kW
r	radius, m
R	individual gas constant, $kJ \cdot (kg \cdot K)^{-1}$
R_e	Reynolds number
s	specific entropy, $kJ \cdot (kg \cdot K)^{-1}$
T	temperature, K, °C
T,	total or stagnation temperature, K
U	overall coefficient of heat transfer, $W \cdot (m^2 \cdot °C)^{-1}$
v	velocity, $m \cdot s^{-1}$
w	entrainment ratio $(\dot{m}_s / \dot{m}_p)$
x	mass concentration, %
x_c	mass concentration of strong solution, %
x_d	mass concentration of weak solution, %

Greek

a	ratio of mass flow rate, $\dot{m}_H$ *frit*
λ	solution circulation factor, $\frac{x_d}{x_c - x_d}$
η	efficiency of solution heat exchanger
η_d	diffuser pressure recovery factor
η_N	stagnation pressure loss factor in primary nozzle
η_s	secondary flow stagnation pressure loss factor
Y	specific heat ratio, $\frac{C_p}{C_v}$
p	density, $kg \cdot m^{-3}$
e	enhancement ratio
ν	kinematic viscosity, $m^2 \cdot s^{-1}$
μ	dynamic viscosity, $N \cdot s \cdot m^{-2}$

a	surface tension, $N \cdot m^{-1}$
6	film thickness, m
Γ	mass flow rate per unit width, $kg \cdot (ms)^{-1}$

Subscript

a	absorber
b	back-pressure
c	concentrated
con	condenser
d	dilute
dp	design point
e	evaporator
f	liquid
g	generator, gas
H	high pressure
i	inside tube
in	input
int	internal loop
1	liquid
L	low pressure
m	mixed flow
0	outside tube
od	off-design or part-load
P	ejector primary flow
rec	rectifier
ref	reference state
s	ejector secondary flow
sat	saturated
,T	total
th	throat
v	vapour
w	wall
0,1,2...	numbers for the states

CHAPTER 1
INTRODUCTION

Global warming (due to greenhouse gas accumulation in the lower atmosphere) and stratospheric ozone depletion are increasingly recognized as two coexistent, partly-related processes threatening to upset the ecological support system of the Earth. A recent analysis of the potential public health impact of climate change concluded that a few degrees increase of average global temperature would lead to: increased incidence of heat strokes and heat-related death in chronic diseases; geographic shifts in tropical and infectious diseases; increased occurrence of death, injury and epidemics due to weather-related emergencies and flooding of coastal areas (Slooff et al 1995).

In order to curb the global warming and ozone depletion, two important documents, The United Nations Framework Convention on Climate Change (FCCC) and Montreal Protocol, were signed by many countries. According to these two documents, CFC and HCFC fluids, which are widely used in vapour compression refrigerators and heat pumps will be gradually phased out and the emission of greenhouse gas CO_2 should be reduced to their 1990 levels. In some EU countries, this ban extends to HFC fluids.

The ban on CFC, HCFC and HFC fluids has encouraged research into environmental friendly refrigerants such as water. The lower CO2 emission requires not only reduction in fossil fuel consumption but also improvement of energy efficiency of refrigerators and heat pumps. Utilization of low-grade energy is also an effective way to reduce CO_2 emissions. For the latter, heat powered refrigeration cycles can provide the answer. There are several heat powered refrigeration cycles that can be considered. They are:

- Adsorption cycle - similar to absorption cycle but using solid substance as absorbent. Regeneration of the absorbent could be a problem if continuous cooling load is required. Adsorption

machines are suitable for particular applications but are not proven commercially.

- Ejector cycle - using an ejector to compress refrigerants. Water can be used as refrigerant. Simple in structure and low cost but low energy efficiency.
- Absorption cycle - proven commercially, good energy efficiency and environmentally friendly but may be complex when pursuing high efficiency.

Of the three types of heat powered cycles, the absorption cycle is considered to be the best in terms of energy performance today and it has the potential to be improved. So, the absorption cycle has potential to be widely used if its efficiency can be increased further and its construction can be made simpler. This project was concerned with a novel absorption cycle which could deliver a better performance than a single-effect cycle.

The absorption machine was invented in the mid-nineteenth century by a Frenchman, Ferdinand Carre. Since then, the popularity of absorption systems has risen and fallen due to economic conditions and advances in competing technologies. The benefits of absorption systems have remained constant and include the following:

- absorption systems are able to be driven by low grade thermal energy.
- otherwise wasted heat can be utilized to power the absorption refrigeration cycle.
- absorption units are quiet and vibration free.
- absorption units pose no threat to global environmental ozone depletion and may have less impact on global warming than most other options.
- absorption units are economically attractive when the fuel costs are substantially less than electricity costs.

Absorption refrigerators and heat pumps using ammonia-water or water-lithium bromide as working fluid pairs are commercially available. For above 0°C cooling applications, water-lithium bromide systems offer higher efficiencies than ammonia-water systems do. Compared with aqua-ammonia systems, LiBr-water units are simpler in construction because the rectification process, required in aqua-ammonia, is absent. The only drawback for the water-lithium bromide system is that water will freeze at subzero evaporator temperatures. However, near subzero temperature operation is made possible by adding a small amount salt in the evaporator. The real problems for water-lithium bromide systems are crystallization and corrosion when the solution concentration and temperature are high. Current commercial available lithium bromide absorption systems are not suitable for working at a solution concentration greater than 65% and a solution temperature greater than 200°C for reasons of crystallisation and corrosion. This temperature limitation inevitably reduces the second law efficiency when using high temperature heat sources to drive conventional lithium bromide absorption cycles. The concentration limitation results in the increase of circulation rate. The ammonia-water system does not have the crystallization problem that water-lithium bromide system has. However, the high-pressure of the ammonia system makes it impractical at above 200°C. Therefore, efficient use of high temperature heat sources becomes a challenge to the researchers in the field of absorption refrigeration. Much research has been carried out in recent years but the problem still exists. The current trend to use multi-stage, multi-effect cycles and find new working pairs to improve performance seems to have some way to go. Chapter 2 reviews the current state-of-the-art with regard to the improvement of absorption refrigeration cycles and working fluids.

In this research, a novel cycle, which can be driven by high temperature heat sources, is proposed and investigated. This cycle uses an ejector to enhance the concentration process, rather than the evaporating process usually found in previous work on ejector-absorption cycles, which are reviewed in Chapter 2. The ejector entrains the refrigerant vapour evolved at the generator and re-compresses it to such a state that it can be re-used to concentrate the solution.

The entrained vapour, together with the driving flow, are then used to heat the solution. A schematic diagram of the novel cycle is shown in Figure 1.1. From this diagram, it can be seen that the novel cycle is similar to a steam powered single-effect absorption cycle which is shown schematically in Figure 1.2 for comparison. The difference is that an ejector is used to enhance the concentration process in the cycle. Because of the ejector being introduced into the cycle, the solution temperature and concentration in the concentrator can be set to optimum points no matter how high the heat source temperature. In addition, the useful work, which is lost in the conventional absorption cycles due to temperature limitation, is used by the ejector to generate more vapour from the solution. Therefore, this novel cycle can not only avoid crystallization and corrosion but also can increase the second low efficiency when it operates with high temperature heat sources. This novel cycle can be classified as a double effect cycle because the input heat is used twice. So, this cycle is single-effect construction but with double-effect performance. Compared with multi-stage, multi-effect cycles which are believed to have the potential for excellent energy efficiency in use of high temperature heat sources, this cycle offers a practical answer. Furthermore, since this cycle uses the well-established and approved working fluid, H_2O-LiBr, it is easier for it to be commercialized.

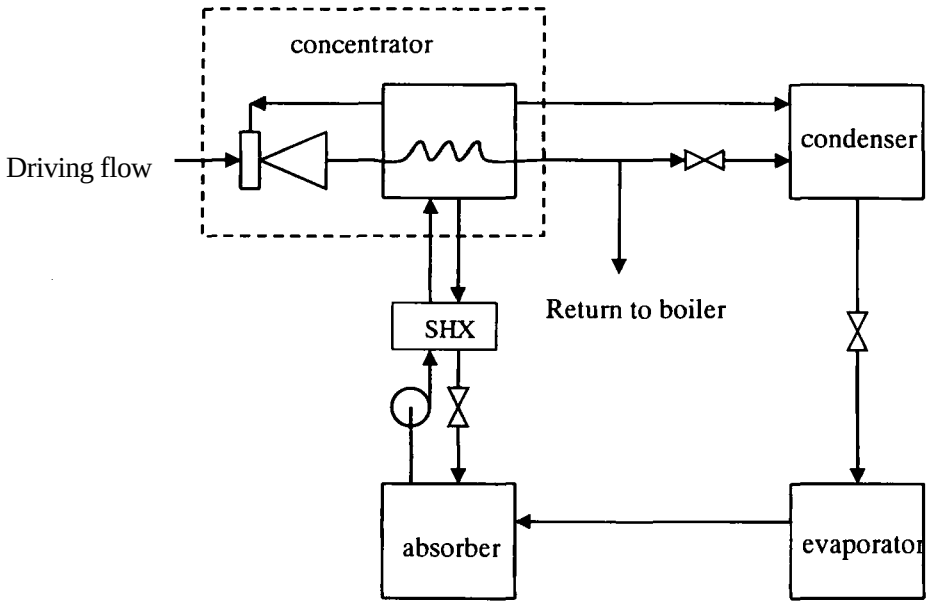

Figure 1.1 The novel absorption cycle

The objectives of this research programme were to:

- Establish the state-of-art in regard to absorption cycle design in order to place the invention within context.
- Experimentally and theoretically determine the performance characteristics of the novel cycle over a range of operating conditions.

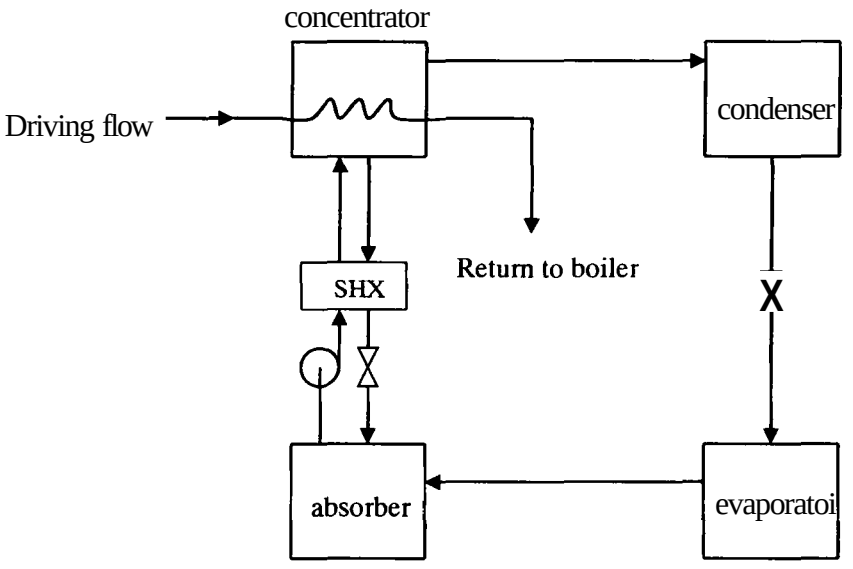

Figure 1.2 Single-effect lithium bromide absorption cycle

To achieve these objectives:

- A detailed literature review was carried out. The results of this are described in Chapter 2. In this chapter, recent developments in advanced absorption cycle design are reviewed, including multi-stage multi-effect absorption cycles, Generator-Absorber heat Exchange (GAX) cycles and hybrid absorption cycles. Since working fluids are strongly related to the cycle design, a review of recent research activity on multi-component fluid is also included.

- A detailed theoretical study of the novel cycle was undertaken. This included a theoretical analysis of the novel cycle with regard to the

cycle performance and the factors that influence its performance; the ejector behaviour in the concentration process.

- Experimental study of this novel cycle was carried out. A preliminary experiment on the steam ejector for the experimental study on the novel cycle is described in Chapter 4. The design and manufacture of the 'concept approve' test rig are presented in Chapter 5. The experimental results of the novel cycle are given in Chapter 6.

- The discussion and conclusion are made in Chapter 7. In this Chapter, the advantages of this novel cycle over the conventional absorption cycle are highlighted. The problems which occurred in this research are discussed. The suggestions for future study on this novel cycle are also included.

CHAPTER 2
PAST RESEARCH ON ABSORPTION REFRIGERATION

Similar to vapour compression refrigeration, absorption refrigeration also uses a phase change process to produce a cooling effect. The main differences between them are: (a) the refrigerant vapour in an absorption cycle is absorbed by a liquid before being compressed by a pump. Therefore, the mechanical work required in absorption cycles is much less than that in the vapour-compression cycles and (b) low-grade heat energy can be used to drive the absorption cycle whereas high-grade work is required to drive vapour-compression machines.

The Coefficient of Performance (COP) is a measure of refrigerator energy efficiency. For absorption refrigerators, COP is defined as the ratio of the evaporator cooling capacity to heat input at the generator. In terms of COP, absorption systems are less efficient than vapour-compression systems. However, when the primary energy is considered, the difference in overall COP (or Energy Efficiency Ratio, EER) is not so great. Environmental concern encourages developing more efficient absorption refrigeration machines

Finding ways to improve absorption system efficiency has been a great challenge for the researchers in recent years. Works was mainly focused on inventing new or hybrid cycles, finding new working fluids and improving the heat and mass transfer of the absorption refrigerator. In the following sections, the past works on the absorption (or hybrid) cycles and working fluids are reviewed. The terms 'desorber', 'generator' and 'concentrator' used in this chapter are all referred to the concentration devices for the cycles.

2.1 THE ABSORPTION CYCLES

2.1.1 Single- and double-effect absorption cycles

Among the varieties of the absorption refrigeration cycles, the single-effect and double-effect machines are the most popular and are commercially available. The coefficient of performance of the lithium bromide-water absorption machines, based on single- or double-effect cycles, typically varies over the range 0.7< COP <1.2 for refrigeration temperature above 0°C. Ammonia-water machines allow refrigeration temperature down to –77.7°C but coefficient of performance is typically around 0.5 (Herold 1996).

The single or double-effect absorption cycles using water-LiBr as working fluid are suitable to work at the solution temperature under 200°C. Above this temperature, corrosion and crystallisation of the working fluid can be problematic. If the solution temperature increases with the heat source temperature, the solution concentration will increase. This makes the solution become not only more corrosive to the construction material, but also suspectable to crystallisation when it is cooling down through the solution heat exchanger. If the solution temperature does not increase with the heat source temperature, the second law efficiency of the cycle will decrease due to the irreversible loss in heat transfer. In other words, the use of a high temperature heat source, such as gas combustion products, to drive conventional single- or double-effect absorption cycles is wasteful of energy. The research on advanced cycles, for example, multi-stage, multi-effect absorption cycles, has concentrated on reducing this waste.

2.1.2 Multi-stage, multi-effect absorption cycles

For high temperature heat sources, multi-effect absorption refrigeration cycles have well-proven potential to attain a performance which is superior to the performance of conventional cycles (Ziegler 1985, Alefeld 1983). The Four-Pressure Triple-effect Cycle using water-lithium bromide was a natural development from conventional double-effect cycles. This cycle has one more high-pressure generator on top of the conventional double effect cycle, and the

vapour evolved from this generator is used to drive the double-effect cycle as shown in Figure 2.1. Therefore, in this machine the input heat is recycled three times to improve the efficiency. It was reported that the calculated COP for this cycle is 1.645 (Herold 1996). Although the triple-effect absorption cycle can reduce the energy loss for high temperature heat source, the corrosion will be problematic for the machines using lithium bromide-water pair since this cycle requires a high solution temperature. Special materials may be required to prevent the corrosion in this case. However, this is a costly answer with current technology. Some companies have tried to use other working fluids to produce triple-effect chillers. Until now, there is no other form of triple-effect cycles proposed for water-lithium bromide pair.

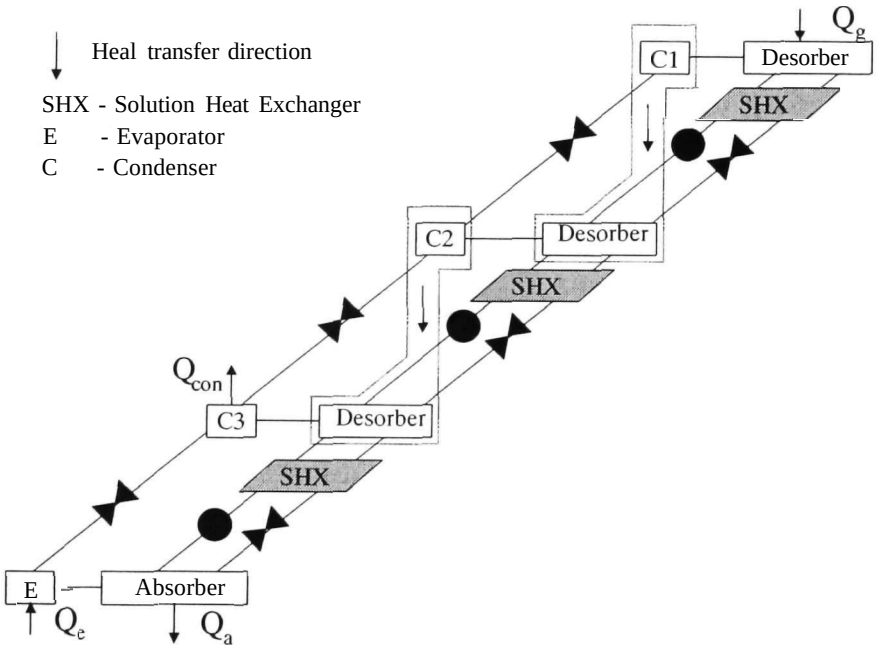

Figure 2.1 Cycle schematic for the triple-effect cycle

Previous work has shown that there are theoretically a large number of cycles that fall into the category of "triple-effect". However, DeVault et al (1990) indicated there were only three basic triple-effect cycles if by limiting the cycles to air conditioning of buildings and by limiting the cycles to basic combinations of cycles using standard evaporator, condenser, absorber and generator components. Among the three cycles, only Two-stage, Triple-effect

cycle is suitable for using the ammonia-water pair as a working fluid, which is shown in Figure 2.2 (Alefeld 1983). Refering to Figure 2.2, while the refrigerant NH_3 from the high-pressure generator releases condensing heat to the low-pressure generator, the heat from the high-temperature absorber is also transferred to the low pressure generator. So, the input heat is used three times. The calculated COP for this cycle is 1.41 (Herold 1996). This cycle was also investigated theoretically by other researchers and its COP is in the range of 1.4 - 1.5 for a temperature lift of about 30°C (DeVault 1990, Ivester 1993, Garimella 1994, Ziegler 1993). Garimella et al (1994) compared working fluids NH_3-H_2O/NH_3-H_2O with NH_3-H_2O for the triple-effect cycle. In their investigation, the NH_3-NaSCN pair was used for the low-pressure sub-cycle in the triple-effect cycle while the NH_3-H_2O was used for the high-pressure cycle. They found that both working fluids are essentially indistinguishable in terms of performance and temperature-pressure considerations, with the primary difference being that the NaSCN cycle resulted in the same overall performance without the use of a low cycle rectifier. Ivester and Shelton (1996) also discussed the optimised evaporator and generator temperature for this cycle. Their result shows that the COP of this cycle was 1.38 when the generator temperature was 200°C, evaporator temperature 5°C and condenser temperature 35°C.

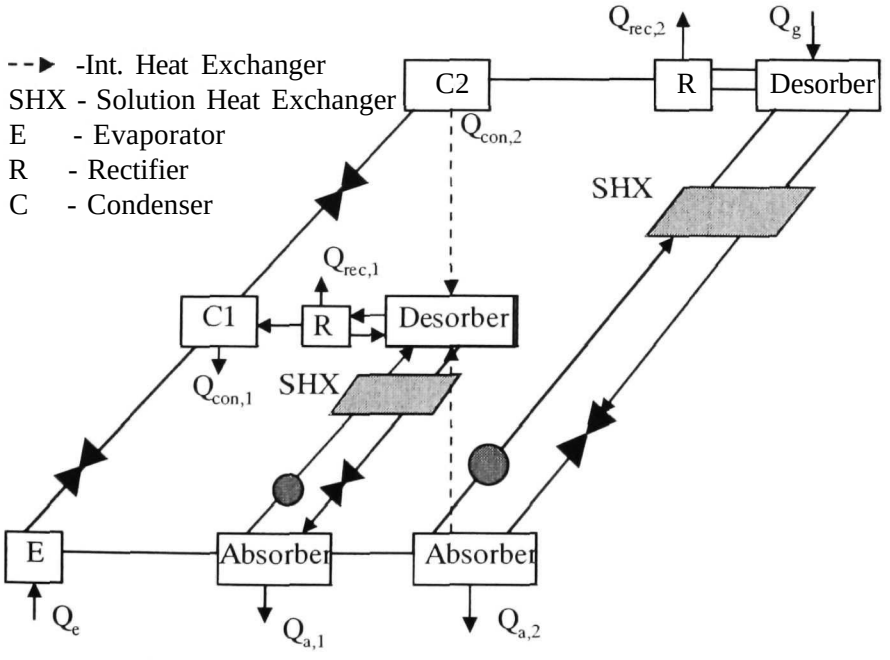

Figure 2.2 Two-stage triple-effect ammonia-water system

The Two-stage, Triple-effect Ammonia cycle requires the generator to work at high-pressure, which increases the manufacturing cost. Gopalnarayanan and Radermacher (1996) reported a low-pressure triple-effect, ammonia-water cycle for multiple application modes as shown in Figure 2.3 for cooling mode. In this cycle, the high temperature desorber (D1) works under the same pressure as the low temperature desorber (D2). The cooling load is produced from the evaporator (E) and the desorber (D3). They claimed that the major advantages of this cycle over the Two-stage triple-effect cycle were a lower operating pressure and temperature in the high-pressure generator and a comparable COP. Their calculations indicate that the optimum COP of the cycle in cooling mode with a pinch point temperature difference of 5°C and a temperature lift from 5 - 35°C is of the order of 1.46. However, this cycle has three different solution circuits. To obtain optimum COP, the concentrations of the three solution circuits need to be controlled precisely, which is not easy to achieve.

Triple-effect cycle can also be formed with two independent cycles using different fluids. Inoue et al (1993) simulated such a triple-effect cycle which used H_2O-LiBr for the low temperature sub-cycle and NH_3-H_2O for the high temperature sub-cycle. The low temperature sub-cycle was driven by the heat from high temperature cycle's absorber and condenser. Their simulation result showed that the COP of 1.33-1.48 was achievable when the generator temperature was above 205°C, the evaporator temperature was at 5°C, the condenser and the absorber temperatures were in the range between 32°C and 42°C.

The triple-effect cycles generally require higher temperature heat source to drive them. For triple-effect chillers, the solution temperature needs to reach 205-230°. For this reason, triple-effect chillers will most likely be direct-fired. This presents significant challenges in the area of absorbent solution chemistry, materials of construction, and component design. Yet, several

companies are now developing triple-effect chillers with targeted fuel-based COP value of 1.4-1.5 (Burgett 1999).

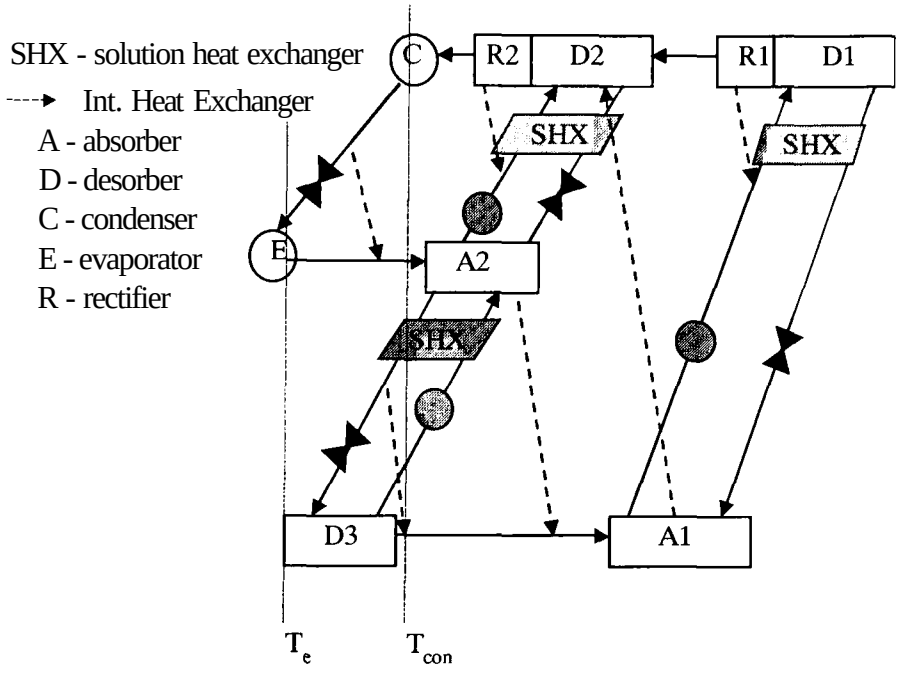

Figure 2.3 Low pressure triple effect cycle - cooling mode

2.1.3 Generator-absorber heat exchange cycles (GAX)

While multi-effect absorption cycles deliver high efficiency, the configuration of the cycles tends to be more complicated. In contrast to the multi-effect cycles, Generator-absorber heat exchange (GAX) cycles provide potentially high energy efficiency at single-stage configuration. This cycle was first described by Altenkirch and patented in 1914 (Altenkirch 1914). A schematic GAX cycle is shown in Figure 2.4. The potential high efficiency of the GAX cycle has attracted a lot of recent interest. In a GAX cycle, absorber heat is directly supplied to the desorber to generate refrigerant vapour, which results in less heat input to the desorber and less rejected by the absorber. By careful arrangement of the heat transfer between the absorber and the desorber, an improved COP is achievable. It was reported that a 250 kW, gas-fired GAX cycle was installed in a government building in Maastricht, The Netherlands (Bassols 1994). This machine uses ammonia-water as a working fluid and returned a seasonal average COP of 1.53.

The basic GAX cycle has a problem that the amount of heat provided by the **high** temperature end of the absorber is less than the heat requirement of the low temperature end of the desorber under most operation conditions. This problem can be solved by increasing the mass flow rate in the high-temperature end of the absorber only. This is accomplished with the so-called branched GAX cycles as shown in Figure 2.5. A second solution pump is used. The configuration with a second solution pump is termed the branched GAX cycle (Herold 1991, Rane 1994). The performance improvement due to the second pump is in the range of 5%.

There are many possible GAX cycle arrangements. Anand and Ericson (1999) conceptualised and documented a total of 21 advanced GAX cycles for space conditioning. Among these cycles, they recommended a SVX GAX cycle as the most promising cycle which has COP improvement of at least 30% over basic GAX and is independent of any unproven advances in pumping technology.

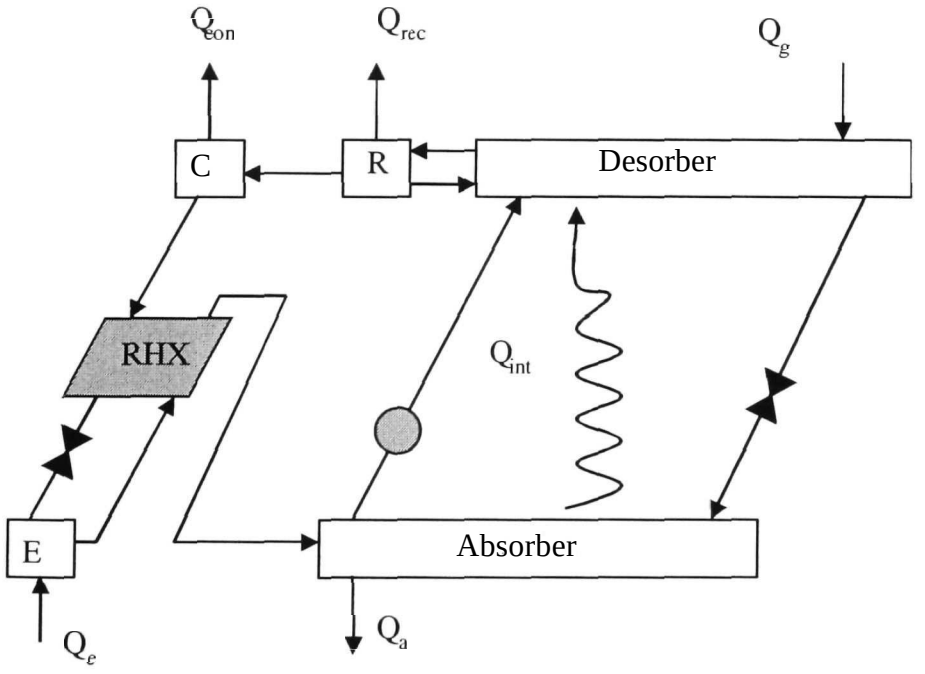

Figure 2.4 Cycle schematic for GAX cycle

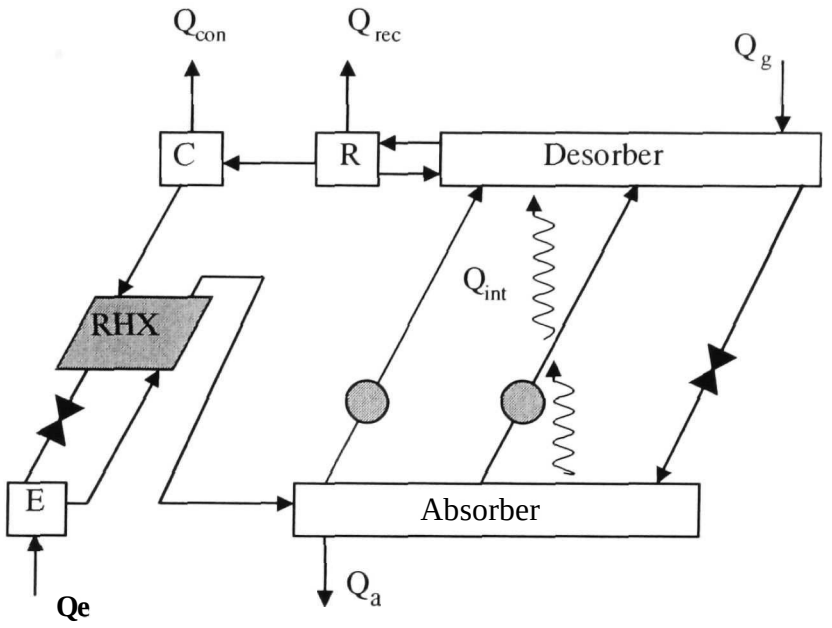

Figure 2.5 Branched GAX cycle

Zaltash and Grossman (1996) used their computer model to simulate a GAX cycle with the binary working fluid NH_3/H_2O and the ternary fluid $NH_3/H_2O/LiBr$. Their simulation results showed that with the ternary fluid $NH_3/H_2O/LiBr$ at higher firing temperatures (greater than 204°C) the cycle COP achieved was over 21% higher than that alternated with the binary working fluid NH_3/H_2O. The presence of salt (LiBr) resulted in a significant decrease in the rectifier duty. Their performance simulation results showed the potential of using advanced cycles with advanced fluid mixtures (ternary or quaternary mixtures).

Cheung et al (1996) reported their performance assessments of nine multi-stage absorption cycles which were classified into three groups: water-lithium bromide cycles, ammonia-water absorption cycles and cascaded absorption cycles. They suggested that the three-stage, triple-effect cycle for water-lithium bromide group, GAX for ammonia-water group and single-stage,

water-LiBr cycle cascaded with a single-stage, ammonia-water cycle for the cascaded group deserved further consideration.

The key problem for a GAX cycle is the heat transfer between the absorber and the generator. The normal GAX configuration requires the use of two pumps. The second pump is used to circulate a heat transfer fluid between the absorber and the generator. If the second pump could be eliminated, a large cost saving would be realised. Dence et al (1996) suggested positioning the high temperature section of the absorber directly into the generator. To achieve this, the generator and absorber must have similar temperature profiles. Further, one has to assure that heat transfer between the absorber and the generator must be matched precisely. They proposed a method to design such a GAX heat exchanger.

2.1.4 Other absorption cycles

There are some other lithium bromide absorption cycles. The Half-Effect and the resorption cycles are among them. The Half-effect cycle is suitable for applications where the temperature of the available heat source is less than the minimum necessary to fire a single-effect cycle. The resorption cycle, however, has the potential of expanding the design options of water-lithium bromide technology, i.e., a wider range of the solution concentration but the COP of both cycles is low (Herold 1996).

2.2 HYBRID ABSORPTION CYCLES

While the research activities to improve the absorption system efficiency have focused on the multi-stage, multi-effect absorption cycles, some researchers have been working on combining other refrigeration cycles with absorption cycles to achieve better energy performance. The majority of those reported are the combination of the vapour-absorption and vapour-compression cycles. This, perhaps, is the result of similarity between them. Either mechanical or thermal compressors have been found in the combinations. A combination of vapour-compression and absorption cycles, which is known as the sorption-

compression system, can be achieved in a number of ways (Morawetz 1989). The basic sorption-compression cycle is shown in Figure 2.6. The refrigerant vapour in this cycle is compressed by a mechanical compressor from the desorber to the absorber. The cooling load is provided by the desorber while the heat is supplied from the absorber. The sorption-compression cycles can deliver higher energy efficiencies and have simple configurations but they require mechanical work. Feldman et al (1998) reported an absorption refrigerator based on the absorption-compression cycle but which used an organometallic absorbent and hydrogen or nitrogen gas as a refrigerant. The resulting value of COP for cooling was 3.06.

Cacciola et al. (1990) analysed an absorption heat pump using two combinations of working fluids, NH_3/H_2O and KHO/H_2O. Their cycle is shown in Figure 2.7. This cycle reduced the highest system pressure and avoided the need for a rectifier in the water/NH_3 system. Riffat et al (1994, 1996) reported a rotary absorption-recompression heat pump. In this novel arrangement, a gas engine was used to drive a screw compressor which compressed vapour evolved at the generator. In this machine, the evaporator, absorber, condenser and generator assembly rotated at about 800 rpm. The rotation of the assembly improved the heat and mass transfer condition in the system, due to the thin and highly sheared liquid films caused by centrifugal acceleration. The theoretical primary energy ratios for cooling were 1.96 with working fluid $H_2O/LiBr$ and 1.3 with H_2O/NaOH-KOH-CsOH. The configuration of the system was quite complicated and the sealing was found to be problematic.

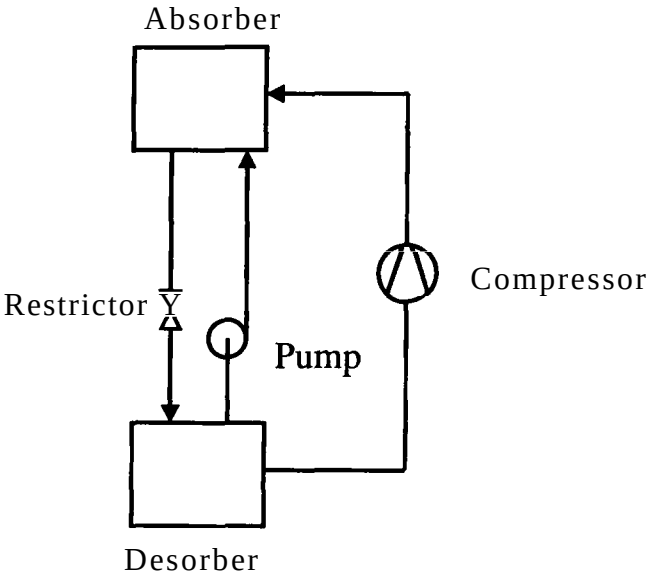

Figure 2.6 Absorption-compression cycle

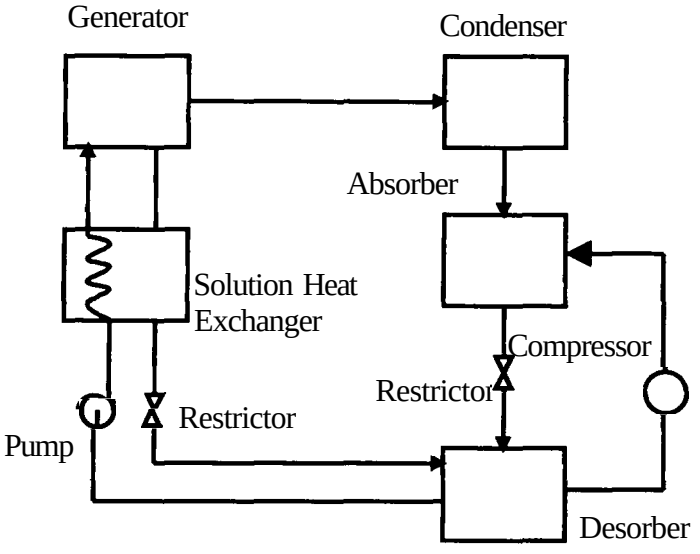

Figure 2.7 An absorption heat pump by Cacciola (1990)

Using an ejector as a compressor in absorption cycles is another way of combining the vapour-absorption cycles with the vapour-compression cycles, and this approach avoids the use of mechanical work. The ejector function in the absorption cycles can be classified as three forms, i.e., to enhance the evaporation process, to enhance the absorption process and to enhance the concentration process. Kuhlenschmidt (1973) proposed a cycle that used an ejector to entrain the vapour from the evaporator and discharged it to the

absorber as shown in Figure 2.8. In the cycle, the ejector was driven by the vapour from the low-pressure generator of a double-effect absorption cycle. This cycle increased the temperature lift and eliminated the need for a condenser, but COP could not be improved. Neither theoretical nor experimental results for this cycle are yet available. Chung et al. (1984) and Chen (1988) used the returning solution (DMETE/R21 and DMETE/R22) from the generator as a primary fluid to entrain the refrigerant vapour from the evaporator. The mixture fluid was discharged into the absorber. Since this arrangement allowed the absorber pressure to be higher than the evaporator pressure, the circulation ratio of the solution could be reduced, therefore, COP was improved. However, this system can only be operated using high-density refrigerant vapour because a liquid driven ejector is not suitable for low-density vapour such as water vapour as used in water-LiBr absorption cycles. This cycle is shown in Figure 2.9.

Eames et al (1995) investigated an ejector-absorption cycle both theoretically and experimentally. This cycle shown in Figure 2.10 consisted of two sub-cycles: the steam ejector cycle and LiBr-water single effect absorption cycle. The ejector cycle was driven by water vapour from the generator of the absorption cycle. Because the steam ejector utilised the energy, otherwise lost in a conventional absorption cycle, to enhance the vaporisation process in this novel cycle, a higher COP was expected. The computer simulation of this novel cycle was reported by Sun et al (1996). Experimental COP of this cycle was reported in the range between 0.8 to 1.04 for 5°C cooling temperature (1994). However, this cycle required the generator temperature of at least 200°C and this may result in increased corrosion rates which may be problematic (Eames 1996).

Gu et al (1996) suggested a hybrid cycle that used two ejectors to entrain the refrigerant vapour from the evaporator: one driven by returning solution from the generator and another driven by the refrigerant vapour from the generator as shown in Figure 2.11. This cycle was actually the combination of Chung et

al (1984), Chen (1988) and Eames (1995), but with R21-DMF as working pairs. The calculated COP for this cycle was 0.651. No experimental results were provided.

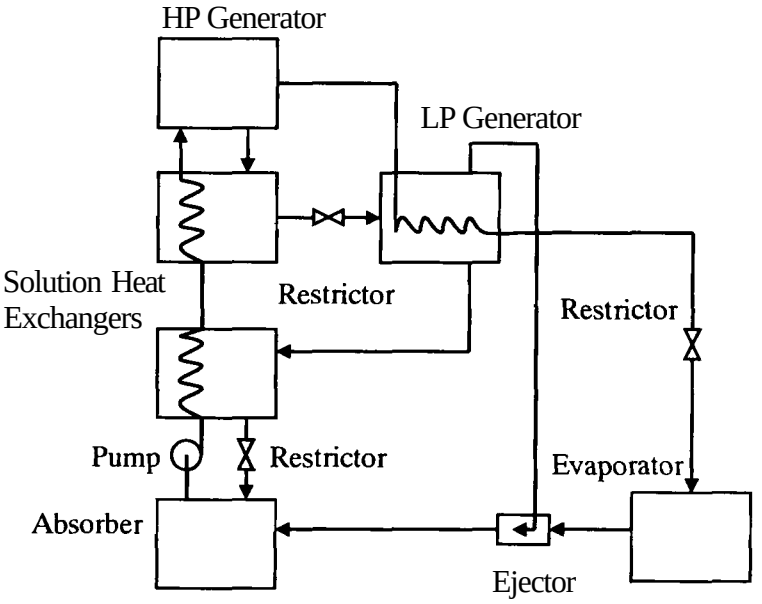

Figure 2.8 An absorption refrigeration cycle proposed by Kulenschimidt (1973)

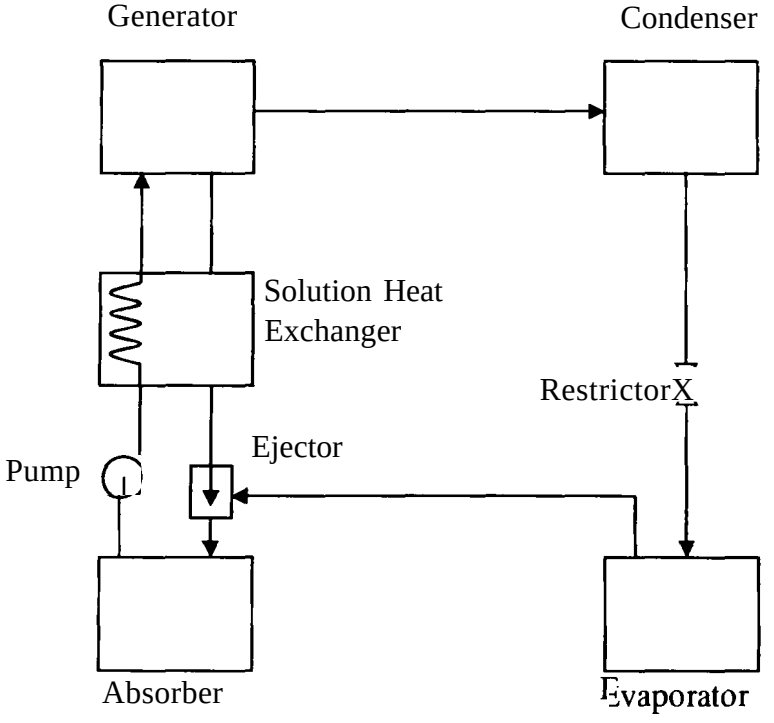

Figure 2.9 Ejector absorber cycle

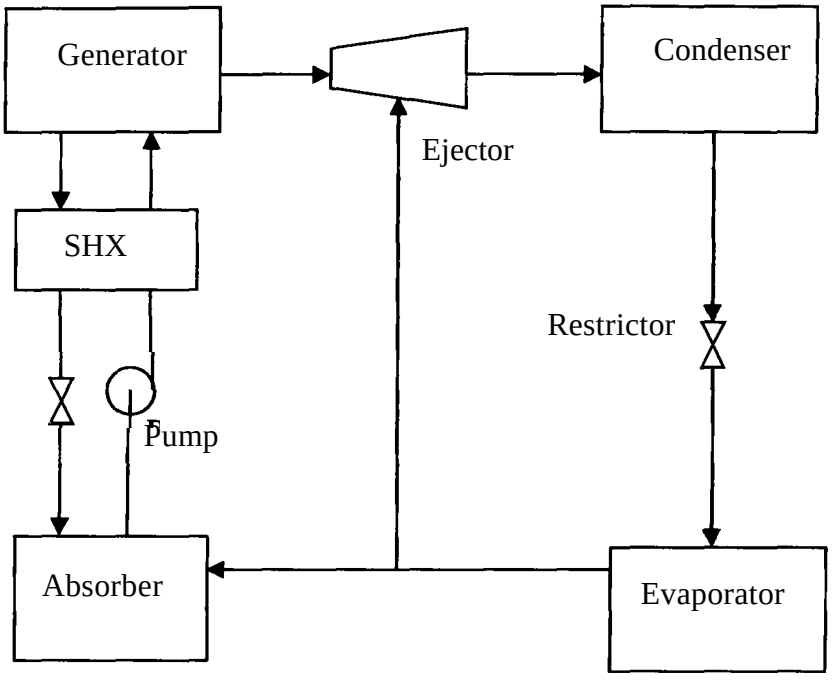

Figure 2.10 Combined ejector-absorption cycle

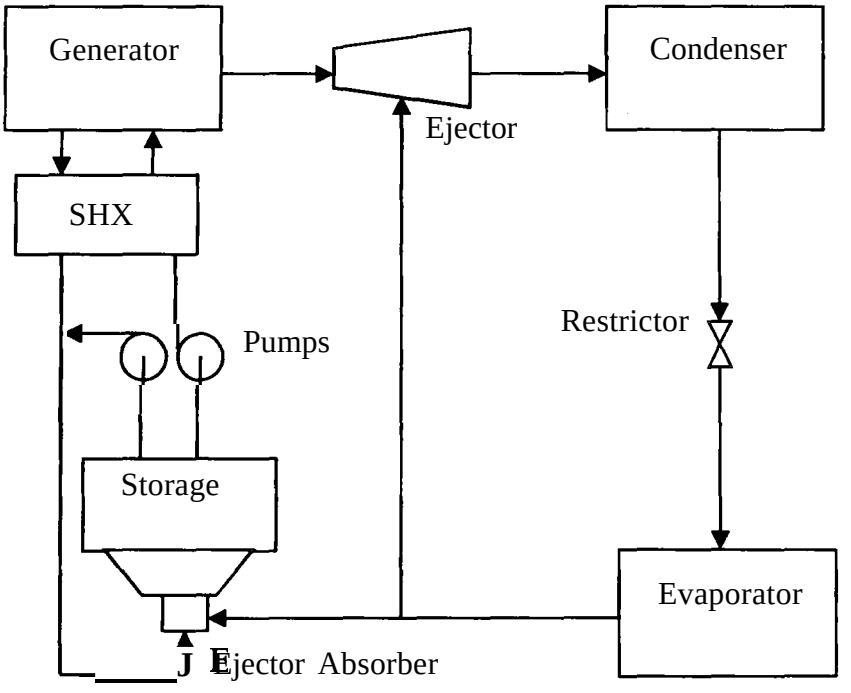

Figure 2.11 Two ejectors absorption cycle

2.3 THE WORKING FLUIDS

The efficiency of an absorption cycle is not only determined by the cycle design, but also determined by the working fluid used in the cycle. Therefore, the working fluid is an important subject in order to improve the efficiency of absorption cycles. For absorption refrigerators, the following pairs are frequently employed or discussed:

NH_3/H_2O

H_2O/H_2O-LiBr

CH_3OH/CH_3OH-salt solution

R22 (CHCIF2)/E181 or other organic solvent

R133a (CH_2ClCF_3)/ETFE

The criteria for working fluids for absorption systems have been discussed by Alefeld et al (1994).

Among the working fluids, H_2O/H_2O-LiBr and NH3/NH3-H2O are the most widely used in proprietory absorption refrigerators. This is because these two working pairs have so far provided the best energy performance compared with others. However, water-LiBr solution is corrosive at high temperatures and crystallisation occurs at high concentrations. Water as the refrigerant also freezes at sub-zero temperatures, which limits its applications. Although the ammonia-water pair does not crystallise and can work at sub-zero temperature, the volatility of water with ammonia and the high vapour pressure of the solution results in increased complexity of construction and high cost. Furthermore, the efficiency of the ammonia-water systems is lower than that of LiBr-water system owing the need for rectification in the former.

In recent years, binary fluids have been studied in order to improve H_2O-LiBr and NH_3-H_2O working pairs. The aqueous solutions of LiBr can be used as an absorber for NH_3 (ammonia) or for CH_3NH_2 (methylamine). In this case, the solution operation-zone is extended towards significantly higher generator

temperatures. For a given desorber temperature and pressure, the solution has a higher ammonia (or methylamine) composition in relation to H_2O content in the liquid phase. This reduces the rectification requirements significantly. Similar improvement can, in principle, be obtained for $H_2O/LiBr$ with H_2O as the working fluid. The crystallisation limit is moved to high temperature by adding a second anti-freeze liquid, for example, glycol (Alefeld 1994).

Homma et al (1996) investigated a novel binary working fluid, $LiBr+LiI-H_2O$, for a double effect absorption cycle. Compared with $LiBr-H_2O$ pair, $LiBr+LiI-H_2O$ working fluid could extend the crystallisation limit by 5°C and it was predicted up to 12% higher thermal efficiency could be expected. The research interest on the working fluids tended towards ternary and quaternary working fluids (Iyoki 1990), (Iyoki 1993), (Kim 1995) and (Saravannan 1998). Saravanan (1998) compared 16 working fluid combinations for a vapour-absorption refrigeration system and concluded that H_2O-LiCl combination was better from the cut-off temperature and circulation ratio point of view and the H_2O-$LiBr+LiCl+ZnCl_2$ combination was better from the coefficient of performance and efficiency ratio point of view.

Lange et al (1999) reported their test results of Water-Lithium Chlorate (H_2O-$LiCLO_3$) in which they claimed that this working pair can increase COP by 5% for heat pumps compared with H_2O-LiBr pair, no crystallisation and no severe corrosion problems were found in first tests. This working pair also allowed the absorber and the condenser to work at a higher temperature.

2.4 CONCLUSION

Recent research activity on absorption refrigeration shows that multi-stage, multi-effect and GAX cycles have been considered as an effective way to improve energy efficiency. Many multi-stage, multi-effect absorption cycles have been proposed and investigated in past ten years although few have been tested experimentally. The simulation results do favour these cycles, and imply that the higher efficiency is possible by increasing the number of effects

and stages. However, more heat exchangers are required in these cycles, which results in increased complexity and cost. From this point of view, a three-stage, triple-effect cycle might be the most complicated one to be practically realised. GAX cycles are similar to a single stage system and it has potential to deliver better energy performance, however, it is not easy to implement the heat transfer efficiently between the generator and absorber which is crucial to GAX cycles. Most research on the advanced cycles has been carried out in simulation methods and few experimental results are reported. So, there is some way to go before many of the proposed advanced cycles can be commercialised.

In general, higher COP carries with it the penalty of increased complexity and therefore cost. Furthermore, the greater complexity generally causes a greater sensitivity to approach temperature (the temperature difference occurring in heat exchanger). Therefore, it is difficult to obtain higher COP by increasing cycle stages and effects in practice.

Hybrid absorption cycles provide an altemative way to improve the energy efficiency of absorption heat pumps. Since mechanical compressors require high-grade energy (electrical or mechanical) to drive them, the hybrid absorption cycles using mechanical compressors lose the ability to utilise low-grade heat sources, which is the one of the most important features of the absorption cycle. The rotary vapour re-compression cycle proposed by Riffat (1994) can be driven by thermal energy at the cost of a gas fired engine and the complexity of configuration. Therefore, the mechanical compressor involved absorption cycles may only be suitable for particular applications.

Using the ejector in the absorption cycle improves cycle performance at low cost, and simulation analysis and experimental results have shown improvements in energy efficiency. The survey shows that the past research on the ejector involved hybrid absorption cycles was focused on using ejectors, driven by the refrigerant vapours or the solutions, to enhance the evaporating

process. While these cycles offered better energy efficiency, the corrosion and crystallisation problems exists for the cycles using $LiBr\text{-}H_2O$ pair. Their performance with high temperature heat sources is just as good as the conventional single- or double-effect cycles. The cycle using an ejector to re-compress the vapour from the generator to enhance desorption process, which is to be investigated in this research project, is not found by this survey.

Although much effort has been made to find and improve working fluids for vapour absorption systems, lithium bromide-water and water-ammonia pairs are still the best in general use. Multi-component working fluids, such as binary, ternary and quaternary solutions, can improve the performance of absorption systems for particular applications, however, there is no evidence that they will soon replace lithium bromide-water or water-ammonia working pairs at this stage. For ejector hybrid absorption cycles, $H_2O\text{-}LiBr$ pair is the most suitable working fluid. This is because (a) water vapour (the refrigerant) can be directly used as a working fluid of ejectors, which is flexible to the cycle arrangement; (b) the construction of the hybrid absorption cycles using $H_2O\text{-}LiBr$ is simple; (c) it can deliver the best energy performance when required cooling temperature is above 0°C.

CHAPTER 3
THEORETICAL STUDY OF THE EJECTOR RE-COMPRESSION ABSORPTION CYCLE

In this chapter, the ejector re-compression cycle will be investigated theoretically. This cycle uses an ejector to enhance the concentration process in a conventional single-effect absorption cycle as has been described briefly in Chapter 1. In order to understand the novel cycle, we start from the conventional lithium bromide absorption cycles. After discussing the single and double effect lithium bromide cycles, a mathematical model of the novel cycle is developed. Since the steam ejector was a key component of the novel cycle, mathematical modelling and designing of the ejector are discussed then. The performance characteristics of the novel cycle are simulated from the two mathematical models. This chapter will provide all the necessary knowledge for further investigation of the novel refrigeration cycle.

3.1 LITHIUM BROMIDE ABSORPTION REFRIGERATION CYCLES

3.1.1 The thermodynamic cycles of the absorption refrigerators

An absorption cycle consists of two pairs of opposite processes that are absorption-desorption and evaporation-condensation. The absorption-desorption process takes place in the solution side, whose function is very similar to the compressor in a vapour compression refrigerator, while the evaporating-condensing process is carried out in the condenser-evaporator system. Since the refrigerant in the absorption machine is compressed in liquid, only a small amount of input energy is required for pumping it. With the solution, most of the energy, however, is used to desorb the solution by boiling. A single-effect lithium bromide absorption machine is schematically shown in Figure 3.1 and its thermodynamic cycle is shown as in Figure 3.2. In the single-effect absorption cycle, the diluted lithium bromide solution is pumped back to the generator through a solution heat exchanger where it is heated by the concentrated solution from the generator. The solution is then boiled in the generator to desorb the water from the solution. The concentrated solution flows back to the absorber to complete the solution cycle, while the

water vapour flows to the condenser and condenses there. Because the concentrated solution has the chemical potential to absorb the water, it causes the water to evaporate in the evaporator, which produces the cooling effect in the evaporator.

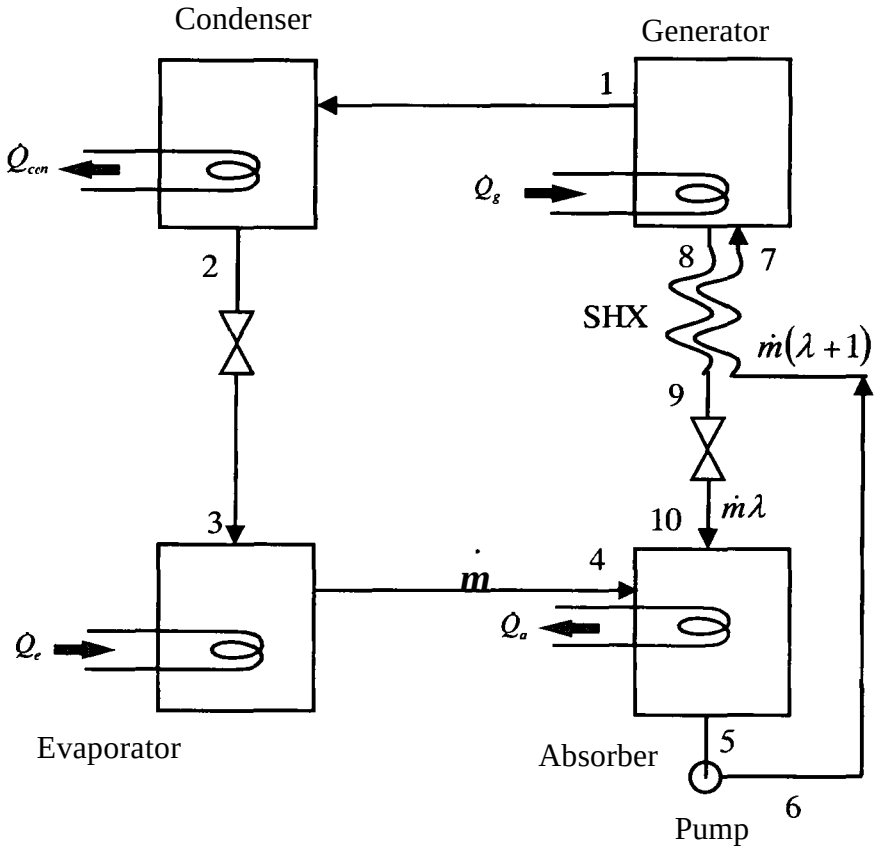

Figure 3.1 Single-effect lithium bromide-water refrigeration system

A double-effect lithium bromide absorption cycle has a similar process to the single-effect, except that there is a low pressure generator to use the condensation heat from the water vapour otherwise wasted in the condenser in order to further concentrate the solution. As a result, the energy efficiency is improved.

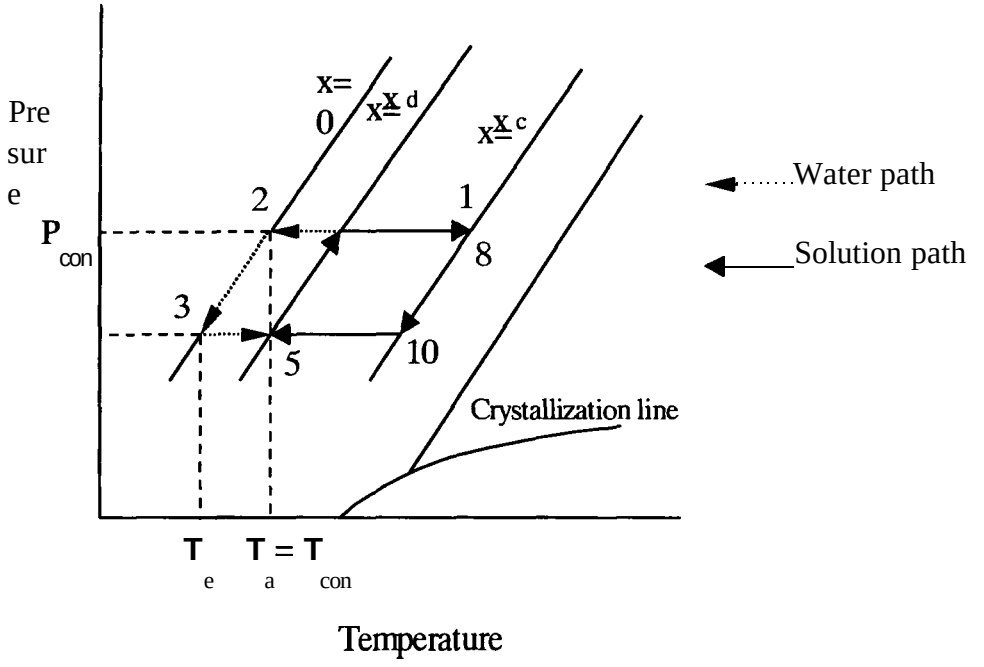

Figure 3.2 Thermodynamic cycle of single-effect lithium bromide refrigerator

3.1.2 Energy efficiency of the lithium bromide absorption refrigeration cycle

The efficiency of a absorption refrigeration cycle is defined as the ratio of the cooling power to the heat power input. It can be obtained by applying the mass and energy balances to the refrigeration cycle. For a single-effect lithium bromide absorption refrigeration cycle, it can be expressed as follow (Gosney 1982),

$$COP = \frac{\dot{Q}_e}{\dot{Q}_g} = \frac{h_4 - h_2}{(h_1 - h_6) + \lambda(h_9 - h_6)} \qquad (3.1)$$

where, λ is the circulation factor which is the mass flow rate of the concentrated solution to absorb unit mass flow rate of vapour from the evaporator. It is determined by the two solution concentrations from the fact that all the lithium bromide which enters with the strong solution leaves with weak solution. Supposing unit mass flow rate from the evaporator, the flow rates of the solutions are X, and $(\lambda+1)$, and the mass balance for lithium bromide gives:

$$\lambda x_c = (\lambda + 1) x_d$$

hence:

$$\lambda = \frac{x_d}{x_c - x_d} \qquad (3.2)$$

It should be noted that the power consumption of the pump and the heat loss from the solution heat exchanger are not taken into account in Equation (3.1). The circulation factor, λ, is important to the energy efficiency of an absorption cycle. The smaller the circulation factor, the higher the energy efficiency, because the low circulation factor reduces power consumption on the pump and solution heat effect in the absorption and desorption processes. The heat rejected from the condenser can be expressed as Equation (3.3),

$$\dot{Q}_{con} = \dot{m}(h_1 - h_2) \tag{3.3}$$

where, h_1 and h_2 are the specific enthalpies of the vapour leaving the generator and water in the condenser. This heat may be used to concentrate the solution in a low pressure generator as it does in a double-effect cycle. A double-effect lithium bromide absorption machine is shown as in Figure 3.3 and its thermodynamic cycle is shown as in Figure 3.4.

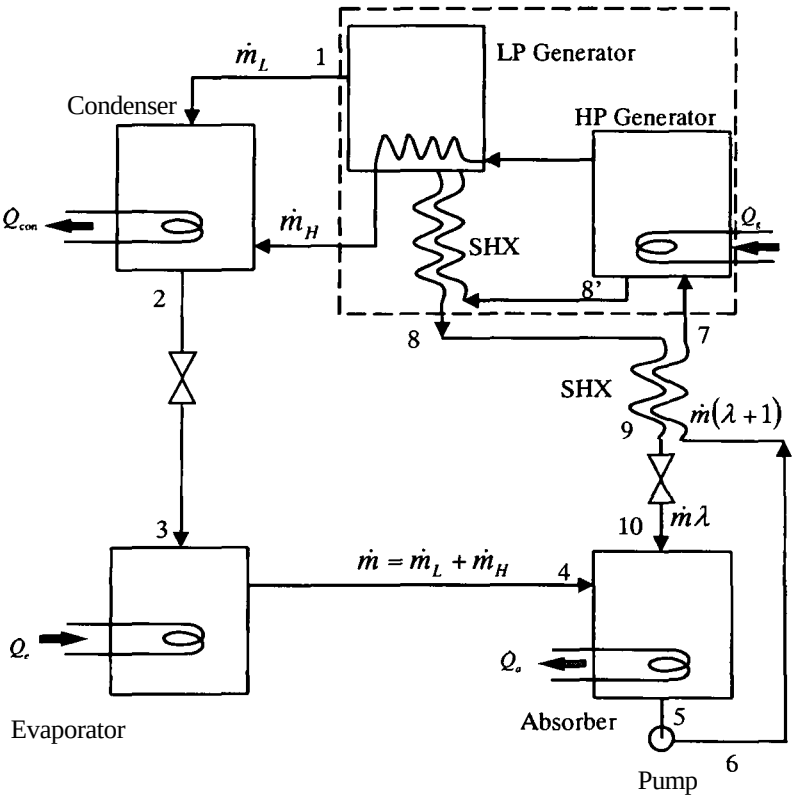

Figure 3.3 Double-effect lithium bromide absorption refrigeration cycle

The concentration process in a double-effect cycle takes place in the high and low pressure generators as shown in Figure 3.3. In the double-effect cycle, the solution is concentrated in the high-pressure, and then it is further

concentrated in the low pressure generator by using the condensation heat of the vapour from the high-pressure generator which is otherwise rejected by the condenser in a single-effect cycle. So, less heat is discharged into the environment from a double-effect cycle and its energy performance is better. Since the vapour from the high-pressure generator has to meet the requirement for concentrating the solution in the low-pressure generator, the minimum temperature of a heat source for a double-effect cycle is higher than a single-effect cycle. If the two concentration processes of a double-effect cycle in Figure 3.3 are considered as a whole, as shown in the dash line square, the energy balance for the concentration process can be written as follows,

$$\dot{Q}_g = \dot{m}_L h_1 + \dot{m}_H h_2 + \dot{m}\lambda h_8 - \dot{m}(\lambda + 1)h_7 \qquad (3.4)$$

The mass balance for the refrigerant of the cycle requires,

$$\dot{m} = \dot{m}_L + \dot{m}_H \qquad (3.5)$$

Substituting $\dot{m}_L$ of Equation (3.4) with (3.5), Equation (3.4) can be expressed as follow,

$$\dot{Q}_g = \text{rti}(/z, -h_7) + \dot{m}\lambda(h_8 - h_7) - \dot{m}_H(h_1 - h_2) \qquad (3.6)$$

If there is no heat loss in the heat exchanger, then the efficiency of the cycle is

$$COP = \frac{\dot{Q}_e}{\dot{Q}_g} = \frac{h_4 - h_2}{(h_1 - h_6) + \lambda(h_9 - h_6) - \alpha(h_1 - h_2)} \qquad (3.7)$$

In Equation (3.7), a is the ratio of the mass flow rates of the refrigerant generated by the high-pressure generator to the total refrigerant of the cycle, i.e., $\alpha = \dot{m}_H / \dot{m}$. The production of $\alpha(h_1 - h_2)$ reflects the energy recovered by the low-pressure concentration process. It is obvious that the double-effect cycle is more efficient than the single-effect one by comparing Equation (3.7) for the double-effect cycle with Equation (3.1) for the single-effect cycle. The value of $\dot{m}_H$ can be determined from the mass balance of the solution cycle.

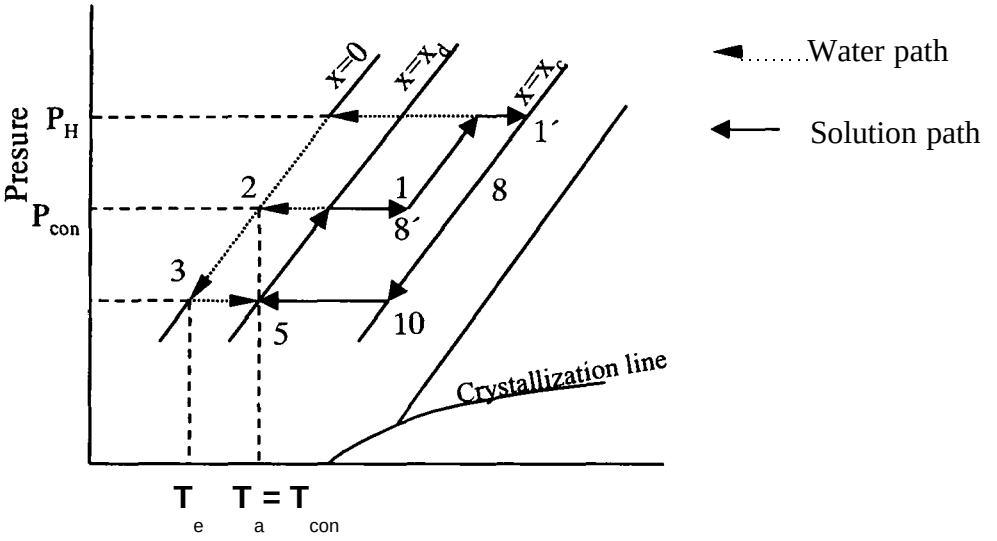

Figure 3.4 Thermodynamic cycle of double effect lithium bromide refrigerator

3.2 THE EJECTOR RE-COMPRESSION ABSORPTION CYCLE

The ejector re-compression absorption cycle is similar to the conventional single-effect lithium bromide absorption cycle which was discussed in section 3.1. The difference between them is that there is a steam ejector in this novel cycle for enhancing the concentration process. Because of the use of the steam ejector in the cycle, the performance and the operating characteristics of the novel cycle are therefore different from the conventional cycle, which are discussed in this section.

32.1 Description of the cycle

The ejector re-compression absorption cycle is shown schematically in Figure *35.* Referring Figure 3.5, the expansion of the high-pressure steam causes a low pressure at the exit of the primary nozzle of the steam ejector, therefore, the vapour at point 8 in the concentrator is entrained by the primary flow. The two streams are mixed in the steam ejector and condensed in the heat exchanger of the concentrator. The condensation heat is used to heat the solution in the concentrator. Obviously, the heat of the entrained vapour is recovered by the steam ejector in this process. Water at point 3 splits into two streams, one flows back to the steam generator and other flows into condenser. In the stable operation, the mass flow rate of the first stream equals to that of

primary flow while the mass flow rate of the second stream equals to that of the entrained vapour. The rest part of the cycle is similar to that of the conventional single-effect lithium bromide absorption cycle

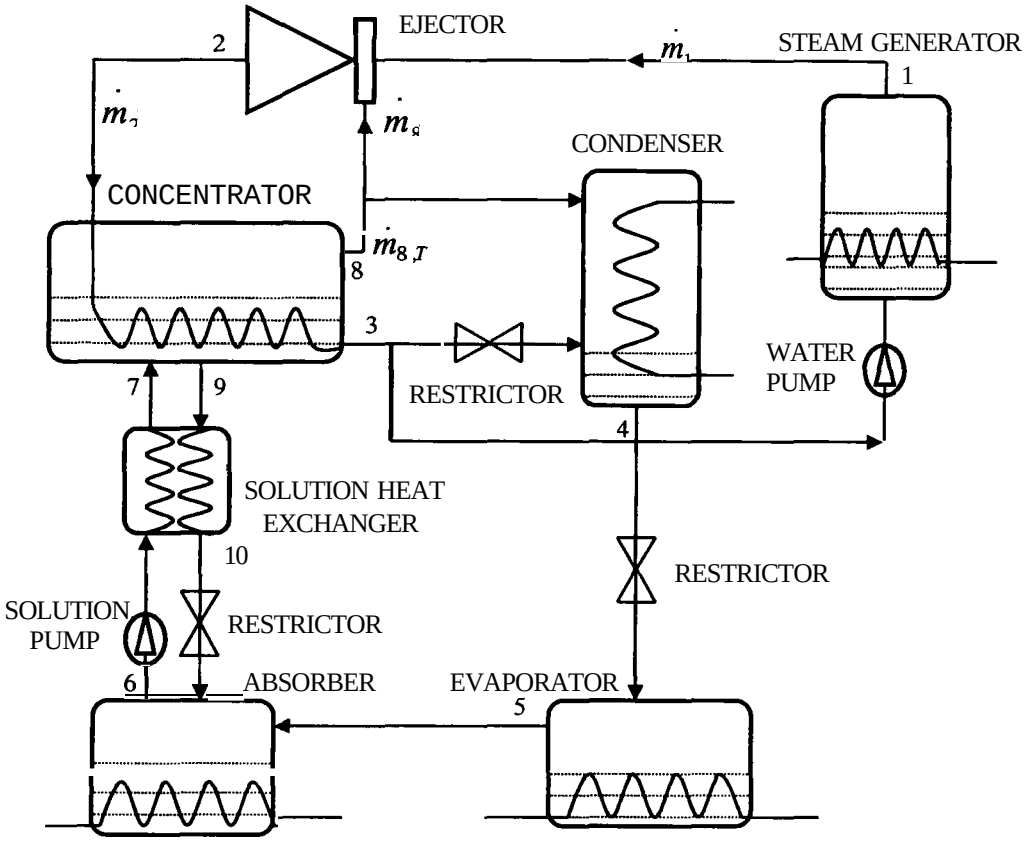

Figure 3.5 The novel refrigeration cycle

Figure 3.6 shows the novel cycle on P-T-C diagram. Referring to Figure 3.6, the cycle 6-7-9-10-6 takes up water at the absorber (10-6) and releases it as vapour at the concentrator (7-9). In the conventional absorption cycle, the vapour is condensed at 8' and the condensation heat is rejected to the surroundings. In the novel cycle, this vapour undergoes a compression process through the ejector to point 2. Since the vapour temperature is greater than the solution temperature in the concentrator, this vapour is used to heat the solution by condensation to point 3. Therefore the heat otherwise wasted is recovered and the energy efficiency is improved. The ejector process on T-s chart is shown in Figure 3.7. In Figure 3.7, the process from points 3 to 5 takes place in the expansion valve and the evaporator while the process from points

5 to 8 is the absorption and desorption of the refrigerant, which takes place in the solution cycle. Points 1_a and 1_b are the states of the steam at the exit of the primary nozzle and in the mixing area of the steam ejector while point 1_b to point 2' is an ideal compression process. The temperature difference between the T_3 and T_g in the Figure 3.6 is required for the heat transfer between the steam exit from the ejector and the solution in the concentrator.

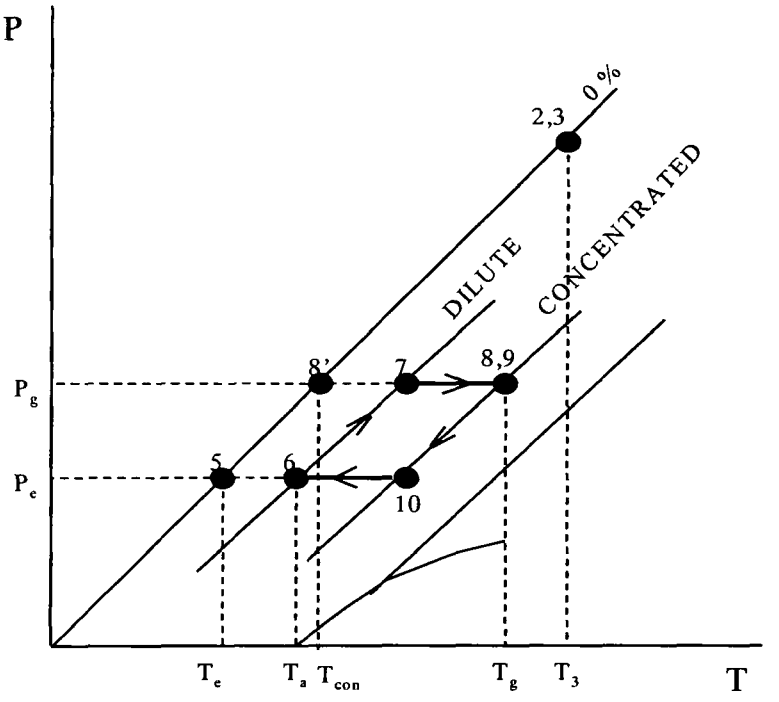

Figure 3.6 Ejector re-compression absorption refrigeration cycle on P-T-C chart

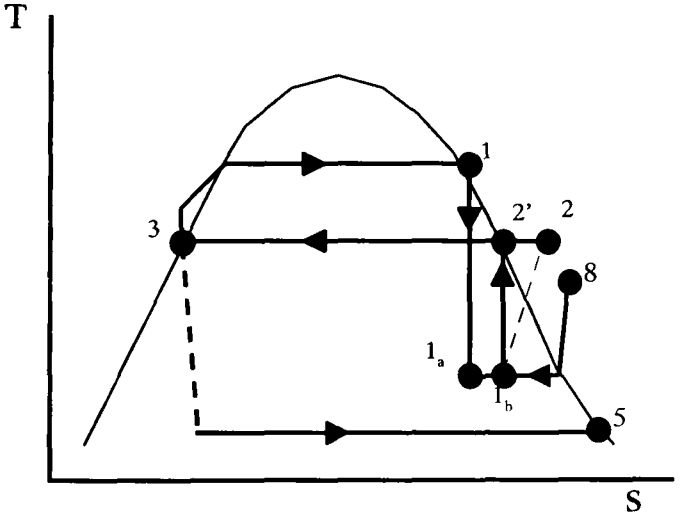

Figure 3.7 Ejector re-compression process

322 Theoretical cooling efficiency of the cycle

Using the state-point information in Figures 3.5, 3,6 and 3.7 and the mass and energy balance, we can theoretically analyse the cycle's energy efficiency. This analysis assumes that the cycle is in steady-state operation and the ejector entrairunent ratio is known.

In order to understand the flows in the concentrator clearly, a schematic diagram of the concentrator is shown in Figure 3.8. It consists of a steam ejector and heating tubes in a sealed glass vessel which is separated into two chambers. The steam ejector sits in the smaller chamber, termed 'ejector housing', while the heating tubes are placed in the larger 'solution chamber'. The chambers are connected by a passage which allows vapour to flow between them. To prevent the droplets of lithium bromide solution from entering the ejector housing, a baffle is positioned in the vapour passage. At the right end of the vessel, there are three outlets: one for the vapour at the top for the vapour to flow to the condenser, the second for the strong solution to return to the absorber and the third at the bottom for discharging the condensed water. The condensed water is then separated into two streams at the outlet: one is pumped back to the boiler, and the other flows to the condenser. The flow rates of two streams can be determined from the mass balance. An inlet is provided at this end for the weak solution retuming from the absorber. The high-pressure steam inlet is at the left-hand end of the concentrator. The heating tubing is placed in the solution chamber in such a way that it can minimise the solution level required to cover the tubes to reduce the gravity influence to boiling. The flow rate of the vapour entrained by the steam ejector is shown as *rii*^, which is the part of the total vapour flow rate $m_{8,T}$ evolved from the solution chamber.

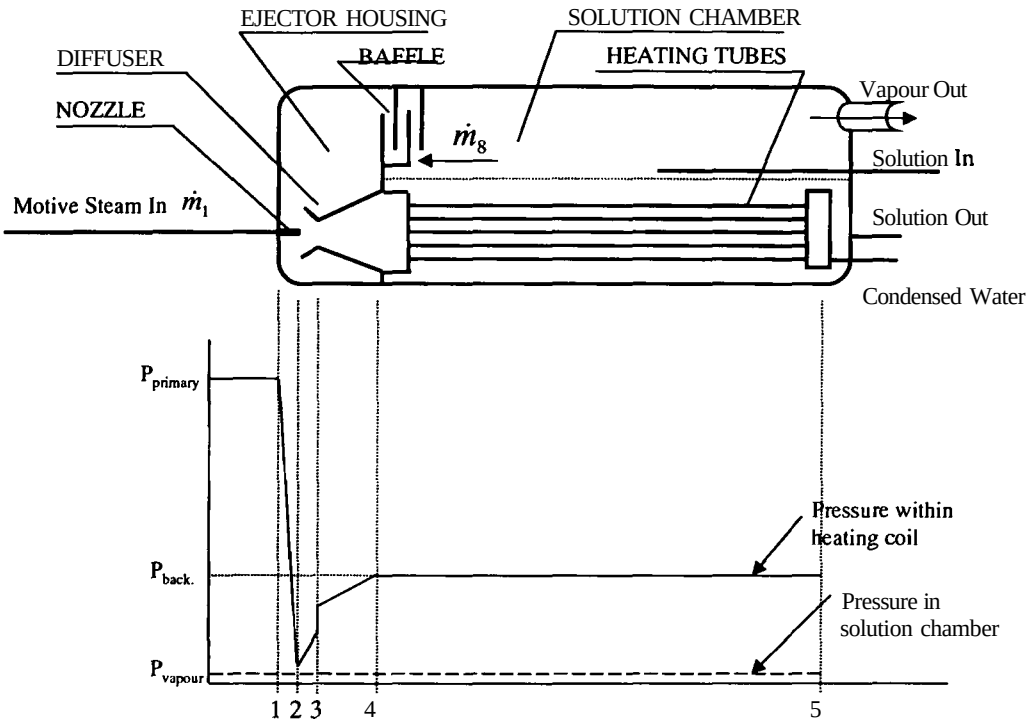

Figure 3.8 Structure and pressure profile of the concentrator

For the mass flow rate, $\dot{m}_8$, entrained by ejector from the vapour evolved from the solution, we can obtain from the definition of the entraimnent ratio,

$$\dot{m}_8 = \dot{m}_1 w$$

where, w is the ejector entrainment and $\dot{m}_1$ is the motive steam flow rate. By mass balance, the mixed steam flow rate $\dot{m}_2$ is as follow,

$$\dot{m}_2 = \dot{m}_1 + \dot{m}_8 = \dot{m}_1 (1 + w) \qquad (3.8)$$

Applying an energy balance to the heat transfer process taking place at the concentrator, the heat released by condensation of the mixed flow $\dot{m}_2$ *in* the process 2-3 should equal that required to evaporate the refrigerant, $\dot{m}_{8,T}$, from its solution at the concentrator. It can be expressed as follow,

$$\dot{m}_2 (h_2 - h_3) = \dot{m}_{ST} \left(h_8 + \frac{x_d}{x_c - x_d} h_9 - \frac{x_c}{x_c - x_d} h_7 \right) \qquad (3.9)$$

Substituting Equation (3.8) for $\dot{m}_2$ then,

$$\dot{m}_1 (1 + w)(h_2 - h_3) = \dot{m}_{8,T} \left(h_8 + \frac{x_d}{x_c - x_d} h_9 - \frac{x_c}{x_c - x_d} h_7 \right) \qquad (3.10)$$

therefore,

$$\dot{m}_{8,T} = \frac{\dot{m}_1(1+w)(h_2-h_3)}{h_8 + \frac{x_d}{x_c - x_d}h_9 - \frac{x_c}{x_c - x_d}h_7} \qquad (3.11)$$

Equation (3.11) gives the refrigerant mass flow rate evolved at the concentrator and shows it is a function of the ejector primary flow $(\dot{m}_1)$ and the entraimnent ratio (w), the states of absorbent, h_7 and h_9, in the concentrator and the difference of the specific enthalpy, (h_2-h_3).

Since the quantity of de-sorbed refrigerant must equal that taken into solution at the absorber, (during steady-state operation), we can use the refrigerant flow, $m_{8,T}$, to the calculate cooling rate at the evaporator.

$$\dot{Q}e = \dot{m}_{8,T}(h_5 - h_4) = \frac{\dot{m}_1(1+w)(h_2-h_3)(h_5-h_4)}{h_8 + \frac{x_d}{x_c - x_d}h_9 - \frac{x_c}{x_c - x_d}h_7} \qquad (3.12)$$

The input heat, $\dot{Q}_{in} = \dot{m}_1(h_1 - h_3)$, and therefore,

$$COP = \frac{\dot{Q}_e}{\dot{Q}_{in}} = \frac{(1+w)(h_2-h_3)(h_5-h_4)}{(h_1-h_3)\left(h_8 + \frac{x_d}{x_c - x_d}h_9 - \frac{x_c}{x_c - x_d}h_7\right)} \qquad (3.13)$$

Equation (3.13) gives the energy efficiency of the novel cycle. If we use the circulation factor, λ, defined in Equation (3.2) to replace the concentrations of Equation (3.13) and ignore the energy loss in the solution heat exchanger, the energy efficiency of the novel cycle becomes Equation (3.14),

$$COP = \frac{\dot{Q}_e}{\dot{Q}_{in}} = \frac{(1+w)(h_2-h_3)}{h_1-h_3}\cdot\frac{h_5-h_4}{h_8-h_6+\lambda(h_{10}-h_6)} \qquad (3.14)$$

In the right-hand of the equation, there are two items. The first one termed 'enhancement factor' describes the improvement of the energy efficiency due to using the steam ejector. The second is the energy efficiency of the conventional single-effect cycle, which has been shown in Equation (3.1). Therefore, the novel cycle is virtually a single effect cycle but its COP is enhanced by the steam ejector according to Equation (3.14).

323 Enhancement factor

The 'enhancement factor' can also be written in following form, which provides more clearly a physical meaning,

$$\varepsilon = \frac{h_2 - h_3}{h_1 - h_3}(1 + w) \qquad (3.15)$$

The ratio, $(h_2\text{-}h_3)/(h_1\text{-}h_3)$, is the fraction of the input energy that can be used to heat the solution and it has the relationship with the ratio, $(h_1\text{-}h_2)/(h_1\text{-}h_3)$, as follow,

$$\frac{h_2 - h_3}{h_1 - h_3} = 1 - \frac{h - h_2}{h_1 - h_3}$$

where, the ratio, $(h_1\text{-}h_2)/(h_1\text{-}h_3)$, indicates the fraction of the input energy that is used to entrain the vapour from the solution chamber into the copper tubes by the steam ejector. For the best energy performance, it is desirable to get the maximum *w* for the minimum $(h_1\text{-}h_2)/(h_1\text{-}h_3)$. Obviously, the ejector has a strong influence on the performance of the novel cycle. Therefore, it is necessary to discuss the ejector performance in order to understand the behaviour of the novel cycle.

3.3 THE PERFORMANCE CHARACTERISTICS OF EJECTOR AND ITS MODELLING

In the section 3.2, it was found that the ejector has a strong influence to the enhancement ratio, e. This means that the improvement of the energy efficiency of the novel cycle largely depends on the ejector performance. In this section, the performance characteristics and the factors that affect the performance are theoretically discussed.

3.3.1 Operation of an ejector

Ejectors are fluidic pumps that use the kinetic energy of a primary fluid to pump a secondary fluid. There are different types of ejectors in use. For this research purpose, only the supersonic steam ejector is considered. A steam ejector consists of a convergent-divergent nozzle and a diffuser. Figure 3.9 shows a schematic construction of a supersonic ejector. In operation, high-pressure steam, coming from a steam generator, is accelerated to supersonic

velocity through the convergent-divergent nozzle. As this high velocity jet emerges from the nozzle it entrains a secondary vapour steam and mixes with the entrained flow at the convergent section of the diffuser. The supersonic mixing flow is slowed down in the convergent section and undergoes a thermodynamic shock at the throat section of the diffuser, where it becomes subsonic flow. The flow is decelerated in the divergent section of diffuser until its pressure equals the back-pressure. This is the process where an ejector pumps a flow from low pressure to high pressure, also called compression process for the secondary flow, because its density is increased in the process. In the process, the primary flow is a driving flow and the secondary is a driven flow. Naturally, the ratio of secondary mass flow to primary mass flow or the entrainment ratio reflects the ejector efficiency. In practice, this is one of the specifications of an ejector. Similarly, the description of the performance for a compressor, a pressure ratio of the back-pressure to the secondary pressure, N_s, is used to describe the pressure lifting ability of the ejector. The entrairunent ratio and the secondary pressure ratio describe the pumping characteristic of an ejector. The effect of the driving flow to the pumping characteristic is described by the primary pressure ratio, Np, defined as the ratio of the primary pressure, Pp, to the back-pressure, P_b. The entrairunent ratio, *w,* the secondary pressure ratio, N_s, and the primary pressure ratio, Np, complete the description of performance of an ejector. Their relationship will be discussed later.

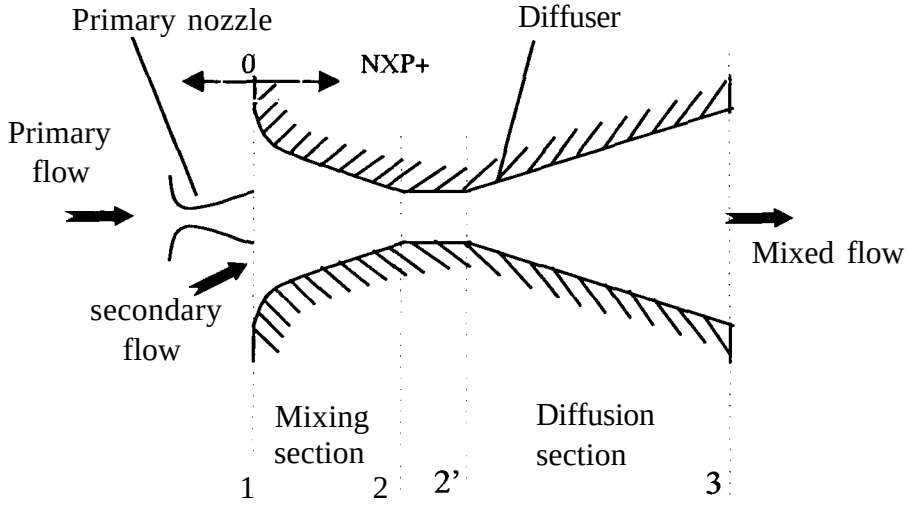

Figure 3.9 Schematic diagram of ejector

33.2 Performance characteristics of ejector

The entrainment ratio and the pressure lift ratio of a ejector are determined by the stagnation pressure of the motive flow, the stagnant pressure of secondary flow and the back-pressure. In general, the entrainment ratio can be represented functionally by:

$$w = \frac{\dot{m}_s}{\dot{m}_p} = f\left(\frac{P_{ts}}{P_{tp}}, \frac{P_b}{P_{tp}}\right) \tag{3.16}$$

i.e., it is dependent on the stagnation pressure and back-pressure ratios. This relationship can also be represented in three dimension surfaces shown as Figure 3.10 (Addy et al, 1981).

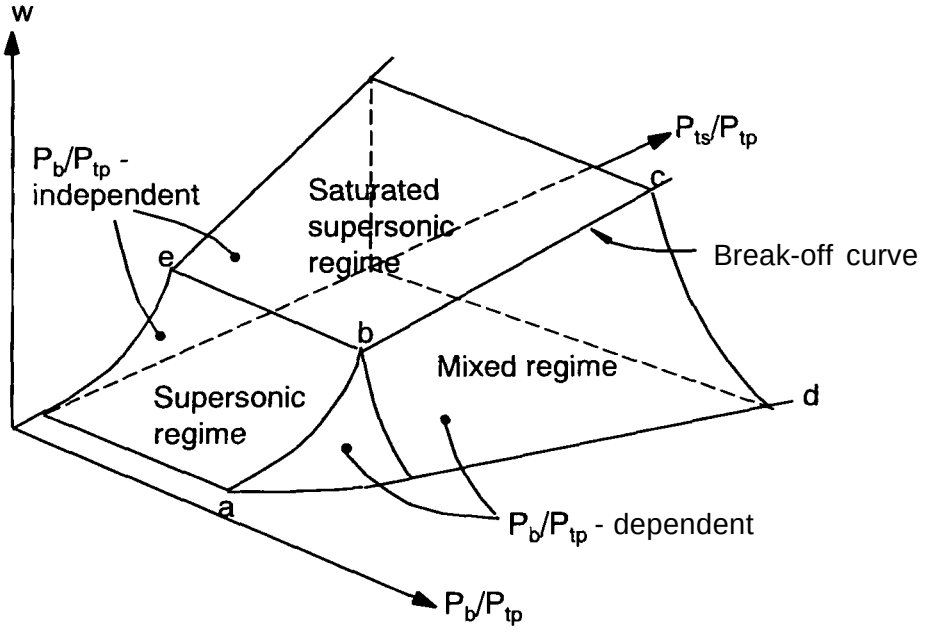

Figure 3.10 Performance characteristics of ejector

The three dimension surfaces consist of 'Supersonic regime', 'Saturated supersonic regime' and Mixed regime' and they are separated by so-called 'Break-off curves shown as Figure 3.10. If the Mach number at the minimum flow area is unity, the ejector operates in either 'Supersonic regime' or 'Saturated supersonic regime', but if this Mach number is less than unity the ejector operates in 'Mixed regime'. The line a-b-c in Figure 3.10 forms a 'Break-off curve' which separates 'Mixed regime' from 'Supersonic' and 'Saturated supersonic' regimes. On the left of the curve, the entrainment ratio is independent of the pressure ratio P_b/P_{tp} and is constant when the pressure

ratio P_{ts}/P_{tp} is fixed. But it becomes P_b/P_{tp} dependent when P_b/P_{tp} falls into the right side of the curve and drops down dramatically for any increase of the ratio. The entrainment ratio will drop to zero when the pressure ratio P_b/P_{tp} reaches to the curve a-d and the ejector has lost its function. The back-pressure Pb at Break-off curve is called the critical pressure.

For efficient use of energy, it is desirable to let the ejector work at as close as possible to the left side of the Break-off curve. However, this is also an unstable condition, because any interruption to the pressure ratio P_b/P_{tp} will cause the entrairunent ratio to drop down dramatically if it moves the pressure ratio to the right side of the curve. So, this factor must be taken into account when determining the pressure ratio Pb/Ptp.

When the ejector operates on the surfaces at the left of Break-off curve, the entraimnent ratio is independent of the ratio of back-pressure to motive pressure. At these surfaces, the entrainment ratio increases as the pressure ratio P_{ts}/P_{tp} increases.

3 3 3 One-dimensional analysis

The purpose of this analysis is to determine the entrainment ratio of a supersonic ejector given a particular maximum required pressure lift and then, if required, the dimension of critical flow passages. Figure 3.11 is the schematic drawing of a supersonic ejector showing the nomenclature used in this section.

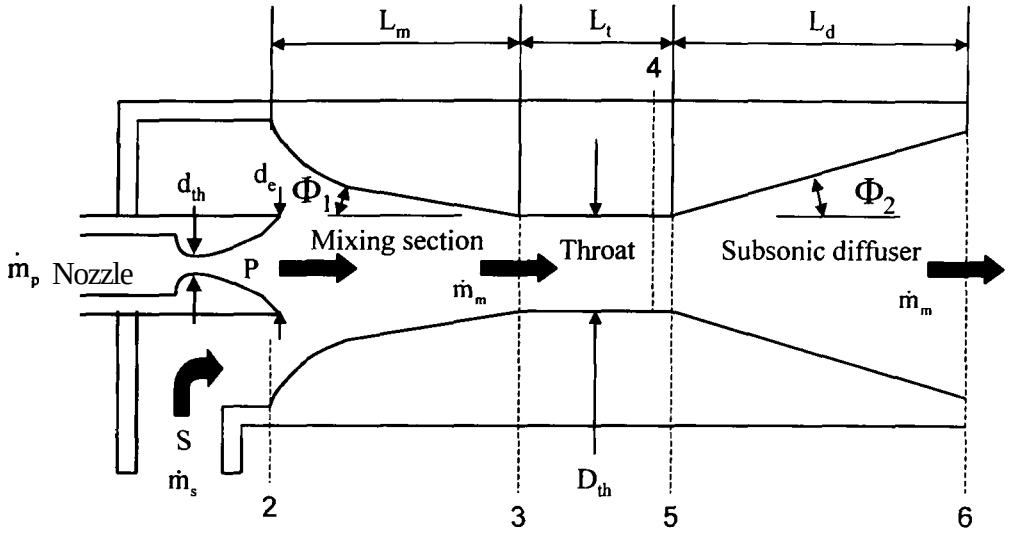

Figure 3.11 Schematic drawing of a supersonic ejector showing the nomenclature used in this section

Primary Nozzle:

Referring to Figure 3.12, high-pressure vapour enters the primary nozzle at the rate, $\dot{m}_p$, with stagnation pressure and enthalpy P_{t0} and h_{t0} respectively, and expands isentropically so that at exit:

$$v'_{p1} = \sqrt{2\left(h_{tp} - h'_{p1}\right)}$$

where: v'_{p1} = nozzle velocity for isentropic expansion

$$h'_{p1} = h\left(P_{p1}, T_{p1}\right)$$

$$s_{p1} = s_{p0}$$

$$P_{p1} = P_{s2}$$

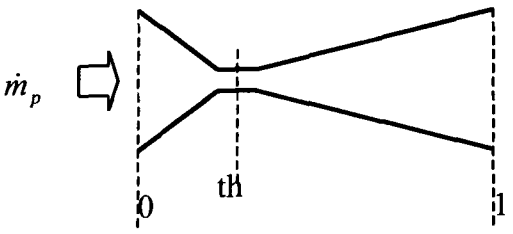

Figure 3.12 Convergent-divergent (de-Laval) nozzle

In practice, fluid friction reduces the flow velocity. To account for this an isentropic efficient factor is introduced:

$$\eta_N = \frac{h_{tp} - h_{p1}}{h_{tp} - h'_{p1}} = \frac{v_{p1}^2}{v_{p1}'^2}$$

From which the actual nozzle velocity is given:

$$v_{p1} = \sqrt{2\eta_N \left(h_{tp} - h'_{p1}\right)} \qquad (3.17)$$

Typical values of η_N lay between 0.97 and 0.99, (ESDU 1986).

Mixing section:

For simplicity, in this section the primary and secondary fluids are assumed to be dry saturated or superheated vapours of the same species.

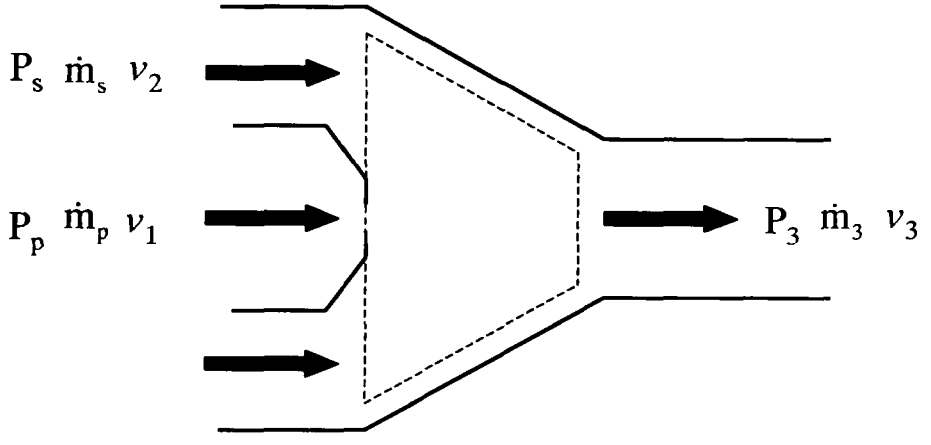

Figure 3.13 Detail of the entrainment model

Referring to Figure 3.13, assuming the walls of the mixing section offer no frictional resistance to the flow, and applying Newton's second law of motion to the control volume yields:

$$\Sigma F = \oint A \cdot dP = \dot{m}_m v_3 - \dot{m}_p v_1 - \dot{m}_s v_2 \qquad (3.18)$$

The solution of Equation (3.18) is complicated by the integration on the left-hand-side. To make this amenable to analytical solution it is usual to assume that either the flow area (A) remains constant (i.e. a constant area design) or the static pressure (P) remains constant and therefore, $dP = 0$. In the present case, for super-sonic ejectors with high secondary pressure ratio, (P_b/P_s), it is usual to apply the later assumption; i.e., that the static pressure is constant

throughout the entrainment region. Experimentally this has been shown to produce designs which produce pressure lifts and entrainment values closer to those predicted using the constant area assumption. Thus, assuming $dP = 0$, Equation (3.18) reduces on rearrangement to:

$$\dot{m}_m v_3 = \dot{m}_p v_1 + \dot{m}_s v_2 \tag{3.19}$$

From mass flow continuity: $\dot{m}_m = \dot{m}_p + \dot{m}_s$ (3.20)

Defining entrairunent ratio: $w = \frac{\dot{m}_s}{\dot{m}_p}$ (3.21)

Substituting (3.20) and (3.21) into (3.19) yields on rearrangement:

$$v_3' = \frac{v_1 + w v_2}{1 + w} \tag{3.22}$$

In the present case, the velocity of the primary flow will be at least two order of magnitude greater than that of the secondary flow. In other words $v_2 \ll v_1$ and in which case, from (3.22) we can write;

$$v_3' = \frac{v_1}{1 + w} \tag{3.23}$$

An effect of fluid friction at the wall of the mixing section will be to reduce the mixed flow velocity. The effect of wall friction can be accounted for by introducing a momentum loss coefficient, K_m:

$$v_3 = K_m v_3' = \frac{\eta_E v_1}{1 + w} \tag{3.24}$$

Typical values of K_m lay between 0.85 and 0.9, (ESDU 1986).

The stagnation enthalpy at the end of the mixing section can be determined by applying the steady flow energy equation across the volume in Figure 3.13. Assuming neither heat nor work transfer occur, then;

$$\dot{m}_3 h_{t3} = \dot{m}_p h_{tp} + \dot{m}_s h_{ts} \tag{3.25}$$

Substituting (3.20) and then (3.21) into (3.25) and rearranging the result gives,

$$h_{t3} = \frac{h_{tp} + w h_{ts}}{1 + w} \tag{3.26}$$

Applying the steady flow energy equation within the diffuser throat yields,

$$h_{t3} = h_3 + \frac{v_3^2}{2} \tag{3.27}$$

Thermodynamic shock process:

At the design-point, it is assumed that a normal shock process occurs at the end of the diffuser throat, between state-point (4) and (5) in Figure 3.11. Because the process occurs over a very short distance, it can be assumed to be adiabatic but never isentropic, and also the flow area can be assumed constant. Therefore, from mass flow continuity:

$$\rho_5 v_5 = \rho_4 v_4 = \rho_3 v_3 \qquad (3.28)$$

Note that if frictionless flow is assumed over the length of the diffuser throat then also,

$$v_4 = v_3 \text{ and } \rho_4 = \rho_3$$

From the steady flow energy equation and noting that $h_4 = h_3$,

$$h_5 + \frac{v_5^2}{2} = h_4 + \frac{v_4^2}{2} = h_{t3} \qquad (3.29)$$

Applying the momentum conservation principle across the shock and noting that $P_4 = P_3 = P_2$ for a constant static pressure entrainment without wall friction, then;

$$P_5 + \rho_5 v_5^2 = P_2 + \rho_4 v_4^2 \qquad (3.30)$$

When determining P_2, it is usual to recognise a loss in total pressure in the secondary flow between the entry to suction pipe and the mixing section. This effect is normally accounted for by introducing a secondary flow total pressure loss coefficient:

$$\eta_s = \frac{P_{t2}}{P_{ts}} \text{ where } 0.95 \le \eta_s \le 1, \text{ (ESDU 1986).}$$

If the Mach number of the secondary flow, as it enters the mixing region, is less than 0.1 then we may assume it to be incompressible (ρ = constant) and the static pressure P_2 is given by Bernoulli's equation:

$$P_2 = P_{t2} - \rho_2 \frac{v_2^2}{2} = \eta_s P_{ts} - \rho_s \frac{v_2^2}{2}$$

Substituting this result into Equation (3.30) and noting that $v_2^2 << v_4^2$ yields:

$$P_5 + \rho_5 v_5^2 = \eta_s P_{ts} + \rho_4 v_4^2 \qquad (3.31)$$

The total pressure at state-point 5, down stream of the shock, is determined by compressing the flow isentropically from P5, h_5 to h_{t5}:

$$P_{t5} = P_5 + \int_{(5}^{5} (\rho \cdot dh)_{s=\text{constant}} \qquad (3.32)$$

Sub-sonic diffuser section:

It is usual to recognise that there will be a loss in total pressure through the diffuser and this is normally accounted for by introducing a diffuser pressure recovery coefficient:

$$\eta_d = \frac{P_{t6}}{P_{t5}} \text{ where } 0.9 \le \eta_d \le 0.96 \text{, (ESDU 1986).}$$

Noting that v_6 will usually be small (M_n < 0.1), then from Bernoulli's equation the maximum back-pressure an ejector can overcome will be,

$$P_6 = \eta_d P_{t5} - \frac{\rho_6 v_6^2}{2} \qquad (3.33)$$

The density, ρ_6, can be determined from P_6 and h_6. The latter is given by applying the steady flow energy equation:

$$h_6 = h_5 + \frac{v_5^2 - v_6^2}{2} = h_{t3} - \frac{v_6^2}{2} \qquad (3.34)$$

Thermodynamic properties

P, V, T, h and s data are required to solve (3.17) to (3.34). If the reduced temperature (T/T_{crit}) of a gas or vapour is greater than 2 and its reduced pressure (P/P_c) is less than 0.1, then it can be usually assumed that its thermodynamic behaviour will be similar to that of an ideal gas:

$$Pv = RT \qquad (3.35)$$

And $h = CpT$ (336)

Where the specific heat value, C_p = constant.

Isentropic expansion and compression of an ideal gas obeys the isentropic law;

$$Pv^{\gamma} = \text{constant} \qquad (3.37)$$

Combining (3.35) and (3.37) gives; $\frac{P^{\frac{\gamma-1}{\gamma}}}{T}$ constant (3.38)

Where the isentropic index, $\gamma = C_p/C_v$ = constant in this case.

If a gas or vapour is assumed to be semi-perfect (sometimes referred to as thermally perfect and calorically imperfect) then the ideal gas equation of state in (3.35) still applies, but the specific heat values are taken to be functions of temperature (only):

$$h - h_{ref} = \int_{T_{ref}}^{T} C_p(T)dT \qquad (3.39)$$

where $C_p(T)$= fl+Z)r+cr'+f/r'+-^ (3.40)

The isentropic index (γ) in this case is also a function of temperature. The simplest method of dealing with this problem is to assume,

$$\bar{\gamma} = \frac{1}{1 - \frac{R}{C_p(T)}} \qquad (3.41)$$

A more accurate solution may be determined by calculating γ using (3.37) at both ends of the process and using the arithmetic average. A still better average value may be obtained by combining the first and second laws of thermodynamics for an open system, and assuming the fluid to be taken as an ideal gas yields:

$$ds = C_p \frac{dT}{T} - R\frac{dP}{P} \qquad (3.42)$$

Substituting Equation (3.40) and noting that *ds = 0* for an isentropic process, integrating (3.42) gives:

$$\ln\left(\frac{P_t}{P}\right) = \frac{1}{R}\left\{a\ln\left(\frac{T_t}{T}\right) + b(T_t - T) + \frac{c}{2}\left(T_t^2 - T^2\right) + \frac{d}{3}\left(T_t^3 - T^3\right) - \frac{e}{2}\left(\frac{1}{T_t^2} - \frac{1}{T^2}\right)\right\} \qquad (3.43)$$

If it is assumed that the vapour expands isentropically across a nozzle from known values of P_t and T, to a given static pressure P, the value of static temperature (T) which satisfies Equation (3.43) must be determined iteratively. Once this value has been calculated the mean isentropic index may be determined:

$$\frac{\bar{\gamma}}{\gamma} = \frac{1}{1 - \frac{\ln(T_t/T)}{\ln(P_t\ IP)}} \qquad (3.44)$$

Equation (3.40) may be applied with confidence at low pressure ($Pr <= 0.1$). By comparing calculated and tabulated values and temperature changes undergone during isentropic compression or expansion process, it can be shown that γ expressed by Equation (3.41) is less accurate than that provided by Equation (3.42) through to (3.44), but the former method is less complicated. However, the error in both cases increases with pressure and pressure ratio, particularly when the state of a dry vapour is close to saturation and near to its critical-point condition. In such cases, it is necessary to use real-gas data; either tabulated, or more conveniently, in the form of equations which provide functional relationships between the required properties. Clearly, the most important of these is the equation of state, and detailed information on these can usually be obtained from chemical suppliers or from the literature. Equations of state and methods for determining related properties of 'real' fluids are covered in most thermodynamic textbooks, (Cengel and Boles 1994).

Method of solution and design

There are several ways to solve Equations (3.17) to (3.34). The aim is to determine the variation in entrainment ratio (w) with secondary pressure ratio, ($N_s=P_6/P_s$) as functions of nozzle pressure ratio (N_n = $P,p/Ps$). However, it should be noted that each solution will only give the predicted design-point performance of a particular ejector. In other words, if w and N_n are altered the flow path geometry (AR, AT, etc) will also change. The preferred solution method is to specify primary and secondary flow stagnation conditions and entrairunent ratio (w) and to calculate the secondary pressure ratio, N_s. Calculations are then repeated over a range of entrainment ratios so that design-point performance charts can be constructed.

Regardless of whether the gas is assumed real, semi-perfect or ideal gas Equation (3.17) to (3.27) and (333) and (334) can be solved directly with little complication, although some iteration is required in terms of property data for the former cases. The solution of Equations (3.28) to (3.32) is a little more complicated, particularly if it is assumed the gas is 'real'. In this case, it

is necessary to devise an iteration scheme, as variables are not separable. However, if the gas is assumed ideal then Equation (3.28) to (3.32) can be converted into Mach Number functions:

Mach Number, $M_n = \frac{v}{\sqrt{\gamma RT}}$ where $\sqrt{\gamma RT}$ = local speed of sound.

By redefining the variables in terms of M_n the solution of (3.28) to (3.32) becomes uncomplicated. The variation in thermodynamic properties across a normal shock wave for an ideal gas are well known. For reference, these are repeated in Appendix A (Hodge and Koenig 1995).

Once Equations (3.17)-(3.34) have been solved, the flow areas through the primary nozzle $(d_t$ and $d_e)$ and diffuser (D_t), and subsonic diffuser exit can be determined from mass flow continuity:

$$A = \frac{rh}{\rho v} \qquad (3.45)$$

Table 3.1 lists recommendations for those geometries which cannot be determined using the one-dimensional model.

Table 3.1: Recommended ejector geometrical features taken from ESDU (1986). (Refer to Figure 3.11 for nomenclature)

Dimension	Recommendation	Comments
Primary nozzle conical divergent expansion tube included angle	10°	The primary nozzle discharge orifice should have a sharp lip
Velocity of steam entering at primary nozzle	50 m-s^{-1}	Maximum value
Radius of convergent steam entry region within primary nozzle	$0.3d_{th}$	Minimum value
ϕ_1	2° - 10°	If a conical inlet to mixing chamber is used then this should be have an included angle of 20° to 40°
Radius of entry region to the mixing section	1D	ESDU recommend that the entry region should consist of a generous bell-mouth. The 1D given here is suggested by the authors
L_m	5 to 10 D	Measured from the exit plane of the constant area section (diffuser throat)
L_t	2 to 4 D	
ϕ_2	3° to 4°	Not great than 7°
Diffuser exit diameter, D_c	< 2.4 D	L_d is determined from ϕ_2 and D_c, however, from the authors experience L_d is usually set at 7 D

3.4 SIMULATION MODEL OF THE NOVEL CYCLE

The COP of the novel cycle can be determined from Equation (3.14) and the entrainment ratio, which is necessary for Equation (3.14), can be determined from Equations for the steam ejector in the section 3.3.3. So, the simulation of the novel cycle can be performed by computing those equations.

3.4.1 The variables used in the simulation

In the simulation, the external conditions are as follows,

Steam temperature, ℃

Condenser temperature, ℃

Absorber temperature, ℃

Evaporator temperature, ℃

Required cooling capacity, kW.

The internal parameters include:

Mass concentrations of the solution, %

Solution temperature of the concentrator, ℃

Steam temperature in the concentrator, ℃

Efficiency of the solution heat exchanger, $\eta = \frac{h_o - h_a}{h_g - h_a}$, where h_o is the enthalpy of weak solution leaving the solution heat exchanger, h_a and h_g are the solution enthalpy in the absorber and the concentrator respectively.

3.42 The properties of working fluids

Equations describing steam properties were taken from Irvine et al (1984). However, because the vapour pressure in the ejector is low, it was assumed that water vapour behaved like an ideal gas. The properties of lithium bromide solutions were calculated from the correlations provided by ASHRAE (1993), Lee et al (1990), Patterson et al (1988) and Hellmann (1996).

3.43 The method of the simulation

In the simulation, the ejector entraimnent ratio was determined from its operating conditions: the state of the motive flow was obtained from its temperature, assuming that the steam was drysaturated. The condition of the secondary flow was determined from temperature and solution concentration in the concentrator (the vapour was superheated); and the back-pressure of the ejector was determined from the state of the mixed steam in the concentrator (the condensing temperature of the mixed steam). From these conditions, the entrainment ratio was determined. Once this was obtained, the calculation of the COP was straightforward. The simulation model was programmed using Microsoft Excel and Visual basic.

3.5 FACTORS AFFECTING THE PERFORMANCE OF THE NOVEL CYCLE AND COP PREDICTION

The computer simulation model was used to exam the factors which effect the performance of the novel cycle. However, attention here was paid only to those effects which are particular to the novel cycle. For brevity, those effects common with conventional absorption cycle refrigeration are not included because they are fully covered in several textbooks including Gosney (1985) and Stoecker (1982).

3.5.1 Effect of the solution states to enhancement factor

From the discussions in Sections 3.2 and 3.3, the solution concentration, x_c, and temperature, T_s, were found to effect the enhancement factor (E) in Equation (3.15). This is thought to because the solution state determines the operating condition of the steam ejector. In this particular application, the suction and the discharge conditions of the steam ejector are linked by the state of the lithium-bromide solution in the concentrator, i.e., the vapour pressure of the solution is the ejector secondary flow pressure while the solution temperature determines the ejector back-pressure. So, any change in the solution condition will effect the entrainment ratio of the ejector. Table 3.2 lists some typical theoretical results.

Table 3.2 Ejector Entrainment Ratio at different solution condition

	Solution Concentration, %					
	55	56	57	58	59	60
Solution temperature	Entrainment ratio					
70 °C	0.4533	0395	0344	0.296	0.255	0.2332
75 °C	0.4364	0382	0.332	0.285	0.243	0.2037
80 °C	0.4196	0367	0319	0.274	0.233	0.1951

Note: The motive steam was assumed to be at 15 bar and the mixed flow temperature equalled the solution temperature.

The results in Table 3.2 suggest that the solution concentration affects entrainment ratio more than its temperature does. Keeping the solution at low concentration will allow the steam ejector operate more efficiently. It should be noted that these calculated results are based on the ejector design conditions and do not represent an ejector's off-design performance. The enhancement factor has a similar characteristic to the entrairunent ratio, as shown in Table 3.3 and Figure 3.14.

Table 3.3 Enhancement factor varied with the solution condition

	Solution Concentration, %					
	55	56	57	58	59	60
Solution temperature	Enhancement factor					
70 °C	1.35	1.303	1.255	1.210	1.173	1.131
75 °C	1.34	1.295	1.248	1.204	1.164	1.127
80 °C	1.33	1.285	1.239	1.198	1.159	1.123

Compared with entrainment ratio, enhancement factor is less affected by the variation of the solution temperature and concentration, but the trend is similar. So, solution concentration should be kept as low as possible to achieve a greatest enhancement factor. However, this will result in low efficiency for the absorption cycle as has been discussed in previous chapter.

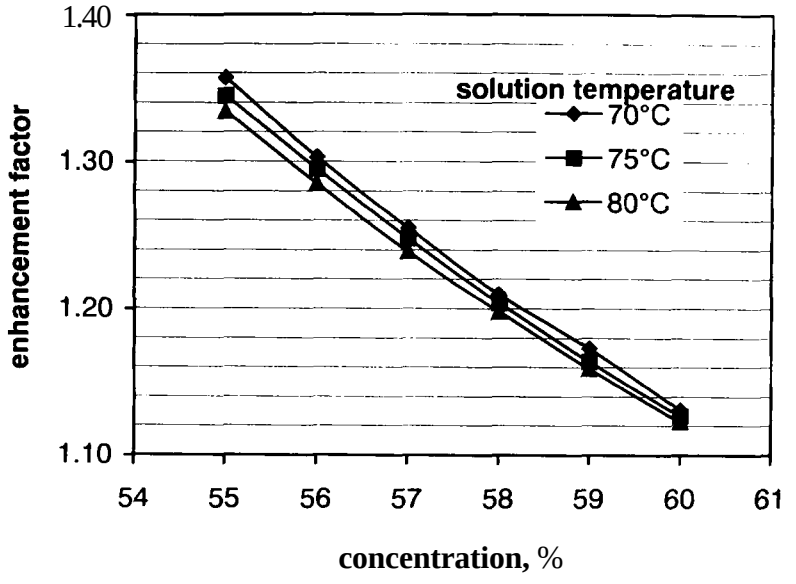

Figure 3.14 Enhancement factor variation with the solution states

3.5.2 Effect of the temperature difference between the solution and steam

The results in Table 3.2 and 3.3 were based on the assumption that there was no temperature difference between the two sides of the heating tubes in the concentrator vessel in Figure 3.8. However, in practice, a temperature difference will exist and this will increase the back-pressure (Pback) to the vapour pressure (Pvapour) ratio. Ejector entrainment ratio will, therefore, decrease and so accordingly will the enhancement factor. The theoretical results indicated that the reduction of the enhancement factor due to the temperature difference is larger at low solution concentrations than at higher values and is proportional to temperature difference, as shown in Figure 3.15. In this figure, the percentage loss of entrainment ratios was referred to their entrainment ratios at zero temperature difference between two sides of the tubes in the concentrator. This is to say that the loss of entrainment ratio at zero temperature difference is naught.

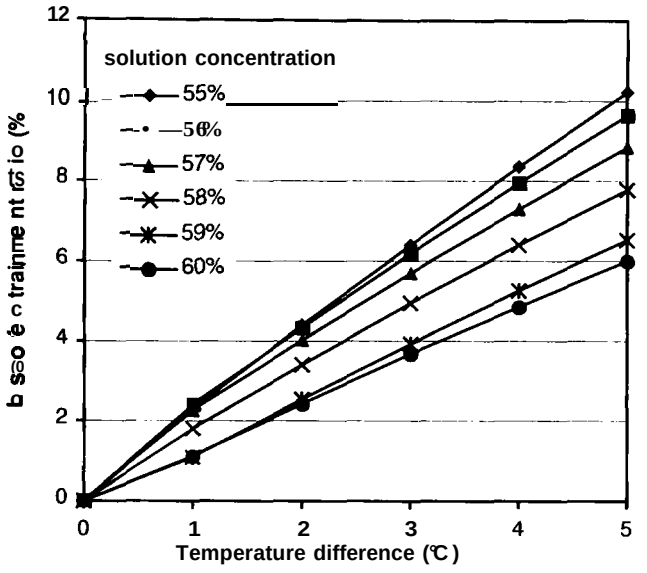

Figure 3.15 The influence of temperature difference to entrainment ratio

3.5.3 COP predictions

The coefficient of performance was calculated by assuming the following conditions:

a. Condensing and absorption temperatures were at 30°C,
b. Evaporating temperature was at 5°C,
c. The heat source was steam at 198.3 °C @ 15 bar,
d. Solution heat exchanger effectiveness was assumed to be 0.7 (Dorgan 1995),
e. The electrical power consumption of the pumps was neglected.

From the calculated results of enhancement factor in Table 3.3, it was found that the values of the enhancement factor were greater than unity. This means that under assumed operating conditions, the COP of the steam ejector re-compression cycle is predicted to be greater than that of the conventional single-effect cycle provided that the heat source can drive the steam ejector. Estimated values of COP are listed in Table 3.4.

COP values responding to the solution concentration change in the novel cycle were found to differ from those of single-effect cycle. The COP of

conventional cycle increases with the solution concentration. However, for the ejector-enhanced cycle, there is a concentration at which the cycle has a maximum COP value. This is a result of the ejector entrairunent ratio decreasing as concentration increases while the COP of the single-effect cycle increases with the concentration. Figure 3.16 compares the variation in COP with solution concentration between the novel and conventional cycles.. Another difference between the novel cycle and the conventional single-effect cycle is that the maximum COP of the novel cycle decreases as the solution temperature increases, as shown in Figure 3.17. In the conventional absorption cycle, there is a solution temperature at which the cycle COP reaches maximum value.

Table 3.4 COP Cost Comparison between the single-effect and the ejector cost single-effect cycles

		Solution temperature											
		70° C		71 C		72 °C		73 °C		74 C		75 C	
		S	N	S	N	S	N	S	N	S	N	S	N
solution concentration	57.0%	0.768	1.015	0.764	1.008	0.762	1.003	0.758	0.997	0.756	0.992	0.752	0.996
	57.5%	0.784	1.016	0.781	1.012	0.778	1.007	0.775	1.002	0.773	0.997	0.770	0.992
	58.0%	0.786	1.016	0.783	1.011	0.781	1.006	0.778	1.002	0.776	0.997	0.773	0.992
	58.5%	0.788	1.011	0.785	1.007	0.781	1.003	0.778	0.998	0.776	0.994	0.774	0.990
	59.0%	N/A	N/A	0.811	1.002	0.807	0.997	0.807	0.993	0.805	0.990	0.802	0.985
	59.5%			N/A	N/A	0.815	0.991	0.814	0.986	0.812	0.982	0.810	0.977

Condensing temperature 30C Evaporating temperature 5 °C, Absorption temperature30° C
S – Single-effect absorption cycle
N – Novel Cycle

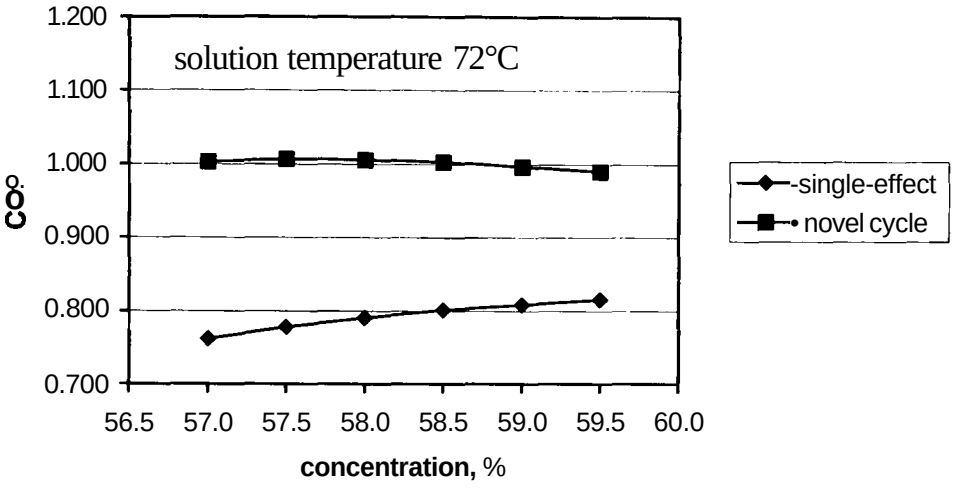

Figure 3.16 Comparison of COP vs. solution concentration

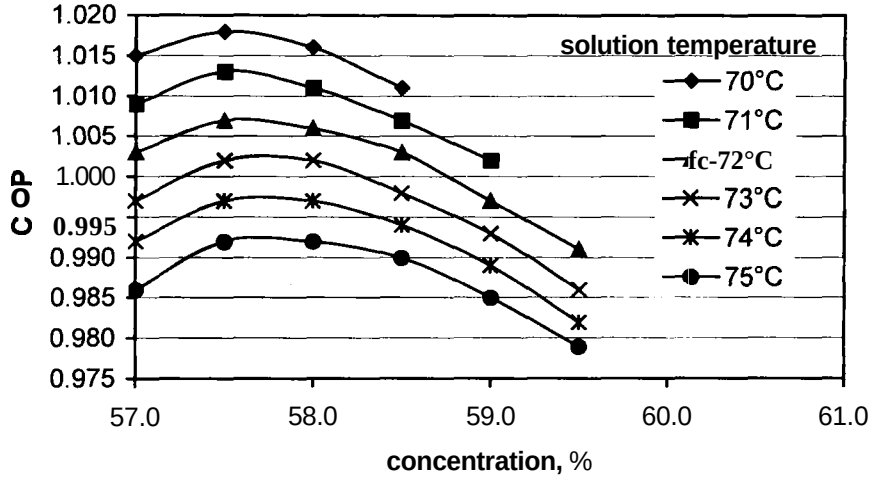

Figure 3.17 COP variation with the solution temperature

• the novel cycle, COP was found to increase with the heat source temperature, ile the solution temperature remains unchanged. Figure 3.18 shows the predicted ıd in COP with the steam temperature. In these results, the solution concentration :he concentrator was 59% and the solution temperature was 71°C.

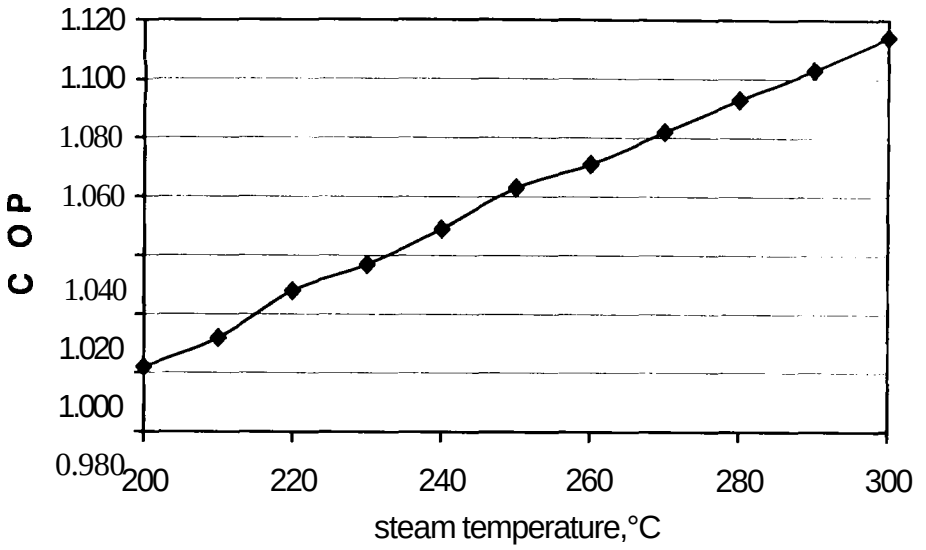

Figure 3.18 COP variation with ejector steam supply temperature

5 CONCLUSIONS

this chapter, the theoretical energy efficiency of the novel refrigeration cycle was cussed. From the theoretical results, it can be concluded that the novel cycle, using ejector to re-compress the vapour for re-heating the solution, can increase the cycle IP. However, a high temperature heat source is required to drive a steam ejector for :h a cycle. The improvement of the COP of this novel cycle largely depends on the rainment ratio of the ejector. Since the steam ejector is introduced into the rigeration cycle, the cycle performance characteristics are profoundly affected by ejector. As a result, the COP responses to the variation of the operation condition the novel cycle are different from those for the conventional cycles. These ferences are:

- The novel cycle COP decreases as the solution temperature increases while there is a solution temperature where the conventional cycle COP reaches maximum value.
- There is a solution concentration where the novel cycle COP reaches maximum value while the COP increases with the solution concentration in the conventional cycle.

• The novel cycle COP increases with the heat source temperature, however, the COP of the conventional single-effect absorption cycle can not always increase with the heat source temperature.

• The novel cycle COP is more sensitive to the temperature difference between the steam and the solution.

erefore, an efficient steam ejector is essential to obtain high COP from the novel ;le. In the meantime, the following requirements should be met if the novel cycle is ɔe mn efficiently,

• The solution temperature should be kept as low as possible.

• The solution concentration should be chosen for the maximum COP.

• The temperature difference AT for the heat transfer between the steam and solution should be kept low as it affects the performance significantly.

ese requirements are the results of using a steam ejector in the concentration ·cess. They may not be necessary for the conventional cycles.

CHAPTER 4
PRELIMINARY EXPERIMENTAL STUDY OF THE STEAM EJECTOR

It is quite normal for a refrigerator to operate at part-load conditions, so, it is important to know the part-load performance. For the novel cycle, the part-load operation means that the steam ejector is also operated under off-design condition. Therefore, it is necessary to know the off-design characteristics of the steam ejector to predict the part-load performance of the novel cycle. In Chapter 3, an ejector model has been developed which can be used to predict the steam ejector performance. However, this is not sufficient to reveal the novel cycle performance under part-load conditions, because this model is only suitable for predicting the ejector entrainment ratio at its designed working condition. It is difficult to predict the ejector off-design performance from a mathematical model because the flow inside the ejector becomes complicated. So, experiment remains a good way to find out the off-design performance. In this chapter, a preliminary experimental study was carried out in order to find out the ejector off design performance.

4.1 THE EXPERIMENTAL APPARATUS

The test facility is shown schematically in Figure 4.1. The apparatus consisted of five principle components: a 7 kW electrically powered steam generator assembly, an ejector assembly, a flash-evaporator, an 8 kW water cooled condenser and a 2 kW evaporator heater. A photograph of the apparatus is included in Figure 4.2.

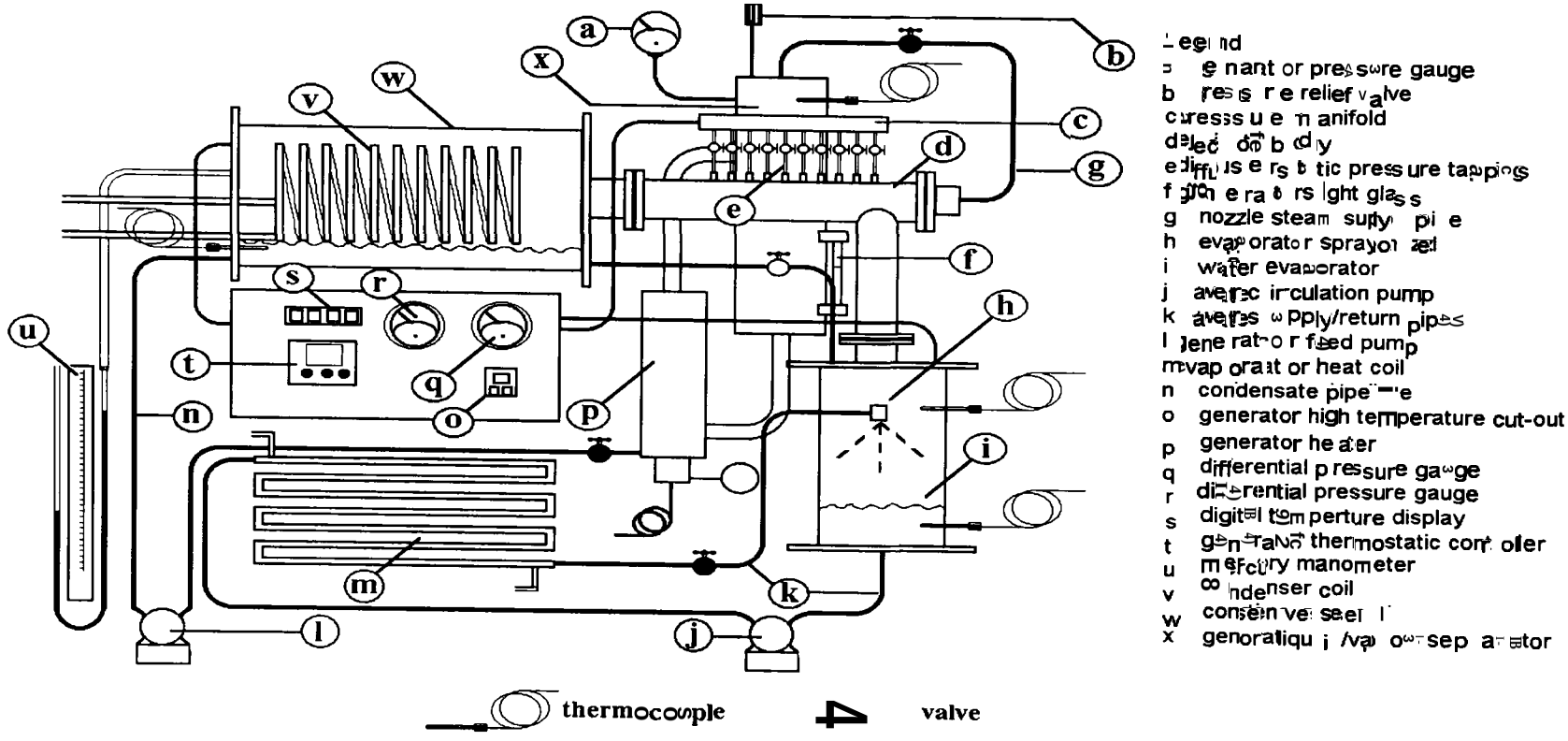

Legend
a pressure gauge
b pressure relief valve
c pressure manifold
d calorimeter body
e diffuser for static pressure tappings
f generator sight glass
g nozzle steam supply pipe
h evaporator sprayer
i water evaporator
j average circulation pump
k average supply/return pipes
l generator feed pump
m evaporator heat coil
n condensate pipework
o generator high temperature cut-out
p generator heater
q differential pressure gauge
r differential pressure gauge
s digital temperature display
t generator thermostatic controller
u mercury manometer
v condenser coil
w conservation vessel
x generator/vapour separator

Figure 4.1 Schematic diagram of the experimental rig

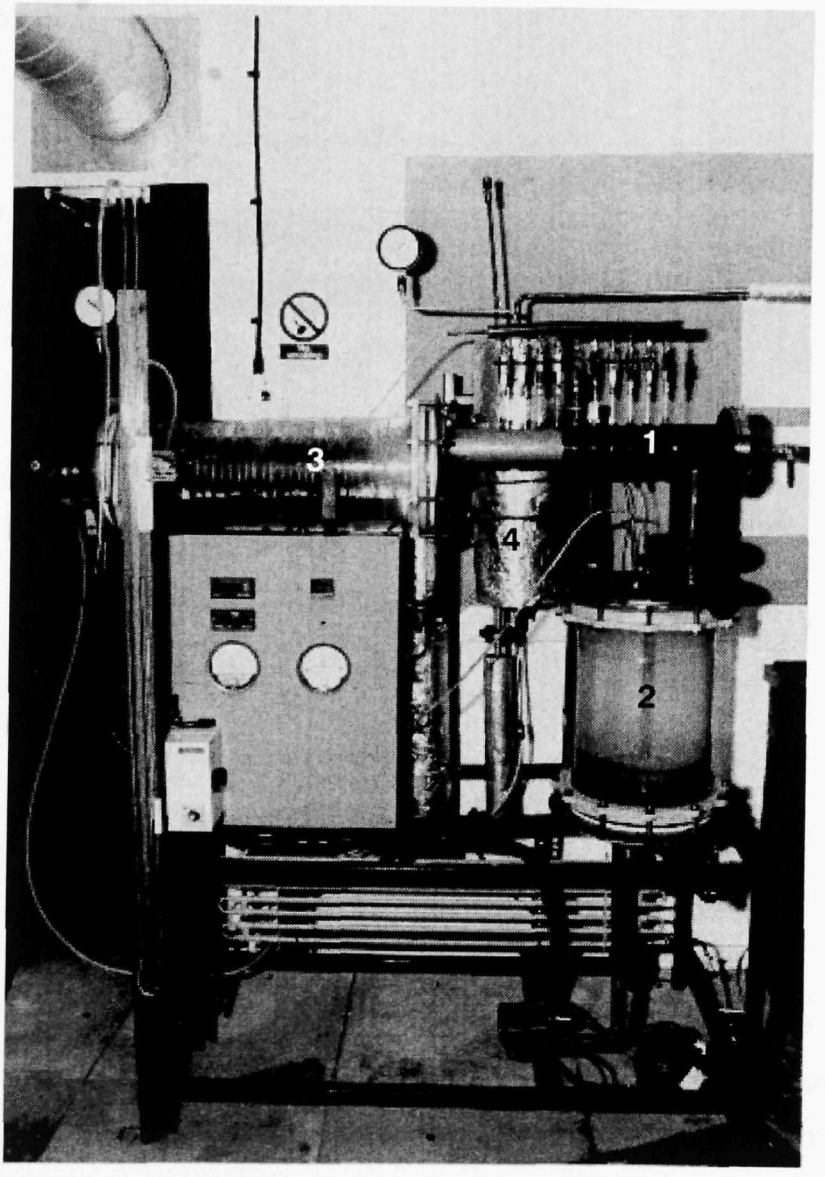

1 - Steam Ejector 2 - Evaporator

3 - Condenser 4 - Steam Boiler

Figure 4.2 Photograph of experimental rig

The ejector assembly is shown schematically in Figure 4.3. The ejector used in this study was designed using the semi-empirical method described by Eames and Aphomratana (1995 [1]). The body of the ejector was made from 80 mm O.D. stainless steel pipe fitted with flanges at both ends in order to provide a connection with the condenser and a location for the primary nozzle support

plate. An 80mm O.D. stainless steel suction manifold was welded to the ejector body and provided with a flange to connect it to the evaporator. All flange mating surfaces were sealed with 'O' ring seals to provide an airtight connection.

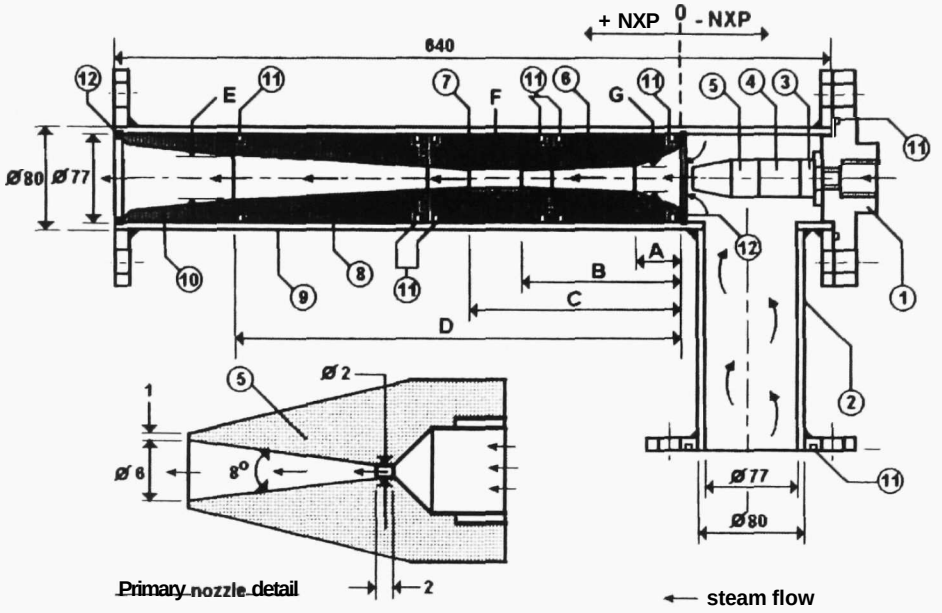

1. Nozzle support flange
2. Suction manifold
3. Nozzle connector
4. Spacer
5. Primary nozzle
6. Mixing section
7. Diffuser throat section
8. Subsonic diffuser section
9. Ejector body
10. Tall piece
11. 'O' seals
12. Fixing rings

Figure 4.3 Schematic diagram of the ejector assembly

Referring again to Figure 4.3; the primary nozzle assembly was made in three pieces: the nozzle itself, a spacer and a screwed connector to connect the assembly to the support flange. The diffuser assembly consists of a mixing section, a diffuser throat section, a subsonic diffuser section and a tail piece. These were manufactured from aluminum. Their diameters were machined in order to provide a push fit into the ejector body, and 'O' ring seals were fitted to prevent steam leaking back from the condenser, between the diffuser and ejector body and into the evaporator. Location lugs were provided to ensure good alignment between the separate pieces of the diffuser assembly.

Figure 4.3 also shows the nozzle exit position (NXP) datum used during the experiments. With reference to this: ten, equally spaced, wall static pressure

tapping were included along the length of the diffuser on 40 mm centres from NXP = 20 mm. Each tapping was connected to a pressure manifold via a short length of pipe, and an isolation valve positioned above for switching the measuring point on/off. The static pressure in the diffuser was measured by comparing its difference with the pressure in the condenser, which was measured using a mercury manometer.

4.2 THE EXPERIMENTAL APPROACH

The objectives were to investigate the part-load operation of steam-steam ejectors and to determine the significance of the primary nozzle position, the nozzle exit area and the diffuser throat area with regard to performance and operating stability.

The apparatus was operated at a steady state condition until the water level in the generator reached its safe lower limit. During this time the water levels, temperature and pressure readings around the apparatus were recorded. From these data, the entrainment ratio and the pressure lift were determined. Experiments were repeated a number of times for different ejector configurations, and the results presented here represent averaged values. The back-pressure of the ejector was adjusted by cooling water flow rate to the condenser, while the suction pressure was adjusted by hot water flow rate to the evaporator.

Experiments were carried out using three geometries of diffuser, three primary nozzle geometries and every combination of these over ranges of nozzle exit positions and evaporator, condenser and generator pressure (saturation temperature) condition.

4.3 EJECTOR PERFORMANCE CHARACTERISTICS

43.1 Entrainment ratio variation with primary stream pressure

If an ejector was designed to work at the primary pressure ratio, $N_{p,d}$ = $P_{p0,d}/P_{b,d}$, and the secondary pressure ratio, $N_{p,d}$ = $P_{b,d}/P_{s0,d}$, the ejector usually gives a maximum value of entrainment ratio, $w_d = \dot{m}_{s,d} / \dot{m}_{p,d}$, when it works at

the designed pressure ratios, $N_{p,d}$ and $N_{p,d}$. Therefore, the designed nozzle pressure ratio, $N_{n,d}$= Ppo,d/ $P_{s0,d}$, is also determined. When the primary pressure ratio N_p is increased or decreased from $N_{p,d}$ due to the change of the primary pressure, the experimental result shows that the entrainment ratio, w, will decrease, as shown in Figure 4.4. The test ejector was designed to be driven by *15* bar saturated steam (111.4°C) of primary pressure and to entrain 5°C (8.7 mbar) saturated water vapour. The entraimnent ratio reaches maximum at the designed point and falls down at each side of the designed point. This can be explained as follows. In the case of $N_n > N_{n,d}$, the primary flow at the nozzle exit is under-expanded, in other words, its static pressure would have initially been greater than that in the mixing section at the nozzle exit position, causing the flow to expand through a series of expansion waves. During this process it is believed that the secondary flow is increasingly pushed away from the emerging jet until expansion is completed, thus causing the entrainment ratio to fall with rising nozzle pressure ratio, and reducing the effective length of the mixing section. In the case of $N_n < N_{n,d}$, the flow would have been over-expanded as it left the nozzle. The flow would adjust its pressure through a series of compression waves. During this process, it is believed that the secondary flow is drawn towards the jet, thus increasing the entrainment ratio. However, it appears from the results that over-expansion has limited effect. When N_n is reduced, the momentum of the jet will fall due to the decrease of mass flow. Eventually, there is insufficient momentum in the combined flow to overcome the back-pressure at the diffuser exit, causing the entrairunent ratio to sharply fall away.

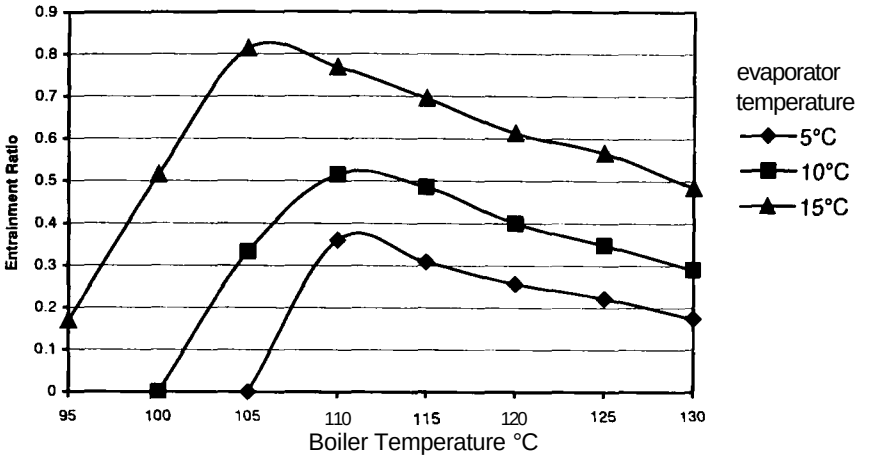

Figure 4.4 Entrainment ratio variation with primary and secondary flows

43.2 Entrainment ratio variation with the secondary stream pressure

Obviously, the entrainment ratio increases as the secondary flow pressure rises, because the higher the pressure, the more momentum is potentially possessed. However, the maximum entrainment ratio tends to appear at lower primary pressure as the secondary pressure increases from its designed pressure, as shown in Figure 4.4. In the figure, the maximum entrainment ratio moves from 1.5 bar (111.4°C) to 1.2 bar (105°C) at 8.7 mbar (5°C) and 17.04 mbar (15°C) curves respectively. The primary flow pressure for the maximum entrairunent ratio moving towards lower pressure is believed to occur as a result of self-adjusting of flows in the mixing section. In this case, the nozzle pressure ratio, N_n, for the maximum entrairunent ratio is much less than the designed nozzle pressure ratio, $N_{n,d}$, therefore, the primary flow at the nozzle exit is over-expanded, which is believed to help the mixing process of the two flows. The loss of momentum of the mixing flow due to reducing the primary pressure is compensated by increasing the secondary pressure, so that the mixing flow can overcome the back-pressure. To keep the nozzle pressure ratio at the designed value it is necessary to increase the primary pressure to 2.94 bar and its mass flow rate is therefore increased. Since the flow area of the diffuser does not increase as the flow rate does, the flow area for the secondary flow becomes smaller. So, the entrainment ratio has to fall.

4 3 3 Back-pressure influence

The back-pressure influence to the entrainment ratio of a ejector is characterized by the critical pressure which divides the entrairunent ratio into back-pressure independent and dependent regimes. When the back-pressure is lower than the critical pressure, the entrainment ratio is independent of the back-pressure. Otherwise, it is dependent on the back-pressure. Figure *45* shows the experimental result of a steam ejector with regard to the back-pressure influence on the entrairunent ratio. In the back-pressure dependent regime, the entrainment ratio is sensitive to the change of back-pressure. Any small increase of the back-pressure causes a large fall in the entraimnent ratio. Therefore, letting the ejector work in this regime should be avoided. Figure *45* also shows the primary pressure ratio, Np, at the critical pressure points. The value of N_p at the critical points varies between 56.7 and 59.2 except the point of 64.1 on the curve for 115°C, which is abnormal due to missing the critical point in the test. That the primary pressure ratios, Np, are so close each other suggests the increase of the critical back-pressure is linearly proportional to the increase of the primary pressure, if the difficulty to catch up the critical condition is taken into account.

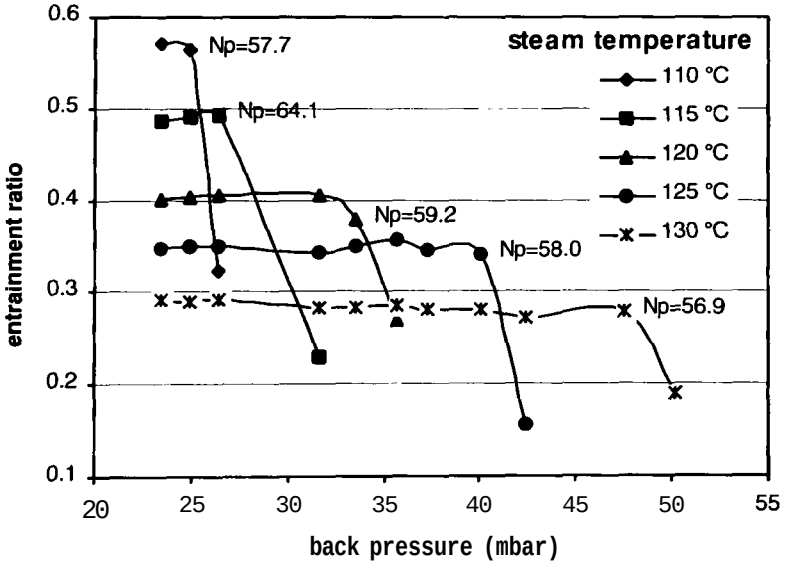

Figure 4.5 Entrairunent ratio variation with back-pressure and primary pressure

43.4 The geometric factors that affect the entrainment ratio

In addition to the operation conditions affecting ejector performance, the intemal geometric factors also have an influence. These are the nozzle outlet area, the nozzle exit position and the diffuser throat area. These effects are discussed here based on our experimental results.

Nozzle outlet area effect

The Mach number of a supersonic nozzle at outlet is determined by its area ratio of the throat and the outlet. The exit area of the nozzle is critically determined by the pressure, N_n, so that the static pressure in the flow equals that in the mixing section. If the exit area is manufactured to be less than the critical value, then the flow will be under-expanded on leaving the nozzle, and the entrainment ratio will be reduced for the same reasons for the increase of the primary pressure. Conversely, if the nozzle is manufactured with an oversized exit area then the flow would be over-expanded and the entraimnent ratio would be reduced also. This is shown as Figure 4.6 from the experimental data. The nozzle geometry for this experiment is described in Table 4.1. No. 1 nozzle with 8mm-exit diameter was the originally designed while No. 2 was purposely manufactured with over-sized exit area. It is shown that the entrairmient ratio with No. 2 nozzle is lower than that with No. 1 over the test range.

Table 4.1 Test Nozzle Geometry

Nozzle Number	Throat Diameter	Exit Diameter	Area Ratio
1	2 mm	8nun	16
2	2 mm	12 mm	36

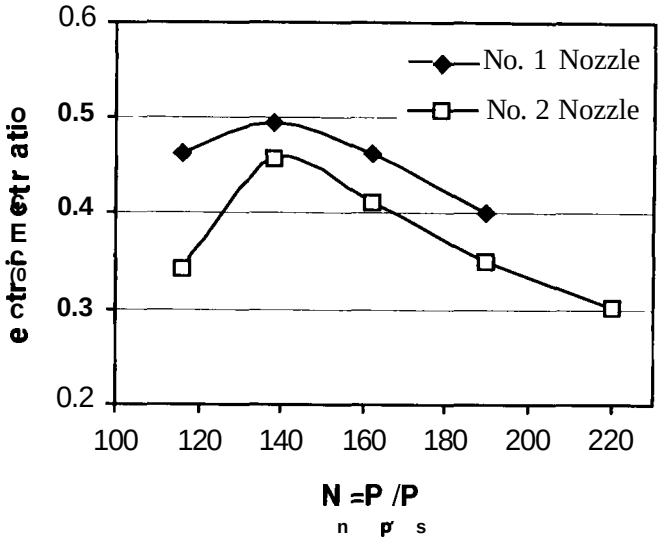

Figure 4.6 Measured variation in entrairunent ratio with nozzle pressure ratio for different nozzle exit/throat area ratio

Effects of nozzle exit position, (NXP)

NXP is defined here as the distance from the exit plane of the primary nozzle to the entry plane of the second conical part of the mixing chamber, as defined in Figure 4.3. Experimental results indicate that the primary nozzle position, NXP, does affect the secondary pressure ratio, N_s. The optimum NXP value, which gives the greatest secondary pressure ratio, N_s, moves towards the diffuser throat as N_p increases, as shown in Figure 4.7. It was also found that the critical pressure could be increased by increasing the ratio of the nozzle position distance to the diffuser throat diameter, NXP/D. Furthermore, if the primary and secondary pressures were maintained, entrairunent ratio was found to be maximum at the optimum NXP/D position.

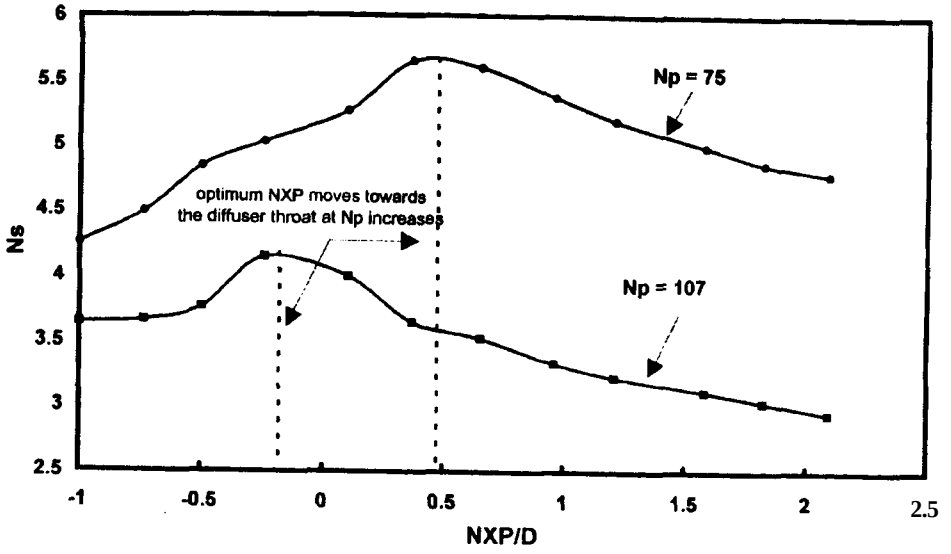

Figure 4.7 Measured variation in optimum nozzle exit position with secondary pressure ratio

Effects of diffuser throat area

The effects of diffuser throat area are shown as in Figure 4.8 and 4.9 from the experiment results. For a constant diffuser throat area ratio, the critical secondary pressure ratio increases with the primary pressure. However, for a constant nozzle pressure ratio, Nn=Pg/Pe, increasing diffuser throat area ratio results in a falling of critical secondary pressure ratio, see Figure 4.8, while the entrainment ratio increases as the diffuser area ratio increases, as shown in Figure 4.9 (Eames 1998). The geometries of the diffusers for the test are shown in Table 4.2.

Table 4.2 Geometries of 3 test diffusers, mm (referring to Figure 4.3)

A	B	C	D	E	F	G
36	98.5	130.9	495.4	52.5	14	17.8
40.6	139.8	176.6	518.1	533	18	24.1
53.8	183.8	219.6	493.6	50.7	22	29.9

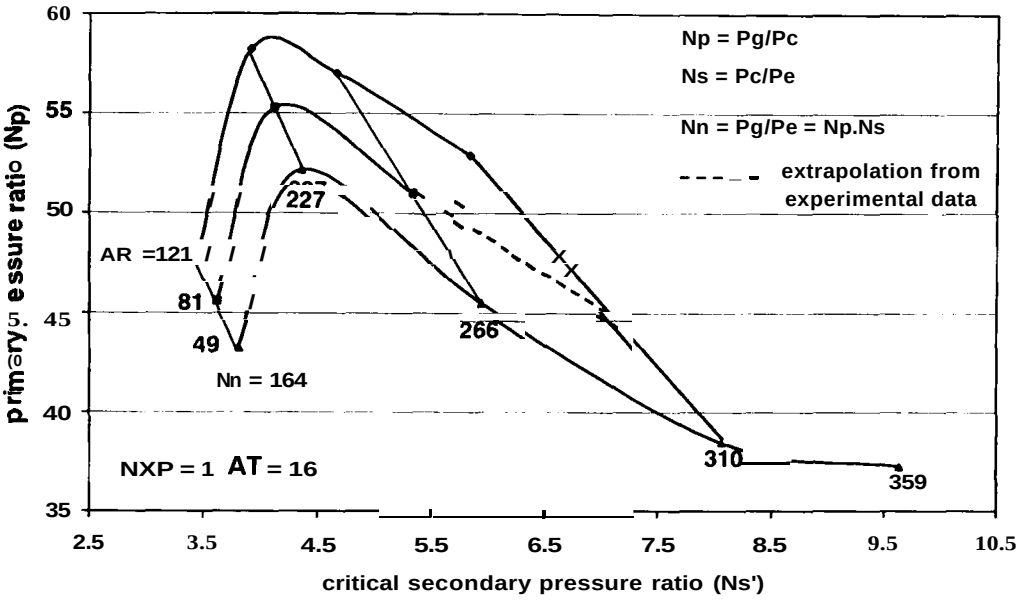

Figure 4.8 Measured effect of primary pressure ratio, diffuser throat area and nozzle pressure ratio on critical condenser pressure

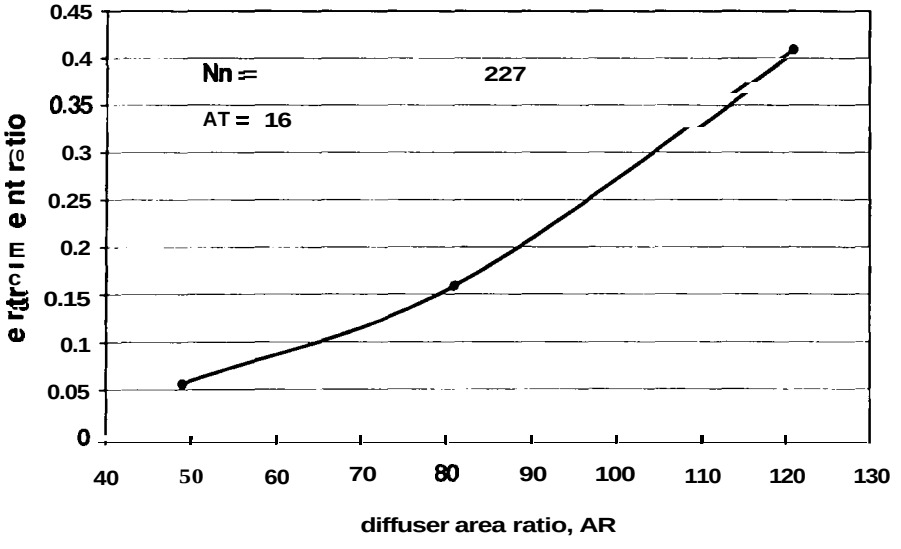

Figure 4.9 Measured variation in entrainment ratio with diffuser throat area ratio

4.4 EFFICIENT USE OF EJECTORS

From the above discussions, the following points should be emphasized regarding the application of a steam ejector in the ejector re-compression absorption cycle:

a. The entrainment ratio of an ejector is reversibly proportional to its secondary pressure ratio which is determined by the operation conditions of the concentration process of the refrigeration cycle. Therefore, the effects on the entrainment ratio must be taken into account when choosing the operation conditions of the concentration process in order to achieve best energy efficiency;

b. The closer to the critical back-pressure, the higher the efficiency from an ejector. However, this is not a stable working condition and the ejector is prone to loss of function under this working condition. It is necessary to leave enough room to allow for unexpected intenuption;

c. The ejector should be operated at design condition as far as possible.

CHAPTER 5
MANUFACTURE OF A REFRIGERATOR BASED ON THE NOVEL REFRIGERATION CYCLE

A proof-of-concept experimental refrigerator was designed and manufactured to test the novel cycle. In layout the machine was similar to a conventional single-effect lithium bromide-water absorption refrigerator except that there was an ejector working within the concentrator. The experimental refrigerator was based on the novel cycle and consisted of six major components plus pumps and valves. The major components included: a steam generator, a concentrator, an absorber, a steam ejector, an evaporator and a condenser. Figure 5.1 shows a schematic diagram of the experimental refrigerator. The photo of the experimental rig is shown in Figure 5.2.

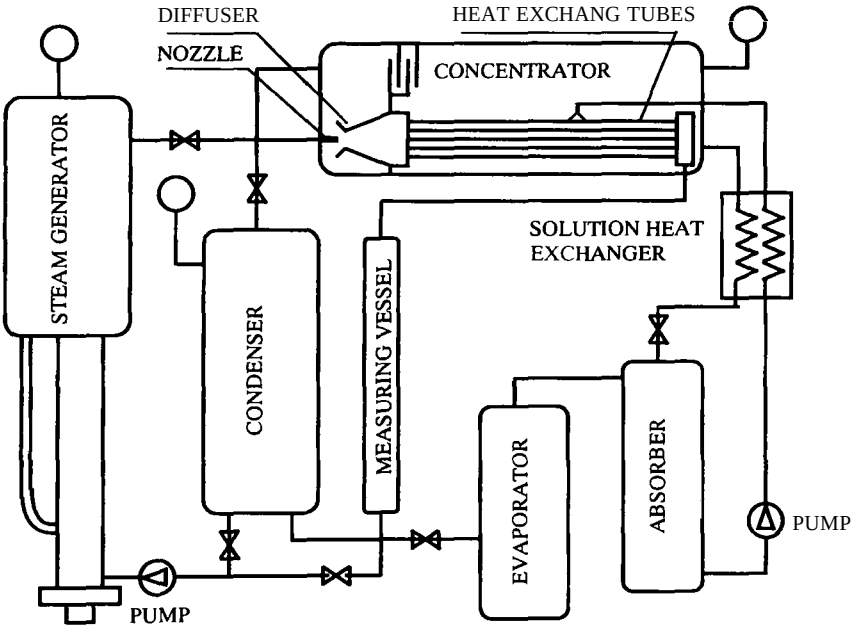

Figure 5.1 Schematic diagram of the experimental rig

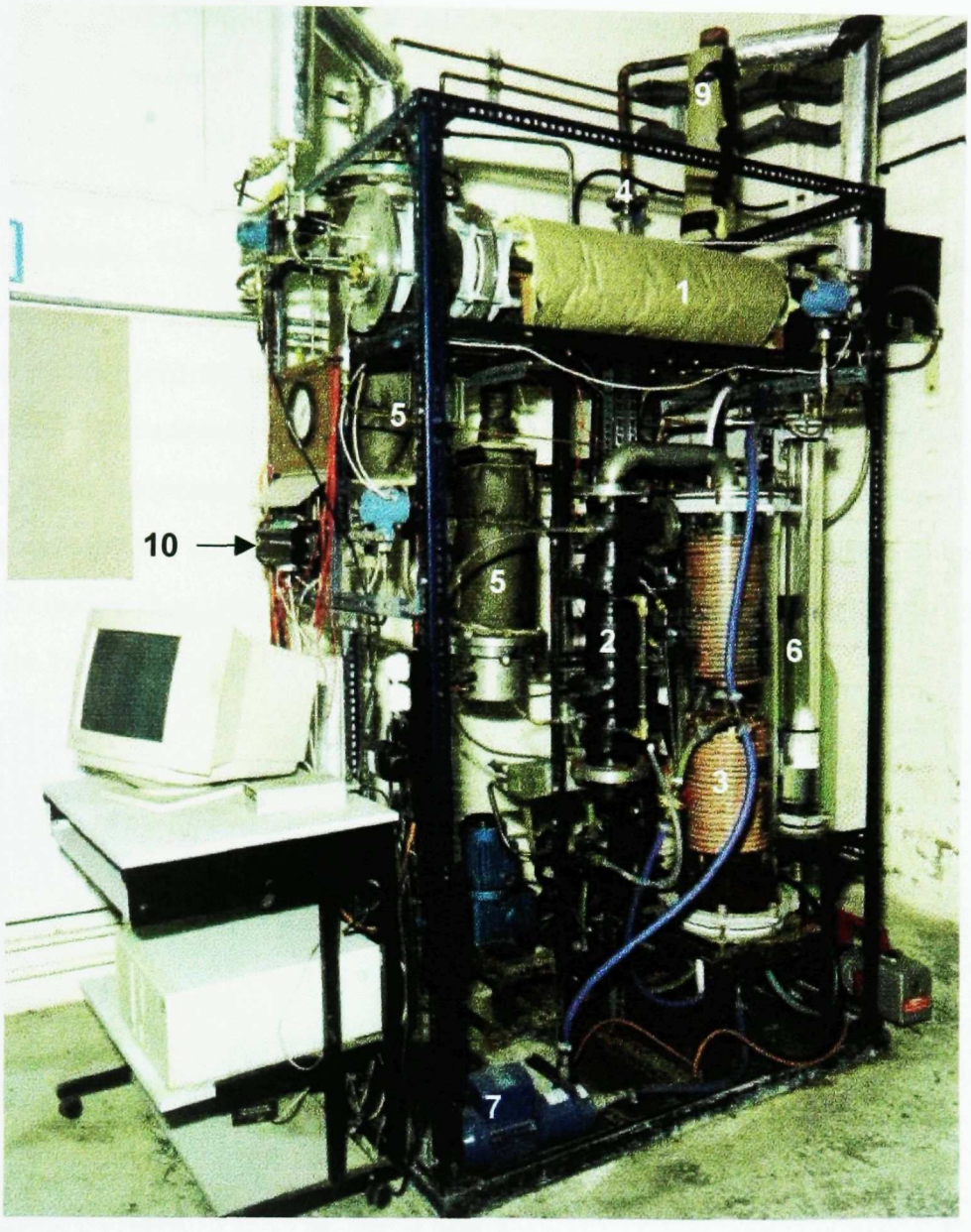

1 - Concentrator 2 - Evaporator 3 - Absorber 4 - Condenser

5 - Steam Generator 6 - Measuring Vessel 7 - Pump 8 - Pump

9 - Baffle 10 - Data Logger

Figure 5.2 Photograph of the experimental rig

5.1 THE STEAM GENERATOR

A 10 kW (max), electrically powered, steam generator was designed and manufactured. It consisted of the water boiler and the steam tank or knock-out

vessel, shown in Figure 5.3. A three-phase electrical heat element was fitted to the water boiler together with a thermostat to protect the heat element from damage by overheating. The steam tank or knock-out vessel was located above the water boiler. Baffle plates positioned inside the knock-out vessel prevented water droplets from entering the steam ejector which could reduce its performance. The water boiler and knock-out vessel were connected by pipe work. The lower liquid retum pipe was coiled to allow for thermal expansion. The steam generator was made of stainless steel and rated at 15 bar operating pressure. Thermocouples and a pressure transmitter were installed to measure the steam temperature and pressure at the knock-out vessel. Steam pressure was chosen as a control parameter because it was found to give better control performance than temperature. A safety pressure relief valve fitted on the top of the knock-out vessel.

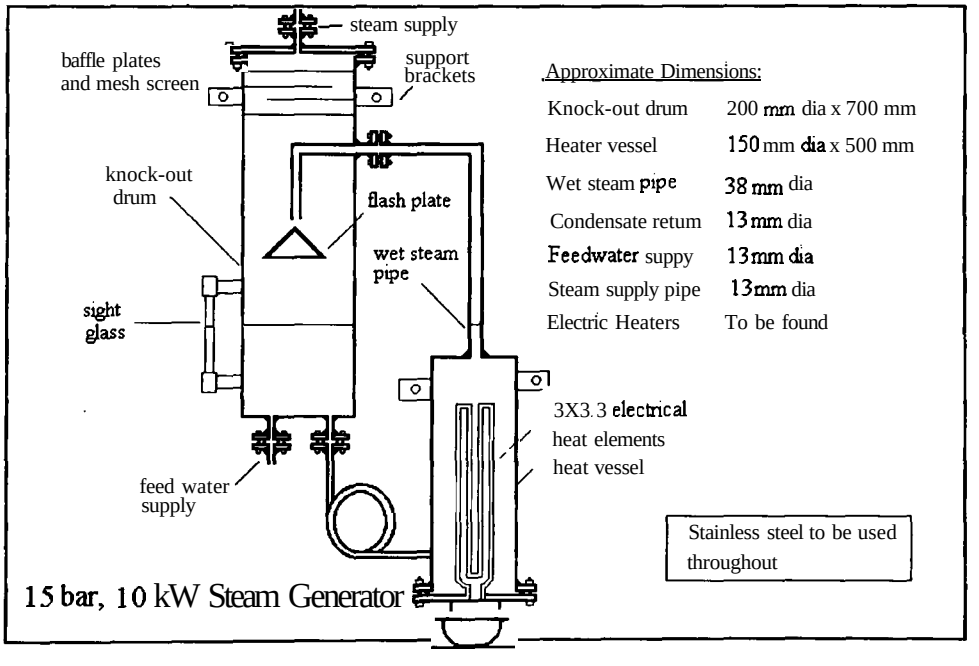

Figure 5.3 Diagram of the steam generator

5,2 THE CONCENTRATOR

The construction of the concentrator is shown in Figure 5.4. The concentrator consisted of two parts; the steam ejector and the concentrator proper. The ejector assembly was made of stainless steel to avoid problems of corrosion.

The motive flow for the ejector was designed for 5 kW of saturated steam at 15 bar, 198 °C. The relative position between the primary nozzle and diffuser was made adjustable in order to optimise their relative positions. The ejector was housed in a 150mm diameter glass pipe. One end of the pipe was sealed using a stainless steel plate and a proprietary flange while the other end was connected to the concentrator housing, which consisted of a 150mm diameter QVF glass pipe. Figure 5.5 shows the construction of the steam ejector.

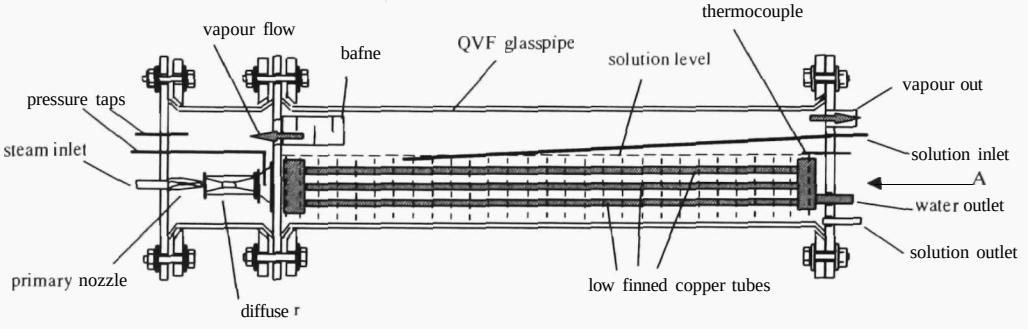

Figure 5.4 Schematic structure of the concentrator

The flow geometry of the ejector was determined from a computer model based on one-dimensional fluid analysis and experimental works which were discussed and described in Chapter 3 and Chapter 4. The ejector working condition was set as follows: The primary flow at 198.3°C, secondary flow at 33°C and back-pressure at 0.6 bar. Its flow geometric sizes are listed in Table 5.1.

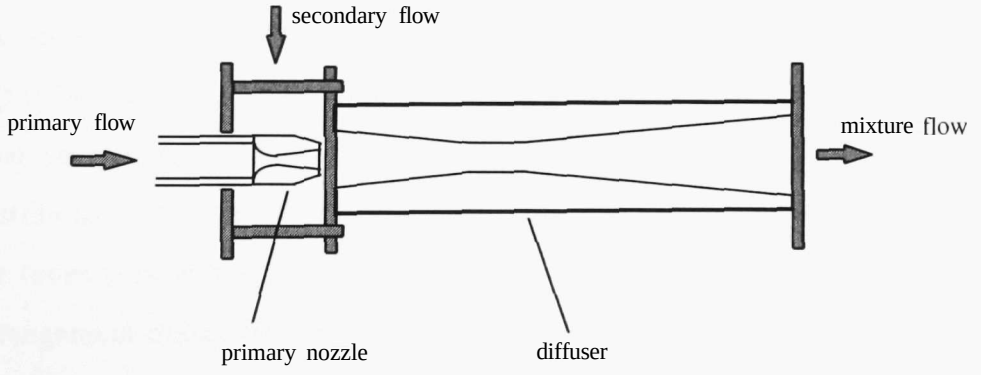

Figure 5.5 Diagram of the steam ejector

Table 5.1 Flow geometric sizes of the ejector

Primary Nozzle	
Throat diameter (mm)	1.23
Exit diameter (mm)	5.12
Constant Pressure Mixing Chamber	
Inlet diameter (mm)	11.98
Exit diameter (mm)	9.26
Length (mm)	15.60
Constant Area Mixing Chamber	
Diameter (mm)	9.26
Area ratio	57.14
Diffuser	
Inlet diameter (mm)	9.26
Exit diameter (mm)	22.69
Length (mm)	96.24

The concentrator heat exchanger was made from low firmed copper tubing. Sixteen copper tubes were used for the tube bank which had a semi-circular shape when viewed from the right in Figure 5.4. From a heat exchange point of view, the tubes were arranged in parallel to the steam flow from the ejector, and connected to manifolds at both ends. The left-hand end (in Figure 5.4) was connected to the diffuser of the steam ejector and right-hand end to a vessel for measuring the condensation water. The numbers of heat exchanger tubes, from top to bottom, were in descending order, 6,5,4,1. This meant that most of the heat energy, carried by high-pressure steam coming from the ejector, was distributed to the top surface of the solution in the vessel. The arrangement of the tubes is shown in Figure 5.6 and the fin size is shown in Figure 5.7. This arrangement makes the vapour easier to evolve, as the density gradient in the solution encourages circulation. A photograph of the steam ejector and the heat exchanger of the concentrator are shown in Figure 5.8 and 5.9.

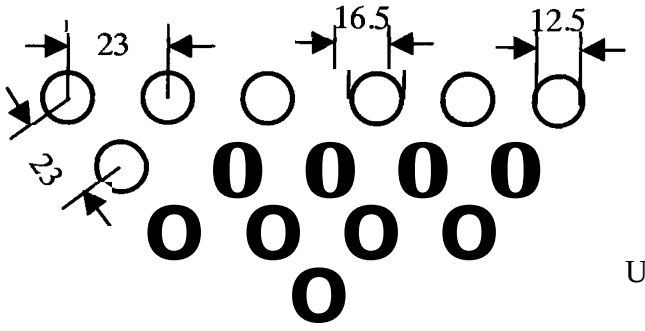

Unit: mm

Figure 5.6 View of concentrator heat exchanger tube arrangement from 'A' direction in Figure 5.4

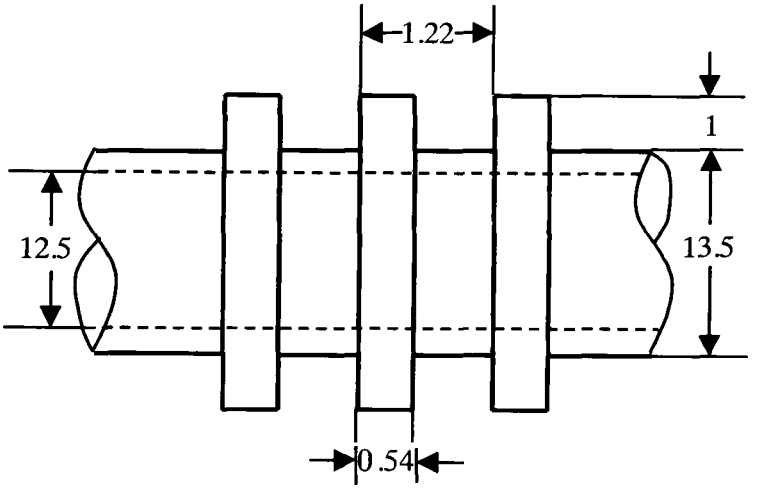

Unit: mm

Figure 5.7 Fin dimension of the copper tube

The solution enters the concentrator at the top and flows back to absorber from the bottom. This causes a flow along and over the copper tubes, which improves the heat transfer coefficient at its surface and avoids weak solution short-cutting to the absorber. There are two exits for the vapour evolved. One is through the baffle on left side of the vessel to the ejector housing and the other is through an outlet on the right side of the condenser. The amount of the flow to either side is determined by the suction ability of the ejector and the condensing pressure. Two pressure tappings are cormected to the pressure meters. One is used to measure the back-pressure of the steam ejector while the other is to measure the vapour pressure of the solution in the concentrator vessel. A thermocouple was fitted on the right side of the concentrator vessel

to measure solution temperature. Solution concentration was determined from its vapour pressure and solution temperature.

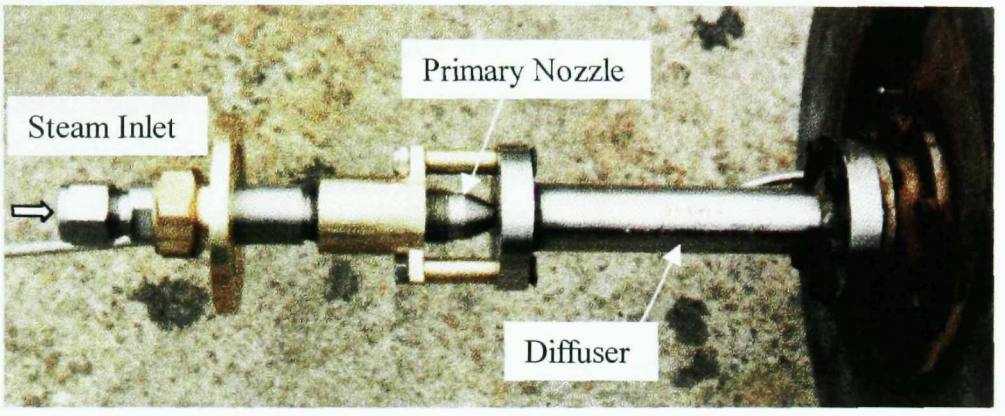

Figure 5.8 Photograph of the steam ejector

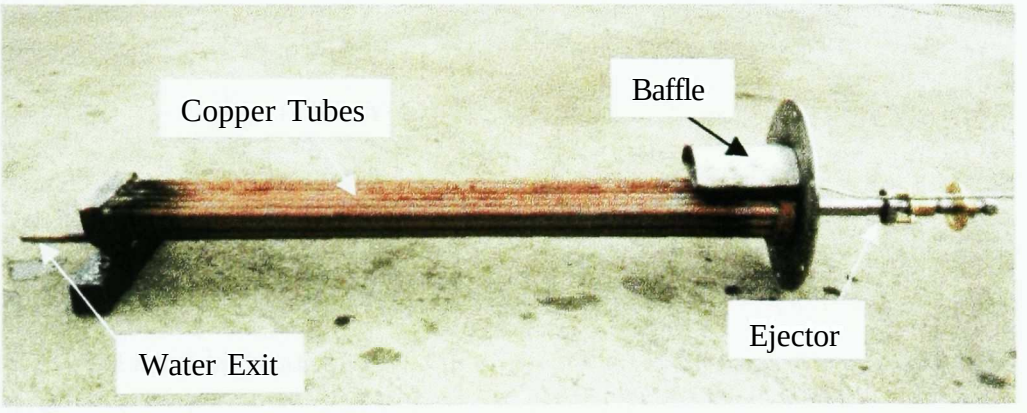

Figure 5.9 Photograph of the heat exchanger of the concentrator

5.2.1 Concentrator heat transfer design calculation

Adrian Bejan (1993) indicates that when,

$$\mathrm{Re} = \frac{\rho_v U_v D}{\mu_v} < 3.5\times10^{4} \qquad (5.1)$$

for a condensable vapour flowing through a horizontal tube, then the condensation process is dominated by natural convection, and the mean heat transfer coefficient, $\bar{h}$, is given by

$$\frac{\bar{h}D}{k_l} = 0.555\left[\frac{D^3 h_{fg} g(\rho_l - \rho_v)}{k_l v_l (T_{sat} - T_w)}\right]^{1/4} \qquad (5.2)$$

This equation was used to calculate the required heat transfer area for condensation. The saturation temperature inside the tubes was assumed to be at 80°C and the inside-diameter of the tube was set at 12.5mm. Substituting the properties of the steam at $80℃$ into Equation (5.2), i.e.

$k_l = 666\times10^{-6}\ \text{kW}\cdot(\text{m}\cdot\text{K})^{-1}$ $\quad D = 0.0125$ mm

$g = 9.8\ \text{m}\cdot\text{s}^{-2}$ $\quad v_l = 0.38\times10^{-6}\ \text{m}^2\cdot\text{s}^{-1}$

$h_{fg} = 2320.8\ \text{kJ}\cdot\text{kg}^{-1}$ $\quad \rho_l = 974.42\ \text{kg}\cdot\text{m}^{-3}$

The heat transfer coefficient for the condensation inside the heat exchanger tubes at different $T_{sat} - T_w$ are:

$\bar{h} = 2.22\ \text{kW}\cdot\text{m}^{-2}\cdot\text{K}^{-1}$, when $T_{sat} - T_w = 2\,°\text{C}$

$\bar{h} = 2.00\ \text{kW}\cdot\text{m}^{-2}\cdot\text{K}^{-1}$, when $T_{sat} - T_w = 3\,°\text{C}$

$\bar{h} = 1.76\ \text{kW}\cdot\text{m}^{-2}\cdot\text{K}^{-1}$, when $T_{sat} - T_w = 5\,°\text{C}$

Therefore, for the condensation capacity of 5kW at $T_{sat} - T_w = 5°\text{C}$, 0567m; of heat transfer area was required. The inside diameter and length of the tubes used for the heat transfer were 12.5mm and 950mm, respectively. Sixteen tubes were used in parallel for the heat exchanger. The total cross-section area for the steam flow was $1.963\text{x}10^{-3}\ \text{m}^2$. For 5kW steam condensation in the tubes, the Reynolds number of the vapour flow inside the tubes was 12,816. This satisfied the requirement expressed by Equation (5.1) for using Equation (5.2) to calculate heat transfer coefficient. The total surface areas inside tubes for heat transfer was 0.5966 m^2, which was greater than the required heat transfer area by 5.2%. The required heat transfer area was met.

Outside the tubes, heat transfer was assumed to be boiling LiBr-water solution at 59% concentration by mass at 75°C. Referring to Figure 5.4, the heat exchanger tubes were immersed in the shallow lithium bromide solution which acted as heating element. Therefore, this was a typical pool boiling case whose heat transfer coefficient varied from the boiling types. The boiling type could

be determined from the excess temperature (T_w-T_{sat}), (°C). Since the condenser temperature was set at 30°C and the concentration of the solution in the concentrator was 59%, the solution temperature should be at least 70°C for the cycle operation. The wall temperature of the tube had been determined at 75°C in the previous calculation. So, the maximum excess temperature was 5°C. The possible boiling type for this excess temperature was nucleate boiling (Bejan 1993). For nucleate boiling heat transfer lithium bromide solution on a low firmed tube, Hou et al (1992) suggested the following correlation,

$$\overline{Nu} = 0.16\left(\frac{1+2l_3/l_1}{1+l_1/l_2}\right)^{0.275}\cdot\left(\frac{\dot{q}\cdot d}{\mu_l h_{fg}}\right)^{0.8588}\cdot\left(\frac{\rho_v}{\rho_l}\right)^{-0.7108}$$
$$\cdot\left(\frac{\dot{q}^2\cdot d}{\sigma_l\sigma_v h_{fg}^2}\right)^{-02104}\cdot \mathrm{Pr}^{0.2173}\left(\frac{P}{P_a}\right)^{03483}\cdot e^{-7.836\times10^{-2}x} \qquad (5.3)$$

where, l_1 channel width of the fin, mm

l_2 the fin width, mm

d inside diameter of the tube, mm

l_3 the fin height, mm.

This correlation was used to determine the coefficient of the heat transfer. The properties of the lithium bromide solution and other data used in this calculation are listed as follow,

Solution properties:

$h_{fg} = 2461.7\ \mathrm{kJ\cdot kg^{-1}}$ $\sigma_l = 0.0799\ \mathrm{N\cdot m^{-1}}$

$\rho_v = 0.0318\ \mathrm{kg\cdot m^{-3}}$ $\rho_l = 1669.6\ \mathrm{kg\cdot m^{-3}}$

$\mathrm{Pr} = 11.835$ $\mu_l = 2.83\times10^{-3}\ \mathrm{N\cdot s\cdot m^{-2}}$

$k_l = 445.2\times10^{-3}\ \mathrm{W\cdot(m\cdot K)^{-1}}$

Finned tube sizes and area:

$l_1 = 0.68\mathrm{mm}$ $l_2 = 0.54\mathrm{mm}$ $d = 13.5\mathrm{mm}$

$l_3 = 1\mathrm{mm}$ $L = 0.95\mathrm{m}$ $A = 1.71\mathrm{m^2}$

working condition:

$P = 42\ \mathrm{mbar}$ $P_a = 1\mathrm{bar}$ $x = 0.59$

$\dot{q} = 3.44\ \mathrm{kW\cdot m^{-2}}$

The calculated Nusselt number was 35.09 and the coefficient of the heat transfer can be obtained from Equation (5.4).

$$\bar{h} = \frac{Nu \cdot k_l}{D} \tag{5.4}$$

The excess temperature can be calculated from following Equation (5.5).

$$\Delta T = \frac{\dot{q}}{\bar{h}} \tag{5.5}$$

From Equation (5.4) and (5.5), the coefficient of boiling heat transfer was 1.157 $kW \cdot m^{-2} K^{-1}$ and the excess temperature was $2.97°C$. In other words, it was sufficient to meet the heat transfer requirement if there was the excess temperature of $3°C$ between the tube wall and solution. This was less than the maximum excess temperature allowed. So, the heat transfer requirement was satisfied.

The overall heat transfer coefficient between the steam and solution could be calculated from Equation (5.6),

$$\frac{1}{U} = \frac{1}{h_o} + \frac{t}{k} + \frac{1}{h_i} \tag{5.6}$$

where, t is the wall thickness of the tubes.

5.3 THE ABSORBER

A falling film absorber was manufactured, because this type has a low pressure drop and simplicity of construction, as shown in Figure 5.10. The outside vessel was made from a 225mm diameter glass pipe fitted with two stainless steel end-disks to provide sealing at the two ends. Solution distributors were fitted above the coils. The distributors consisted of two copper rings with diameters of the copper coils. In order to distribute the solution evenly to the surfaces of the heat exchange coils, flow guiders were employed to direct the flow from the holes in the rings onto the surface of each coil. The total surface area of the coils was 2.393 m^2. A temperature sensor was placed at the bottom of the vessel and a pressure transmitter at the top. A pump was used for the circulation and distribution of the solution in the absorber.

Absorption is a combined mass transfer with the heat transfer process. So, the coefficients of mass and heat transfers should be considered in the design of the absorber. For falling film mass transfer, the average coefficient of mass transfer can be determined by the following Equations (5.7) and (5.8) (Treybal 1986). Equation (5.7) is for small flow rate or long times contact of contact of the liquid with the gas (usually for film Reynolds numbers less than 100) while Equation (5.8) is for for a larger Reynolds numbers or short contact time,

$$k_{L,av} = 3.41\frac{D_{AB}}{5} \tag{5.7}$$

$$k_{L,av} = \left(\frac{6D_{AB}\Gamma}{\pi\rho\delta L}\right)^{1/2} \tag{5.8}$$

where $k_{L,av}$ average mass transfer coefficient $(m \cdot s^{-1})$

D_{AB} molecular diffusivity $(m^2 \cdot s^{-1})$

8 film thickness (m)

Γ mass flow rate per unit width $(kg \cdot (s \cdot m)^{-1})$

L length of wetted wall (m)

Thus the average mole flux for the entire gas-liquid surface per unit width can be calculated from the following equation,

$$N_{A,av} = k_{L,av}\frac{c_{A,L} - c_{A,0}}{\ln\left[\left(c_{A,i} - c_{A,0}\right)/\left(c_{A,i} - c_{A,L}\right)\right]} \tag{5.9}$$

where $N_{A,av}$ average mole flux $(kmole \cdot (s \cdot m)^{-1})$

$c_{A,i}$ LiBr concentration at liquid-vapour interface $(kmole\ m^3)$

$c_{A,0}$ concentration at the beginning of the wall $(kmole \cdot m^3)$

$c_{A,L}$ concentration at the end of the wall $(kmole \cdot m^3)$

Cooling water flows through inside of the tube coils to carry away the heat created by the absorption process. The heat transfer for this side of the coils is fairly straightforward. The Nusselt number is determined by using the following correlation for turbulent flow in a coil (Rohsenow 1985),

$$\overline{Nu} = 0.023\,\mathrm{Re}^{0.85}\left(\frac{r_i}{R}\right)^{0.1}\mathrm{Pr}^{0.4} \qquad (5.10)$$

where, r_i is the inside radius of the tube and R is radius of the coil.

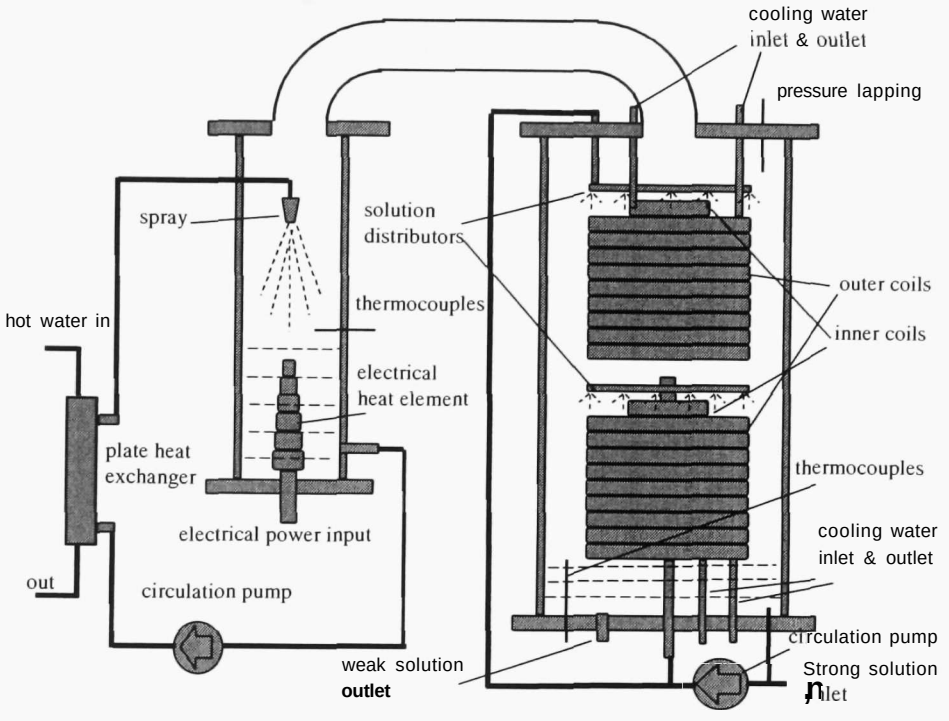

Figure 5.10 The absorber and evaporator system

5.4 THE EVAPORATOR

A flash-type evaporator design was manufactured. The evaporator vessel was made from a 76.2mm diameter (ID) stainless steel tube as shown in Figure 5.10. A 3kW electrical heat element was fitted at the bottom to provide a cooling load. Further cooling load was provided via hot water supplied from an electrical immersion heat tank through a plate heat exchanger shown in Figure 5.10. A spray nozzle positioned on the top of the evaporator nozzle was used to create large surfaces to assist the refrigerant to vaporize. A sight-glass was fitted on the evaporator vessel to observe and measure the water level change inside the evaporator. The evaporation rate, and thus cooling capacity, was measured from the water-level changes in the evaporator vessel. Thermocouples were positioned at the mid-height position in the centre of the

vessel. The temperature signal was fed to a data logger and was used to control the electrical heating element to maintain the evaporator temperature at a pre-set value. The hot water supply to the plate heat exchanger was turned on only when the cooling capacity was more than the heat provided by the electrical heating element alone.

5.5 THE CONDENSER

A shell and coil type condenser was manufactured. The heat exchange coil was made from 13.5mm OD soft copper tubing. This was formed into two diameter coils of 12 cm and 9 cm fitted concentrically within the vessel. For film condensation on a copper tubing wound coil vertically positioned, the coefficient of heat transfer can be determined with following correlation (Lienhard, 1987):

$$\overline{Nu} = \frac{\bar{h} d \cos\alpha}{k} = \left[\frac{(\rho_f - \rho_g)\rho_f h_{fg} g (d\cos\alpha)^3}{\mu k \Delta T}\right]^{1/4} f\left(\frac{d}{D}, B\right) \quad (5.11)$$

where B is a centripetal parameter:

$$B \equiv \frac{\rho_f - \rho_g}{\rho_f} \frac{c_p \Delta T}{h_{fg}} \frac{\tan^2\alpha}{\mathrm{Pr}} \quad (5.12)$$

and a is the helix angle. The function of the tube-to-helix diameter ratio, d/D, and B can be evaluated numerically. The helix angle α of the coil used in the absorber is so small that the centripetal parameter B can be considered as zero. For d/D = 133/120 = 0.113 and 13.5/90 = *0.15, f(d/D,0)* equals 0.728 and 0.726, respectively according to Karimi's work (1977). An average value was used for Equation (5.13). Therefore, the external heat transfer coefficient was given by:

$$\bar{h} = 0.727\left[\frac{(\rho_f - \rho_g)\rho_f h_{fg} g k^3}{d\mu\Delta T}\right]^{1/4} \quad (5.13)$$

The heat transfer inside coils is similar to that in the absorber, and can be determined from Equation (5.10). The copper coils have a $1.1\mathrm{m}^2$ total surface area. The overall heat transfer coefficient was calculated to be around 2500 $\mathrm{W\bullet(m^2\bullet K)^{-1}}$. The shell was constructed from a Schedule 10s, 152.4mm bore

pipe, 80cm in length. A level indicator (sight-glass) was fitted to enable the condensation rate to be measured.

5.6 THE MEASUREMENT AND CONTROL SYSTEM

Type 'K' thermocouples were used throughout for temperature measurement. The temperatures were collected by a data logger and displayed on the computer screen. Three Rosemount absolute pressure transmitters, Model 2088, calibrated for the ranges from 0 to 1 PSI and 0 to 20 bar respectively, were used to measure the vapour pressures in the absorber, concentrator and steam generator vessels. The pressure transmitter used to measure the concentrator was also used to measure the condenser pressure by switching a valve between them. These signals were also fed to the data logger and the steam pressure was fed back to control the steam generator heaters. A pressure gauge was used to monitor the back-pressure of the steam ejector which was displayed on the meter. The circulation flow of the solution was measured with a rotor meter, calibrated for lithium bromide solution from 0 to 2.8 $L \cdot min^{-1}$ @ 40 °C. The heat power input to the steam generator and the evaporator were calculated from measured voltages and the currents inputs to the heating elements. All the data was collected by a Data Electronics data logger DT505. Figure 5.11 shows the diagram of the measuring and controlling system used in the rig. All the measurement points are listed in the diagram except two meters without signal out to the data logger. They were the flow meter and a pressure gauge for measuring the back-pressure of the steam ejector.

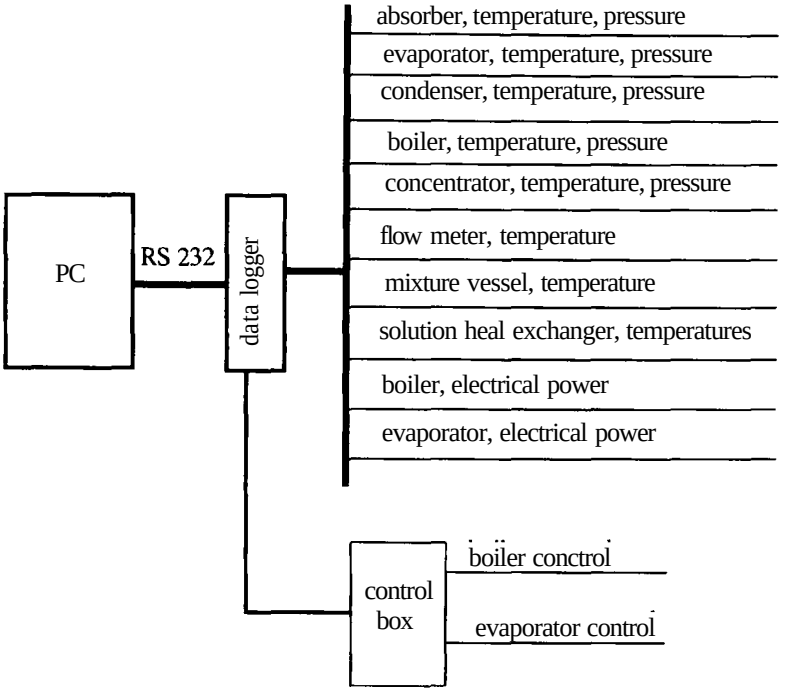

Figure 5.11 Diagram of the measuring and controlling system

5.7 COMMISSION OF THE EXPERIMENTAL RIG

Following the construction, the rig was pressurized with compressed air to 1 bar gauge for the leakage test. Since this was an experimental rig which needed to be modified late, many removable joints and gaskets and fitting were used. Thus perfect leak tightness was impossible. After the leakage test, the system had a leaking rate below 1 mbar per hour when the system was vacuumed down to 20 mbar. This would cause the air accumulation in the system over the period of experiment, which could deteriorate the cycle performance. A vacuum pump was used to evacuate air and all non-condensable gases from the system before starting an experiment and during the operation if it was necessary.

The condenser, the evaporator and the measuring vessels would be used to measure the flow rates in experiments. Their height-to-volume relationships were calibrated before the rig was used. A measuring cup was used to measure the volume of water filling into the vessels during the calibrations. The height of the water level corresponding to the volume of water filled was recorded and the water temperature was measured. These data were correlated into

formulas for calculating the flow rate from the level change. The volume - height relationships for the three vessels were listed in Appendix B.

The primary flow rate of the ejector was also measured in the commission stage in order to use it as power input to the cycle. Two primary nozzles were used: one with the throat diameter of 1.0mm, another with 1.1mm. Each primary nozzle was fitted to a same diffuser in tum to comprise an ejector. The ejector was tested under primary pressures of 10 bar, 12.5 bar and 15 bar. The measurement was carried out as follows: (a) blocking the secondary flow passage of the ejector, (b) opening the steam valve to the primary nozzle when the generator pressure reached to the set point, (c) adjusting back-pressures to operate the ejector in the choke condition, (d) taking reading of level change from the measuring vessel in a fixed time interval when the ejector was in stable operation. The measurement was repeated several times and an average value was used for the primary flow rate.

CHAPTER 6
EXPERIMENTAL STUDIES ON THE REFRIGERATOR

In this chapter, the experimental study of the novel cycle was discussed. The aim of this study was to investigate the operation characteristics of the novel absorption refrigerator and the energy efficiency.

6.1 EXPERIMENTAL METHOD

The experimental rig has been described in Chapter 5. As was indicated in Chapter 5 it was necessary to evacuate the system every time before the experiment. A vacuum pump was used to evacuate the system until the evaporator temperature started to fall. Once the system was evacuated, the steam generator was switched on. When the steam pressure reached 2 bar, steam was discharged to the atmosphere for 5 minutes to get rid of the remaining air from the steam generator.

Once the steam generator pressure had reached the set value, the supply valve to the concentrator was opened. In the meantime, the solution circulation started. It took about 1 hour for the system to enter stable operation. Once the rig was in a stable operation, the readings (water levels, temperature, pressure and flow rate) were taken, in tum, every five minutes. There were three water levels (evaporator, mixing vessel and condenser) to be taken from the sight glasses in order to determine the cooling capacity, the ejector entrainment ratio and the amount of refrigerant generated. All three readings were important in determining the cycle performance. The error was reduced by, first, marking each individual water level before taking measurements. The test lasted about 15 to 20 minutes for every operation condition. An average value during the period was used as experimental results.

6.2 CALCULATION FROM THE READINGS

For the purpose of precisely describing the experimental results, some important parameters relating to the refrigerator performance must be clearly

defined. These are the steam power input, the cooling capacity, the steam ejector entrainment ratio and the solution concentrations of the concentrator and the absorber.

62.1 Steam power input to the refrigerator

The power input was determined from the steam flow rate through the primary nozzle. There were two reasons why the electrical power was not used as the power input directly. The first was that the thermal insulation of the steam generator was not good enough. The second was that it was not convenient for the measurement system to carry out the calculation for the power consumption simultaneously. Since the flow rate through the primary nozzle is only determined by the primary pressure when it works under choked condition, it is adequate to calculate the power input from the pre-calibrated nozzle pressure-flow rate data that were ready for use, see Table 6.1.

Table 6.1 Ejector primary rates ($g \cdot min^{-1}$) at different steam pressure

Steam Pressure, bar	Primary nozzle diameter, mm	
	1.1	1.0
15.0	131.14	98.39
125	110.95	80.23
10.0	89.91	60.69

Figure 6.1 and 6.2 were plotted from the data in Table 6.1. The flow rate between the measured pressure points was calculated from those two figures.

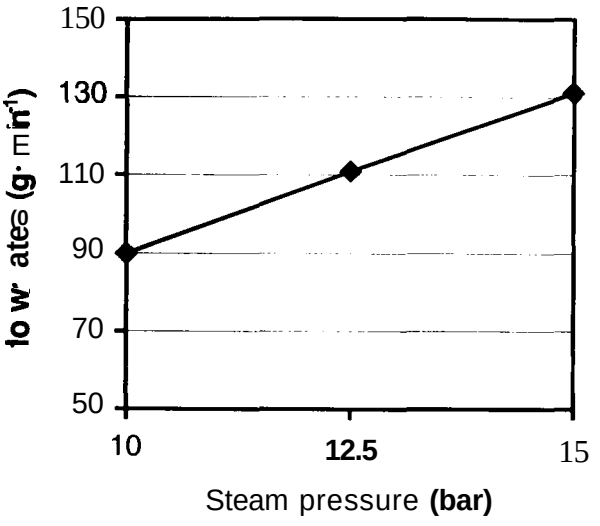

Figure 6.1 Measured primary flow rate (0 = 1.1 mm)

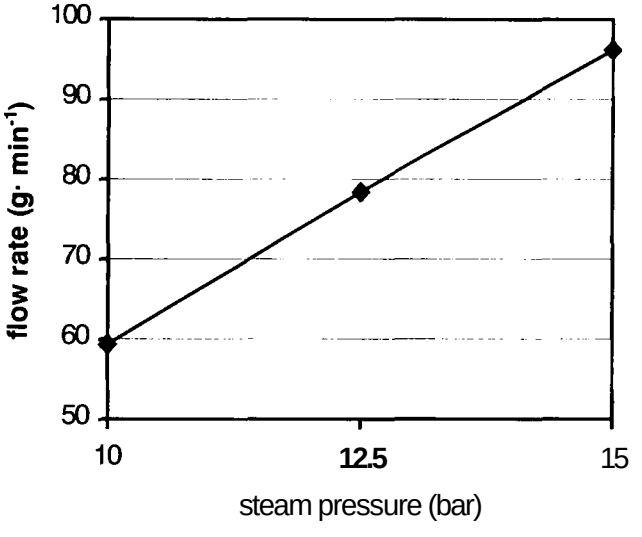

Figure 6.2 Measured primary flow rate (0 = 1.0 mm)

622 Evaporator cooling capacity

The cooling capacity of the refrigerator is proportional to the rate at which the water is vaporized in the evaporator vessel. The water-level changes in the evaporator vessel over a time interval were used to determine the cooling capacity. The volumes against height for the evaporator were calibrated in Chapter 5 and listed in Appendix B.

623 Ejector entrainment ratio

Entrainment ratio is the ratio between secondary to primary flows at the steam ejector. The primary flow rate was pre-calibrated under different primary pressures, which was also used for calculating the steam power input described earlier. The secondary flow was measured from the water-level changes in the measuring vessel shown in Figure 5.1 by taking away the known primary flow at the steam generator pressure (Figure 6.1). The secondary flow rate, therefore, is equal to the difference between the mixture and primary flow rates. The volume versus height of water level in the measuring vessel was calibrated in Chapter 5 and listed in Appendix B.

6.2.4 Vapour evolved from the solution of the concentrator

The flow rate of the vapour leaving from the LiBr-water solution in the concentrator during the concentration process describes the capability of the concentrator. This flow rate consists of two parts in this experimental rig: one, which equals the secondary flow to the ejector and two, the flow to the condenser. The former was known from determining the entrainment ratio, and the latter was measured from the water level change of the condenser. So, the total flow rate of the vapour is evolved from the secondary flow rate plus the flow rate to the condenser.

6.2.5 Solution concentration

The solution concentration in the concentrator was calculated from temperature and vapour pressure measurements, while that in the absorber was measured using a hydrometer. This is because the equilibrium solution temperature in the absorber is difficult to measure accurately in this case.

Except for the measurements discussed, others were straightforward. All the measurements were taken on a time-averaged basis.

6.3 EXPERIMENTAL RESULTS

63.1 The steam ejector performance

The ejector was the combination of one diffuser with each of two primary nozzles. The first nozzle (with 1.1mm throat diameter) was designed for the diffuser, which means that this nozzle matches the diffuser under design condition. The second nozzle, however, had a reduced throat diameter (with 1.0 mm throat diameter) to reduce the steam input. The geometrical sizes of the ejector were listed in Chapter 5. The distance between the nozzle exit and the mixing entrance is defined as the nozzle position (NPX). NPX was made to be adjustable within the mixing chamber entry to optimise the ejector performance, which has also been described in Chapter 5.

Maximum pressure lift ratio

The maximum pressure lift ratio is the ratio of the back-pressure to the suction pressure when the secondary flow is zero. This ratio indicates the pressure lift ability of an ejector. In the present application, that the highest solution concentration in the concentrator can be used is determined by this ratio. In practice, the steam ejector should not be designed to work under such conditions because no benefit will be from the use of an ejector in the cycle. Test results of the pressure lift ratios with steam generator pressure at 10 bar, 12.5 bar and 15 bar are listed in Table 6.2. These data show that the maximum pressure lift ratio increases with the primary pressure. They also show that the lift ratio for the 1.0mm diameter throat is lower than that for the 1.1mm diameter throat. It was found in the test that the pressure lift ratio was unstable and an intermittent flow to the ejector housing was observed if the back-pressure was too high. This is the result of the back-pressure being at or higher than the critical back-pressure. The maximum pressure lift ratio for the 1.1mm nozzle ejector is shown in Figures 6.3 to 6.5. The critical pressure increases as the primary pressure increases. It was found experimentally that the critical back-pressure was 394.3 mbar for 15 bar steam pressure, 342 mbar for 12.5 bar steam pressure and 268 mbar for 10 bar steam pressure for the present ejector design. Figures 6.6 to Figure 6.8 show the pressure lift ratio of the

ejector with a smaller throat diameter nozzle. The critical pressures for the smaller throat area nozzle were also decreased, which could be the result of mismatch between the nozzle and diffuser. The test results indicate that the ejector with a 1.1mm throat diameter give better performance. Therefore, in the following experiment, the nozzle with 1.0mm diameter would not be used.

Table 6.2 Pressure lift ratio of the steam ejector

Throat diameter (mm)	Pressure lift ratio		
	P_g =10 bar	P_g = 125 bar	P_g = 15 bar
1.1	13.41	15.08	15.78
1.0	11.242	12.383	12.437

It should be noted that Figure 6.3 to Figure 6.8 recorded the histories of the change of the pressure lift ratio in the tests. There was a period for the back-pressure to build up in the tests while the suction pressure did not fall because some water existed in the ejector housing. This resulted in the pressure-lift ratios being low at the start. If there was no water in the ejector housing, the pressure-lift ratio should be higher but would be lower than the maximum value according to the discussion in previous chapters.

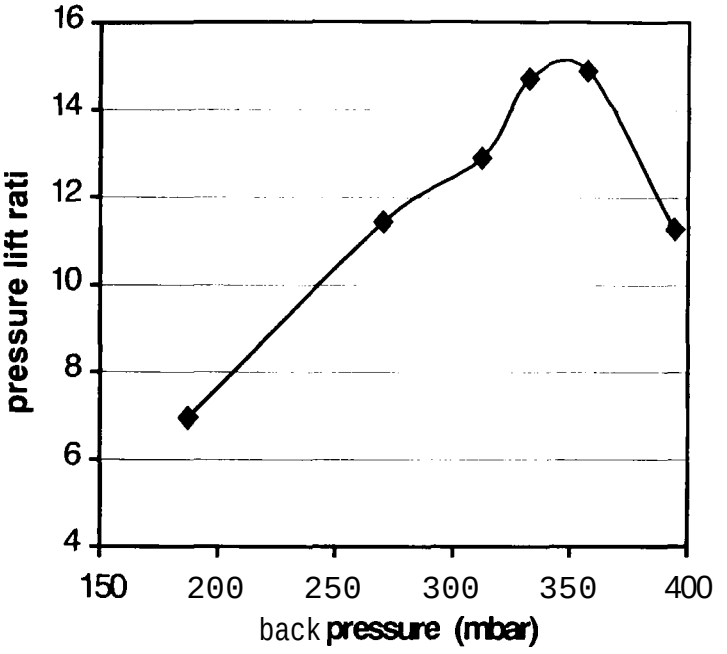

Figure 6.3 Back-pressure and pressure lift ratio

(15 bar, 1.1mm throat diameter)

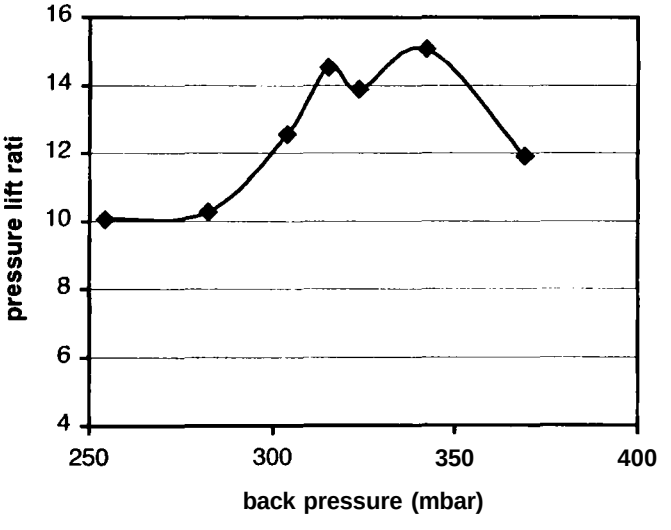

Figure 6.4 Back-pressure and pressure lift ratio

(12.5 bar, 1.1mm throat diameter)

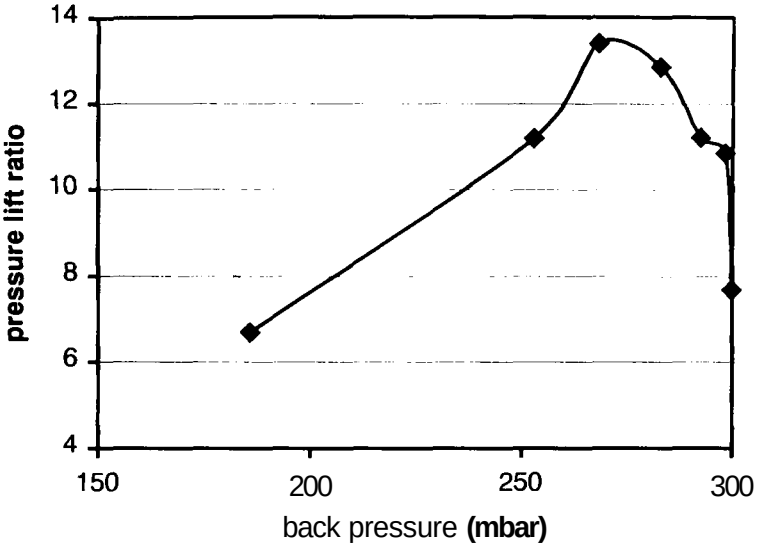

Figure 6.5 Back-pressure and pressure lift ratio

(10 bar, 1.1 mm throat diameter)

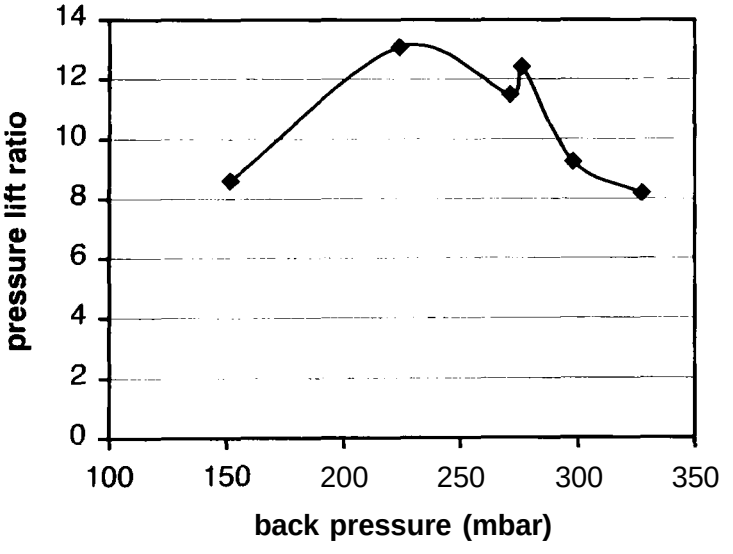

Figure 6.6 Back-pressure and pressure lift ratio

(15 bar, 1.0mm throat diameter)

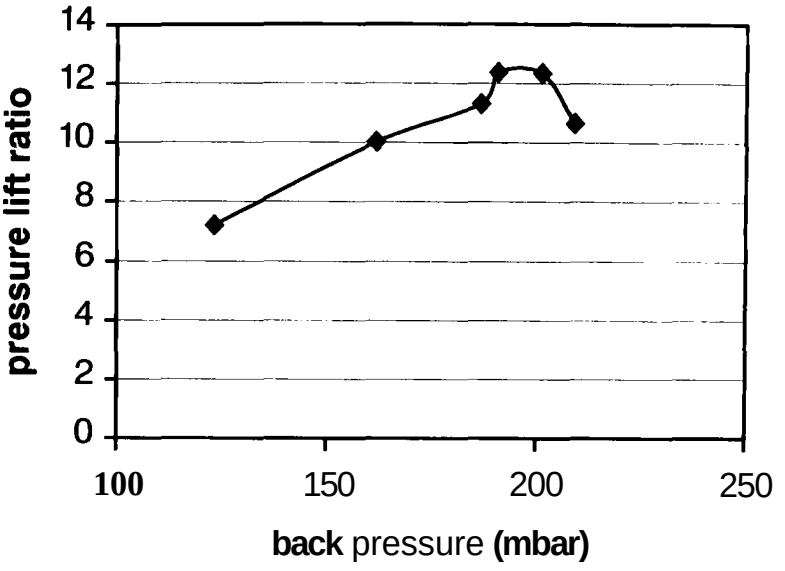

Figure 6.7 Back-pressure and pressure lift ratio
(12.5 bar, 1.0mm throat diameter)

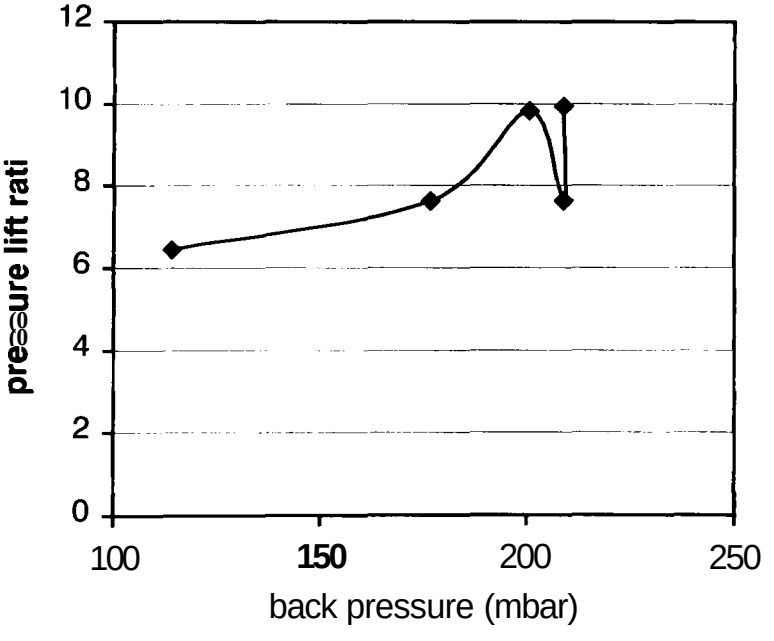

Figure 6.8 Back-pressure and pressure lift ratio
(10 bar, 1.0mm throat diameter)

Ejector entrainment ratio

Since the concentrator was directly connected to the condenser, the vapour pressure of the concentrator was dominated by the condenser pressure. This

resulted in the suction pressure of the steam ejector also being controlled by the condenser pressure. For the refrigeration operation, the condenser pressure was usually kept constant. This meant that the suction pressure of the ejector was in constant while its back-pressure varied with the solution temperature and concentration. That is to say the solution state determines the ejector's pressure lift ratio. From our previous discussion, it was known that when the primary pressure was fixed, the ejector entrainment ratio was varied with the pressure lift ratio. Therefore, the ejector entrainment ratio is determined by the thermodynamic states of LiBr-water solution. Knowledge of the relationship between entrairunent ratio and the thermodynamic state of LiBr-water solution is necessary to understand how the cycle might operate efficiently.

Figure 6.9 is the experimental result of the entraimnent ratio variation with the back-pressure, which was determined by the solution concentration and temperature. This figure shows that the entrairunent ratio remains unchanged almost until the back-pressure is greater than 452 mbar. When the back-pressure is greater than 452 mbar, the entrairunent ratio is unstable and falls dramatically. The test result shows that the ejector lost suction function totally at 469 mbar. In this particular case, therefore, the critical back-pressure lay between 463.64 mbar and 469 mbar where the entrairunent ratio approached zero. The maximum solution temperature of the concentrator should be lower than the saturation temperature of water corresponding to this pressure for the rig to be in operation. The critical back-pressure is also decreased with the suction pressure. Figure 6.10 shows the relationship of entrairunent ratio and suction pressure of the ejector. In Figure 6.10, the entrairunent ratio falls quickly when the suction pressure is lower than 46.8 mbar and approaches zero at about 45.5 mbar. So, the increase of the solution concentration in the concentrator is limited by this pressure. It is concluded from these experimental results that the best operating conditions for this particular steam ejector design are when the back-pressure is less than 452 mbar and suction pressure is higher than 50 mbar. The corresponding temperature and

concentration of the solution in the concentrator for this condition will be around 73°C and 59% respectively.

When the motive steam pressure was reduced from 15 bar to 12.5 bar, the critical pressure of the ejector was also decreased. Figure 6.11 shows the ejector entrainment ratio when the steam pressure was at 12.5 bar. In Figure 6.11, the entrainment ratio does not have significant change, however, the critical back-pressure is dropped to 386.3 mbar. A fall in critical back-pressure due to lowering motive steam pressure resulted in a reduction in solution concentration at the concentrator when the condensing temperature was held constant. Therefore, the optimum solution concentration and temperature operation of the steam ejector used in this case was approximately operation 58% and 70°C respectively. However, this limited the maximum condenser temperature to approximately 30°C. Above this temperature, the ejector entrairunent ratio falls sharply, which results in a reduction of the cycle efficiency.

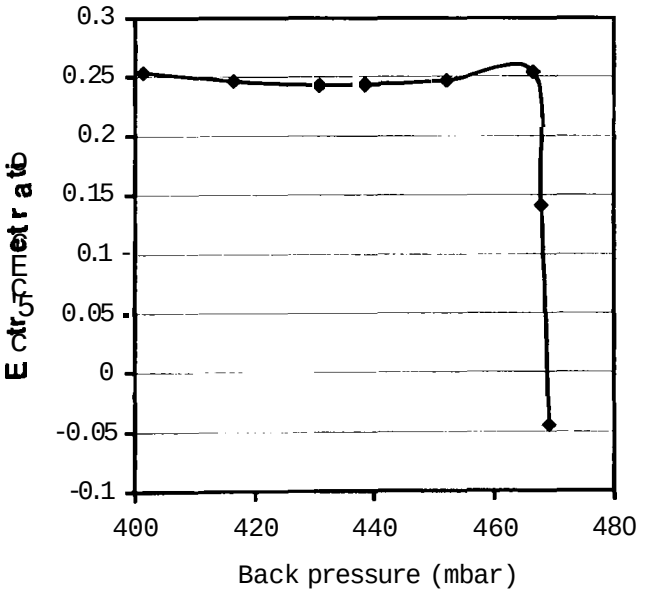

Figure 6.9 Entrainment ratio variation with back-pressure (15 bar)

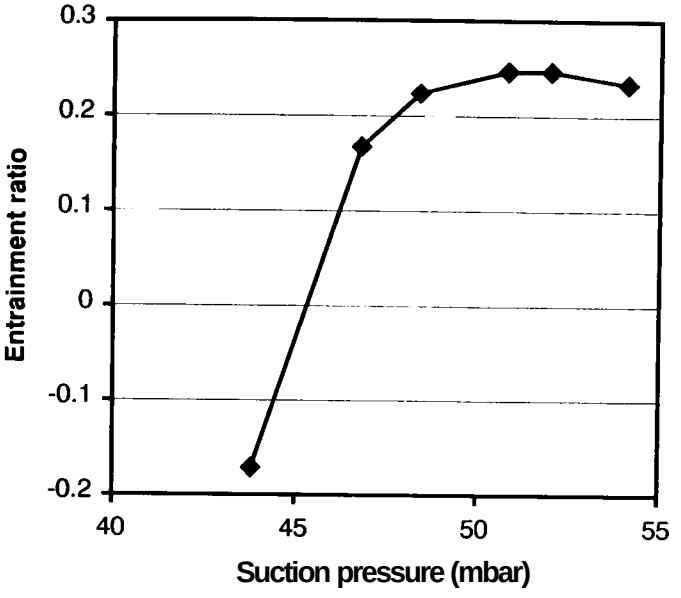

Figure 6.10 Entrainment ratio variation with suction pressure

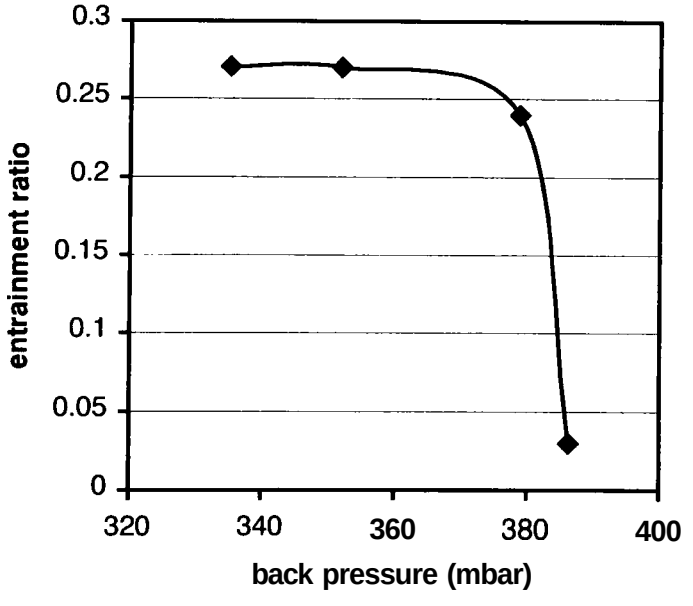

Figure 6.11 Entrainment ratio variation with back-pressure (12.5 Bar)

632 The energy efficiency of the concentrator

The efficiency of the concentration process in the concentrator was defined as the ratio between the mass rates of the vapour evolved from the solution and

the steam input to the concentrator from the steam generator. This efficiency parameter is proportional to cycle COP under steady operation and therefore, it was important to know what factors affected the concentration process, and how they influenced the cycle performance. Experiments were carried out over a range of solution concentrations and motive steam pressures. The results indicated that the solution concentration has a strong influence on the efficiency of the concentration process.

The influence of solution concentration

The concentration of the solution has a significant influence over the mass flow of vapour evolved from the concentrator. Experimental results indicated that this influence increases with concentration. Figure 6.12 shows results of experiments, which were carried out from concentration of 56% to 60.44% with 15 bar motive steam pressure. From Figure 6.12, it was found that the mass ratio decreases as the concentration increases. In the range 56% to 58% concentration, the ratio changes less. The ratio decreases quicker as the concentration increases. In this case the mass ratio was found to decrease rapidly above 60.44% concentration.

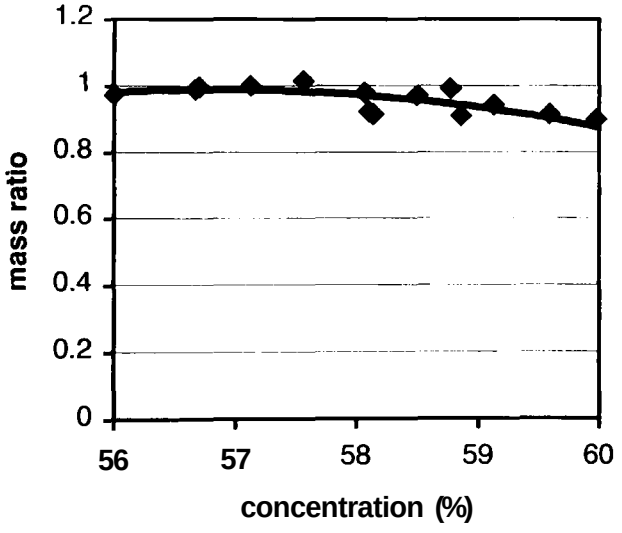

Figure 6.12 Mass ratio of the evolved vapour to the motive steam (15 bar)

Figure 6.13 shows the mass ratio variation in concentrator at 12.5 bar motive steam pressure. In this case, the mass flow ratio of the concentrator was found to decrease as concentration increased in a similar way as when 15 bar motive steam was used, but with reduced values. Comparing Figure 6.12 with Figure 6.13, it can be seen that the concentration range for the solution for the 15 bar steam pressure is greater than that for 12.5 bar. This was thought to be because the ejector was able to entrain vapour at lower pressures when driven by higher motive pressure. When the solution concentration increased to a point at which its vapour pressure was too low to be entrained by the ejector, the motive flow began to bypass the concentrator heat exchanger and flow directly through the secondary passage to the condenser. When this occurred, the mass flow ratio fell dramatically.

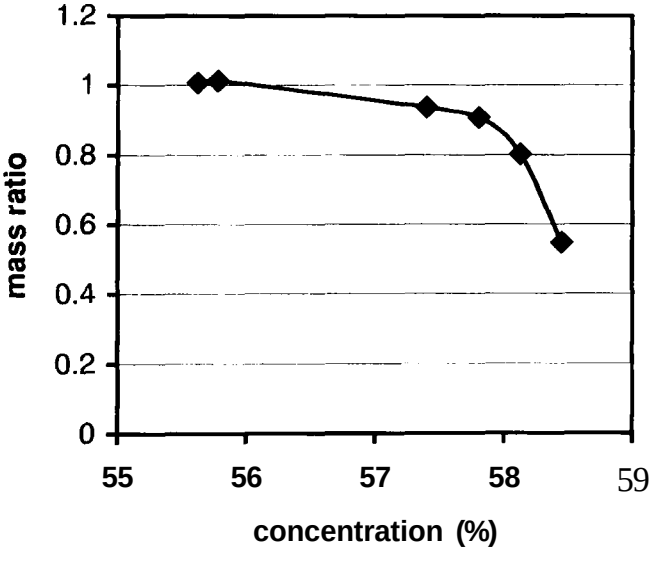

Figure 6.13 Mass ratio of the evolved vapour to motive steam (12.5 bar)

From these experimental results, it was concluded that the lower the solution concentration, the greater the mass flow ratio would be and, therefore, the higher the cycle's COP. This effect, however, is restrained by the evaporating temperature and the power consumption on the pumps, due to high circulation flow rate of the solution.

The temperature difference between the solution and the steam

In Chapter 3, the influence of the temperature difference between the solution and the steam to the entrainment ratio of the steam ejector was discussed. Figure 6.14 and Figure 6.15 show the measured temperature difference between the steam inside the concentration heat exchanger tubes and the solution outside, over a range of concentrations. The temperature difference was at around 4°C in the range 57% to 60% concentration when 15 bar steam was used to drive the cycle. This was reduced to about 3.5°C when the steam pressure of 12.5 bar was used. The decrease in temperature difference due to the low pressure used was the result of lighter heat transfer load to the heat exchanger. The concentration change was not a significant factor to the heat transfer between the steam and the solution. However, the temperature difference was more sensitive to the heat load on the heat exchanger.

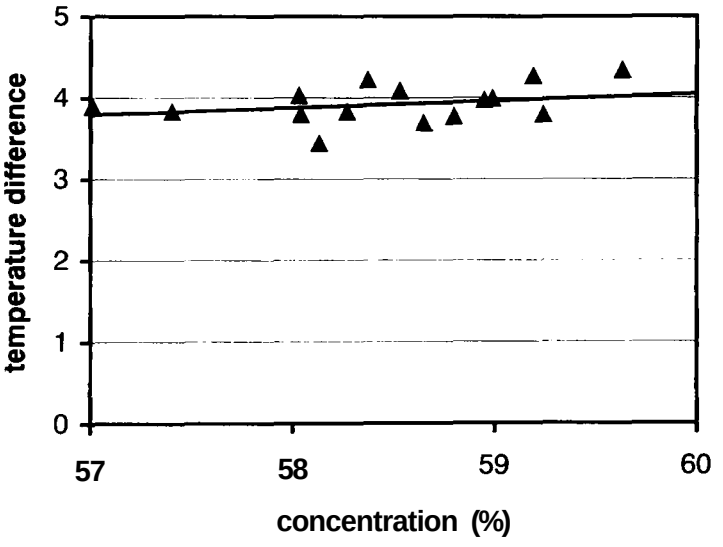

Figure 6.14 Temperature difference between the steam and the solution (at 15 bar motive steam)

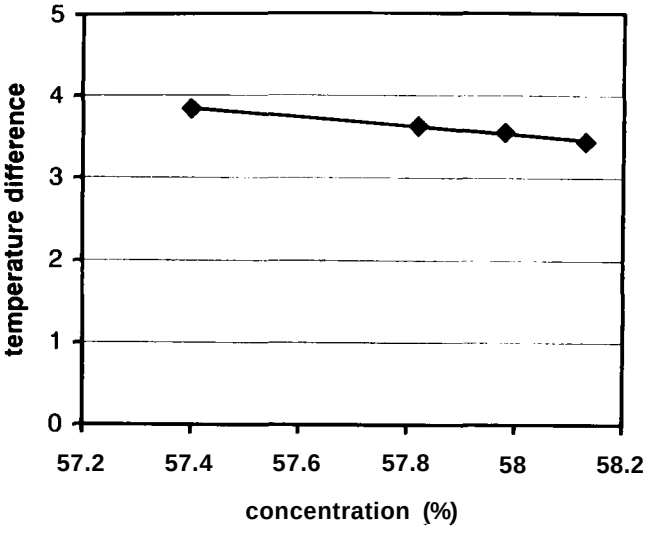

Figure 6.15 Temperature difference between the steam and the solution (at *125* bar motive steam)

6 3 3 The energy efficiency of the refrigerator

The efficiency of this novel refrigeration cycle and its characteristics are the main concern of this research project. A theoretical evaluation of cycle efficiency was discussed in Chapter 4. Experimental results are now described and compared with the theory. Interest is focused mainly on the influence of factors such as the motive steam temperature, the evaporating temperature, the solution concentration and the condensing pressure on cycle efficiency.

COP at different motive steam pressures

Ejector motive steam pressure was found to have a strong influence on its COP and cooling capacity of the novel refrigerator. To determine how the motive steam pressure affects COP and the cooling capacity of this novel cycle, the refrigerator was tested over a range of steam generator pressure from 12.5 bar to 15 bar. In the test, the evaporating and condensing temperatures were held at 5 °C and at 30 °C respectively. Cooling capacity and COP variation with motive steam pressure are shown in Figures 6.16 and 6.18. It was found that cooling capacity and COP increased slowly as steam pressure was varied from 12.5 bar to 13.5 bar. When the pressure was increased above 14 bar, both COP and cooling capacity increased more quickly at first and

reached a maximum value at 15 bar. This was the design condition for the ejector, and the curves of COP and the cooling capacity in Figures 6.16 and 6.18 actually reflect the performance of the steam ejector, and, therefore, it was expected that the entrairunent ratio would be greatest at 15 bar motive pressure. When the motive steam pressure was between 12.5 bar and 14 bar, the back-pressure of the ejector was close to its critical value where the entrainment ratio of the steam ejector approaches zero (the measured entrairunent ratios were 0.03 for *125* bar and 0.07 for 14 bar). With so low an entrainment ratio, the ejector here acts as a resistant device to the steam flow, rather than as a vapour compression device to boost the concentration process. This causes the novel cycle COP to fall to the conventional single-effect system.

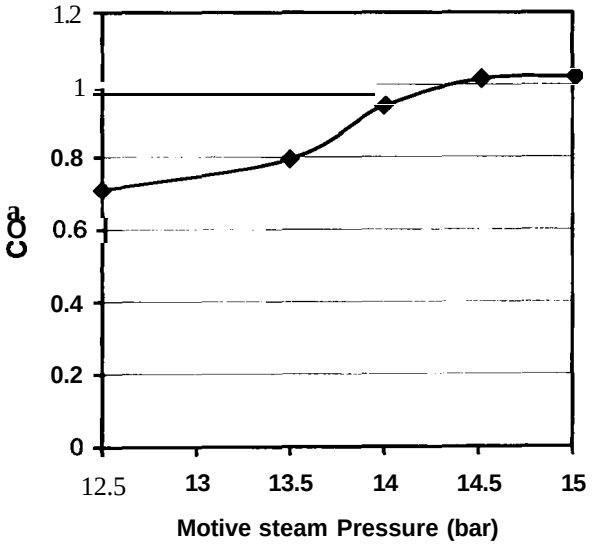

Figure 6.16 COP variation with motive steam pressure

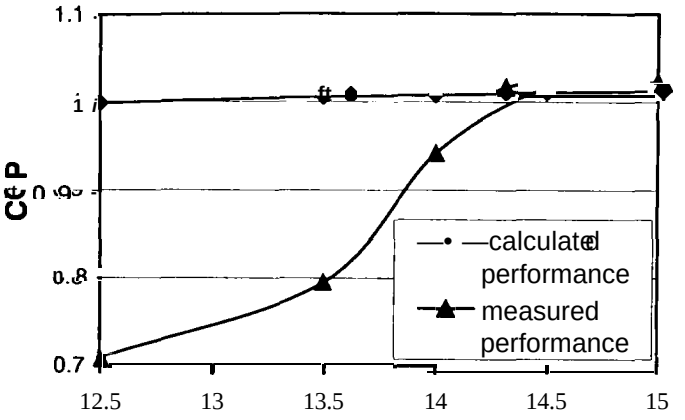

Figure 6.17 COP difference between part-load and design operation

This experiment conceming the steam pressure influence to the cooling capacity and COP of the refrigerator above 15 bar was not carried out for the safety reasons. However, from the trend of the curves in Figure 6.16 and 6.18, and from Figure 4.4 in Section 4.3 of Chapter 4, it can be predicted that further increasing the steam pressure above 15 bar will result in an increase of the cooling capacity but a decrease of COP. The speed of the cooling capacity increasing will slow down because the entraimnent ratio will not increase as the pressure increases, and when the pressure reaches a point where the high primary flow rate blocked the secondary flow, this cycle goes back to the conventional single-effect absorption cycle again. Figure 6.17 compares the part-load operation and with the designed operation in terms of COP. In the figure, the COP for designed operation was calculated from the computer model, which needs several ejectors work at its designed condition to realise. It shows the influence of the ejector to the cycle performance.

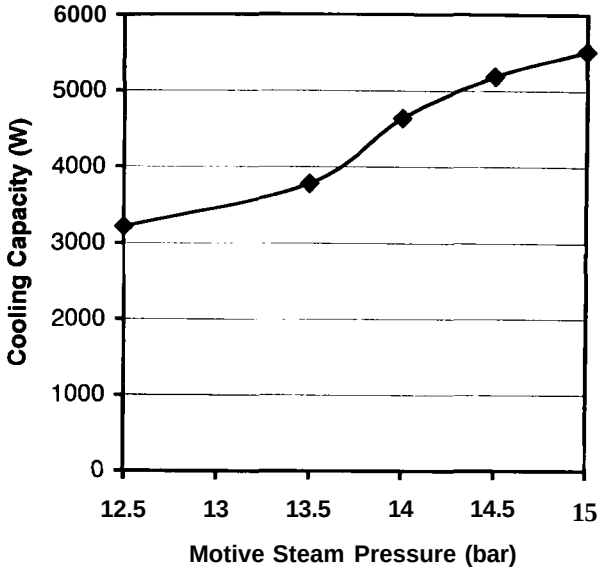

Figure 6.18 Cooling capacity vs. motive steam pressure

COP and solution concentration

The solution concentration in the concentrator influences the cycle COP. Figure 6.19 shows the measured variation in COP over a range of concentration from 57% to 59.5%. COP over the range is approximately unity and its trend increases with the concentration. In the Chapter 3, the effect of the concentration on the COP was discussed, where the theoretical result indicated that there was a concentration where the COP reached maximum value. The concentration alternation to either side of the maximum point would resulted in decrease of the COP. The experimental result, however, did not have such a trend. The experimental COP seemed to increase with the solution concentration in the concentration range. The comparison between the experimental and theoretical results is shown in Figure 6.20. The trend-line difference between them can be explained by the fact that the theoretical analysis was based on an assumption that the ejector was designed to work at the design condition but the steam ejector did not always work at its design point over tested range of concentration. Referring to Figure 6.9, this figure was drawn from the experimental data from which the ejector was operated at 15 bar (motive steam pressure) and 50mbar suction pressure (secondary flow). The entrainment ratio in Figure 6.9, it should be noted, remains approximately

constant until the back-pressure reaches 466.3 mbar. In the concentrator, the back-pressure varies with the solution temperature while the vapour pressure is mainly controlled by the condenser pressure which remained unchanged during the test. This means only the back-pressure is increased with the solution concentration. If the concentration increase does not cause the back-pressure to rise above the critical back-pressure, the entrainment ratio still remains unchanged. Furthermore, it was indicated in the previous chapter that COP of the single-effect system increases with the solution concentration. So, the overall COP of the novel cycle also increases with the solution concentration. However, COP will fall quickly once the concentration reaches a value to which the corresponding back-pressure is above the critical point.

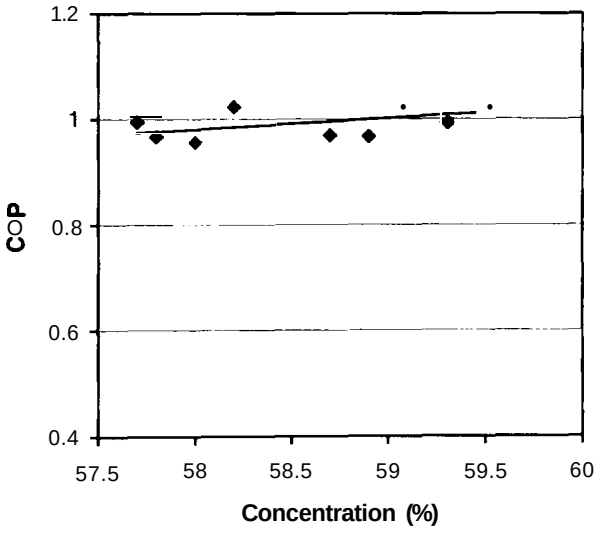

Figure 6.19 COP variation with solution concentration

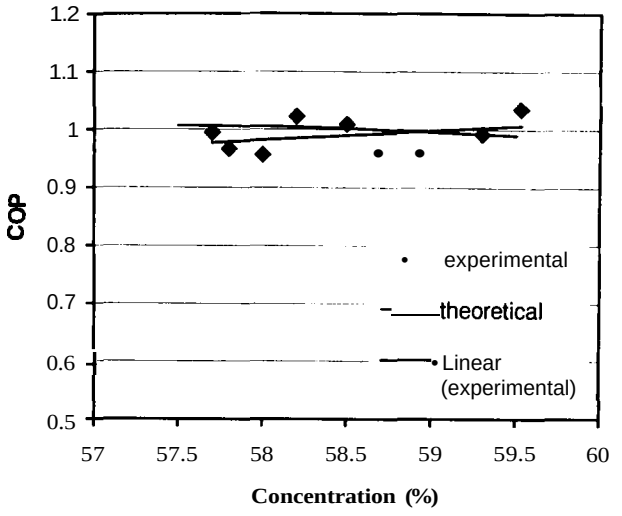

Figure 6.20 Comparison of the experimental and theoretical COPs at different concentration

63.4 Stability of the concentration process

It was observed in experiments that a steam flow periodically appeared from the ejector housing to the concentrator proper when the solution temperature rose to 75°C. This became continuous as the solution temperature further increased and the solution finally stopped boiling. This phenomenon occurred when the absorption process was not working properly. So, the concentration process was unstable when the solution temperature was above 75°C. The unstable concentration process was caused by the pressure lift ratio of the steam ejector. When less water vapour was absorbed, the concentration of the solution entering the concentrator increased, while the input power remained unchanged. Consequently, the bulk concentration of the solution in the concentrator was increased. The increase of the solution concentration not only resulted in lower vapour pressure (the suction pressure) by thermodynamic equilibrium, but also a reduction in the boiling heat transfer coefficient. The latter caused the solution temperature (therefore the back-pressure of the ejector) to increase. Therefore, the ratio between the back-pressure and suction pressure increased. Once the pressure ratio was beyond the maximum pressure lift ratio of the steam ejector, the motive steam would flow through the ejector housing rather than the heating tubes. If the pressure

ratio then fell within the maximum pressure lift ratio, the flow disappeared otherwise the flow remained. Although this phenomenon was found when the absorber did not work properly, it is equivalent to the situation in practice when cooling load demand reduces. The unstable concentration process caused the cycle COP to fall sharply and should be avoided.

6.3.5 The problem with the absorption

The absorber in the experimental rig was found to be rather inefficient in that it was not capable of absorbing the quantity of vapour evolved at the concentrator when the absorption temperature is at 30°C. To balance the absorbing ability of the absorber with the concentrator, the solution temperature had to be decreased. Experimental data showed that at a solution temperature of 23°C, vapour flow balance was achieved between absorber and concentrator with the solution concentration in the absorber maintained at 54%. Perhaps the fault lies with the absorber suction line between absorber and evaporator and therefore, not the absorber. Calculations showed that the pressure resistance between the evaporator and absorber is a major factor responsible for the poor efficiency. The cormecting pipe between them consisted of two 90° elbows, one sudden contraction and one sudden expansion as shown in Figure 5.8 in Chapter 5. Table 6.3 lists the calculated pressure losses at these parts (Munson 1989). The total pressure loss was estimated to be 1.57 mbar, which requires the absorber to operate at least 4°C lower than what it would be without the flow resistance. Considering other inefficiencies in the absorber, such as effects of the film distribution and non-condensable gas to the mass transfer coefficient, 23°C solution temperature seems to be acceptable for this case. Measurement of the solution density has confirmed that the solution concentration remains around 54% at this temperature.

Table 6.3 The pressure loss between the evaporator and absorber

	2xelbows	Sudden expansion	Sudden contraction	Tubing
Velocity, $m \cdot s^{-1}$	157.46	157.46	157.46	157.46
Loss coefficient	0.3	0.9	0.3	
Friction factor				0.02
Pressure loss, Pa	50.2	75.8	25.3	6.1

63.6 Concluding discussion

The results of the experimental investigation showed that COP of the steam ejector re-compression absorption cycle is 25% greater than that of single effect cycle. Although this is not yet as efficient as the double-effect cycle, it is only about another 0.2 COP lower. This could be reduced by improving the steam ejector performance and other parts of the experimental rig, such as a better heat exchanger in the concentrator.

Only one steam ejector was tested and it is believed that this may not have been optimised for the cycle. It was indicated in the Chapter 3 that the steam ejector has a strong influence on the cycle COP. Any improvement in the performance of the steam ejector will proportionally increase the COP. Improvements needed include the raising of both the entraimnent and pressure lift ratios. If the entrainment ratio of the steam ejector could be raised to 0.4, the cycle will be in a strong position to replace the conventional double-effect lithium bromide refrigerator. If the pressure lift ratio was increased at the same time, the solution circulation rate would be reduced, and this too would make the cycle more efficient. So, the entraimnent ratio and the pressure lift ratio of the steam ejector are considered to be important areas for future research in this novel cycle.

The temperature difference between the steam and the solution in the concentrator is a further important factor which determines the cycle COP. The larger the temperature difference, the higher the back-pressure for the

steam ejector and therefore the greater the pressure lift ratio required. In this experimental rig, there was a 5°C temperature difference between them, which was mainly caused by steam condensation heat transfer. If the heat transfer between them can be further improved, the cycle COP will increase.

The absorber used in the experimental rig was not as efficient as it may have been, resulting in a lower than required solution temperature to balance the steam mass flows in concentration and absorbing processes. The low absorption temperature also decreased the heat exchanger efficiency and this tended to reduce the cycle COP.

6.4 CONCLUSION

The novel cycle has been tested experimentally and discussed in this chapter. The experimental results have approved that using a steam ejector in the concentration process can improve the energy performance of a lithium bromide absorption cycle. The part-load performance is also discovered from the experiment work. From the experimental results, we conclude,

- The experimental COP value was 1.01 with T_g = 1983°C, T_{con} = 30°C (42.42 mbar), T_a = 30°C (calculated from concentration and vapour pressure) and T_e = 5°C.

- The experimental results show that the steam ejector can enhance the concentration process, which improves the cycle efficiency. At the design conditions, COP of this novel cycle is 25% higher than that of the conventional single-effect cycle but slightly lower than that of conventional double-effect cycle.

- The steam ejector operation characteristics strongly affect the cycle performance. The solution temperature and concentration in the concentrator must meet the ejector operation conditions, otherwise, the efficiency decreases. In the worse situation, the

operation of the refrigerator is unstable. The COP of the novel cycle is even lower than that of conventional single-effect cycle in the worst case.

• The experimental results compare favourably with the theoretical analysis in Chapter 3.

CHAPTER 7
GENERAL DISCUSSION AND CONCLUSION

The novel absorption refrigeration cycle has been theoretically and experimentally investigated in the previous chapters. The literature survey in this study showed that this novel cycle, which used a steam ejector to enhance the concentration process for a lithium bromide absorption cycle, was investigated for the first time. In the theoretical study, we investigated its energy performance and operational features with the use of the steam ejector. It was found that the steam ejector had a significant effect on the cycle energy performance. For this reason, a detailed one-dimensional analysis and design method for the ejector was discussed. The theoretical study also showed that the solution concentration should be as low as possible to achieve better energy performance. This was different from conventional absorption cycles. Since the one-dimensional analysis was not able to model the off -design performance of the ejector, a preliminary experimental study on steam ejectors was carried out in order to reveal the ejector off-design operation. Finally, the novel cycle was tested under the experimental conditions, which were described in the Chapter 6. Thus, the novel cycle was investigated comprehensively in this research.

One of the most important features of the novel cycle is the improvement of the energy performance, although the experimental results are not better than the conventional double-effect cycle. The theoretical and experimental results showed that the otherwise wasted thermal energy in the refrigerant vapour, evolved from the solution, could be recovered by a steam ejector. The recovered energy could be used to generate more refrigerant vapour from the solution. By doing this, the overall energy efficiency of the cycle was therefore improved. A COP = 1.013 was achieved experimentally when the input steam was at 198.3°C (15 bar), evaporator temperature at 5°C, condenser and absorber temperatures at 30°C. This figure puts the novel cycle in a position between the single and double effect absorption cycles in terms of COP. It could be better if the steam ejector was optimized. The efficiency of

this novel cycle increased with the heat source temperature while it decreased for the conventional single-effect cycle when the heat source temperature was beyond a certain point.

Another feature of the novel cycle is that it can maintain a low generating temperature and concentration without reducing the energy efficiency when a high temperature heat source is used. LiBr-water solution in the novel cycle could be kept well below the temperature at which the solution may attack the constmction material. In other words, using high temperature heat source to drive the novel cycle does not cause the corrosion problem. Compared with the triple-effect machines, which are supposed to be more efficient with the use of high temperature heat source, the machine based on this novel cycle is simple in construction and low in capital cost, but provides excellent energy performance. These features give the novel cycle a very good prospect when using heat sources above 200°C.

Simple construction, low capital cost and less maintenance are also very attractive features. According to the definition of 'effect' for the absorption cycle, the novel cycle is also a double-effect cycle but a steam ejector replaces the high-pressure generator and the solution heat exchanger presented in the conventional double-effect cycle. Since the steam ejector is a simple device, the structure and capital cost of the machine based on the novel cycle are also simpler and lower than those of the conventional double-effect machine. Therefore, this novel cycle also offers potential competition to the conventional double-effect cycle in using below 200°C heat sources. Yet the scope for this novel cycle in this region depends on how much the entrainment ratio of the steam ejector can be increased.

As was indicated in the previous chapters, the steam ejector plays an important part in the cycle energy efficiency. Improving the ejector performance is vital to the novel cycle. For the best result, a high entrainment ratio with required pressure lift ratio is essential. So far, this research work has finished proving the concept. Neither optimising the ejector and the system, nor designing a

better ejector for the system was done. This means that there is potential to improve the cycle COP. The steam ejector used in this rig has 0.25 entrainment ratio and it may not be the best. A different design of the ejector may be necessary to achieve a better performance.

While the steam ejector improves the cycle energy efficiency, it also creates a new problem for the system i.e. the unstable concentration process when the back-pressure of the ejector is greater than its critical value. As was indicated in the Chapter 6, an unstable concentration process decreased the cycle COP, and this must be prevented in practice. Positioning a one-way valve between the ejector housing and concentrator proper may be an answer to prevent the motive flow bypass. In the case of a less demanding cooling load, less heat input is required and it should be adjusted in On/Off mode because this allows the steam at the rated pressure to be supplied to the ejector for it to work at design condition. So, an adequate control system may be required in practice application.

CONCLUSION

The ejector re-compression absorption cycle provides a different way to deal with problems, such as corrosion or low second low efficiency which may be encountered in conventional or advanced absorption cycles when using high temperature heat source. The results of this research confirm that this is a practical way to solve these problems. In the case of using high temperature heat source, the machine based on this novel cycle has the advantages of low cost and simple construction over the advanced absorption cycles such as the triple-effect absorption cycles. A COP of 1.013 was achieved experimentally in this research. The author believes that this figure could be improved if the steam ejector had been optimized. This work has completed the first step in the cycle study. To obtain the best performance from this novel cycle, it is required to optimize the steam ejector and absorption cycle.

REFERENCE

A

Addy, A.L.,Dutton, J. C and Mikkelsen, C. D., (1981), Supersonic Ejector-Diffuser Theory and Experiments, Department of Mechanical and Industrial Engineering, Engineering Experiment Station, University of Illinois at Urbana-Champaign, Urbana, Illinois 61801.

Bejan, A., (1993), Hear Transfer, John Wiley & Son, Inc., ISBN 0-471-50290-1.

Alefeld, G., (1983), Double Effect Triple Effect and Quardruple Effect Absorption Machines, Proc. 16th Int. Congr. Of Refr., Paris 2,:951-956.

Alefeld, G. and Radermacher, R., (1994), Heat Conversion System, CRC Press Inc., ISBN 0-8493-8928-3.

Altenkirch, E.and Tenckhoff, B., (1914), Absorptionskaeltemaschine zur kontinuierlichen Erzeugung vonKaelte und Waerme oder acuh von Arbeit, September 22, German Patent 278,076.

Anand, G., Erickson, D. C, (1999), Identification and Evaluation of Advanced GAX Cycles for Space Conditioning, Munich: Proceeding of the Intemational Sorption Heat Pump Conference, March 24-26, pp.507-521.

Aphomratana, S., (1994), A Theoretical and Experimental Investigation of a Combined Ejector-absorption Refrigerator, PhD thesis, The University of Sheffield.

ASHRAE Handbook, (1993), Fundamentals, American Society of Heating, pp 17.81- 17.83, Refrigeration and Air-Conditioning Engineers, Inc, ISBN 0-910110-96-4.

B

Bassols, J., Schneider, R., Veelken, H., Kuckelkom, B. and Ohrt, D., (1994), 1st Operation Results of a Gas-fired 250 kW Absorption Heat Pump with Plate-fin Heat Exchangers, New Orleans: Procedings of the Intemational AbsorptionHeat Pump Conference, ASME AES-Vol. 31, January 19-21, pp. 73-78, 1994.

Burgett, L. W., Byars, M. D. and Schultz, K., (1999), Absorption Systems: The Future, More Than a Niche?, Munich: Proceedings of the Intemational Sorption Heat Pump Conference, pp.13-24, March 24-26.

C

Cacciola, G., Restuccia, G. and Rizzo, G., (1990), Theoretical Performance of an Absorption Heat Pump Using Ammonia-Water-Potassium Hydroxide Solution, Heat Recovery System & CHP, Vol. 10, No. 3, pp 177-185.

Cengel, Y A. and Boles, M. A., (1994), An Engineering Approach to Thermodynamics, 2"" ed., McGraw-Hill Inc., ISBN 0 07 113249 X.

Chen, L.T., (1988), A New Ejector-Absorber Cycle to Improve the COP of an Absorption Refrigeration System, Aren;t Energy, Vol. 30, pp 37-51.

Cheung, K., Hwang, Y., Judge, J. F., Kolos, K., Singh, A. and Radermacher, R., (1996) Performance Assessment of Multistage Absorption Cycles, Intemational Journal of Refrigeration, Vol. 19 No. 7, pp. 473-481.

Chung, H., Huor, M. H., Prevost, M. and Bugarel, R., (1984), Domestic Heating Application of an Absorption Heat Pump, Directly Fired Heat Pumps, Procs. Int. Conf. Uni. Of Bristol.

D

Dence, A. E., Nowak, C. C. and Perez-Bianco, H., (1996), A Novel GAX Heat Exchanger for Cooling Applications, Montreal: Proceedings of the

Intemational AB-sorption Heat Pump Conference, pp.595-602, September 17-20.

DeVault, R. C. and Marsala, J., (1990), Ammonia-Water Triple-effect Absorption Cycles, ASHRAE Trans. Vol. 96, No. 1 pp. 676-682.

Dorgan, C. B., Leight, S. P. and Dorgan, C. E., (1995), Application Guide for Absorprion Cooling/Refrigeration Using Recovered Heat, ASHRAE, Inc., ISBN 1-883413-26-

E

Eames, I. W. and Aphomratana, S., (1996), Jet-Pump Air Conditioning Powered by Waste Heat From A District Heating System, Built Environment – Trends and Challenges, vol 1, pp 141-151, ASHRAE Conf. Proc, Singapore, June.

Eames, I.W. and Aphomratana, S., (1995), A Novel Ejector/Absorption Cycle Refrigerator for Building Air Conditioning, Proc. CIBSE National Conference, Eastboume.

Eames, I.W., Georghiades, M., Tucker, R.J. Aphomratana, S. and Wu, S., (1996), Combined Ejector-Absorption Cycle Technology for Gas-Fired Air Conditioning, Proc. Ab-Sorption 96, Vol. I, pp. 201-208, Sept. 17-20, Canada.

Eames I. W., Wu, S., (1998), Worrel M., Observations on the Operation of Ejectors for Applications in Jet-Pump Refrigeration Powered by Low-Grade Heat, (in print).

ESDU, (1986), Ejectors and Jet Pumps, Design for Steam Driven Flow, Engineering Science Data Item 86030, Engineering Science Data Unit, London.

F

Feldman, K.T., Jensen, CM., Kim, K J. and Razani, A., (1998), A New Absorption Heat Pump, ASHRAE Transactions, 104, PT 1B, 1427-1433.

G

Garimella, S., Lacy. D. and Stout, R. E., (1994), Investigation of Triple-effect Cycle Absorption Heat Pump for Light Commercial Applications, AES, Vol. 32, pp. 23-32.

Gopalnarayanan, S. and Radermacher, R., (1996), Analysis of a Low Pressure Triple Effect Ammonia-water Cycle in Multiple Operation Modes, Intemational Ab-Sorption Heat Pump Conference, Ab-Sorption '96, Vol. 1, pp. 253-260, ISBN 0-660-16598-8.

Gosney, W. B., (1982), Principles of Refrigeration, Cambridge University Press, ISBN 0521236711.

Gu, Z., Feng, S. and Yu, Y., (1996), Absorption-Ejector Hybrid Refrigeration Cycle Powered by Low Grade Heat, Proc. Ab-Sorption 96, Vol. I, pp. 177-182, Sept. 17-20, Canada.

H

Hellmann, H. M., Grossman, G., (1996), Improved Property Data Correlations of Absorption Fluids for Computer Simulation of Heat Pump Cycles, ASHRAE Transaction, Vol. 102, 1,980-997.

Herold, K. E., He, X., Erickson, D. C, Rane, M. V., (1991), The Branched GAX Absorption Heat Pump Cycle, Tokyo: Proceeding of Absorption Heat Pump Conference, September 30 - October 2, pp. 127-132.

Herold, K. E., Radermacher, R. and Klein, S., (1996), Absorption Chillers and Heat Pumps, CRC Press, INC, ISBN 0-8493-9427-9.

Hodge B. K., Koenig, K., (1995), Compressible Fluid Dynamics, Chap. 23, pp 54-62, pub. Prentice Hall Inc., ISBN 0 13 308552 X.

Homma, R., Fujikura, K., Nishiyama, N. and Nakamura, M., (1996), Development of a High-performance Absorption Chiller-heat by Use of a Novel Working fluid, Proc. Ab-Sorption 96, Vol. I, pp. 51-58, Sept. 17-20, Canada.

Hou, M., Tan, S., (1992), Nucleate Boiling Heat Transfer of Lithium BromideAVater Solution on a Low Finned Tube, ASHRAE Transaction, vol. 98,2,pp.44-50.

I

Inoue, N., lizuka, H. and Ninomiya, Y., (1993), COP Evaluation for Advanced Ammonia-Based Absorption Cycles, AES-Vol. 31, 1-6, Intemational Absorption Heat Pump Conference, ASME.

Irvine, T. F. Jr, Liley, P. E., (1984), Steam and Gas Tables with Computer Equations, Appendix I, III, Academic Press.

Ivester, D. N. and Shelton, S., (1993), Varying Heat Exchanger Parameters in the Triple-effect Absorption Cycle, Intemational Absorption Heat Pump Conference, ASME, AES, Vol. 31, pp243-250.

Ivester, D. N. and Shelton, S. V., (1996), Optimized Evaporator and Generator Temperature for the Triple-effect Absorption Cycle, Intemational Ab-Sorption Heat Pump Conference, Ab-Sorption '96, Vol. 1, pp. 429-441, ISBN 0-660-16598-8.

lyoki, S., Iwasaki, S. and Uemura, T., (1990), Vapour Pressure of the Water-Lithium Bromide-Lithium Iodide System, J. Chem. Eng. Data, 35, 429-433.

lyoki, S., Kuriyama, Y., Tamaka, H., Kira, K., Okable, T. and Uemura, T., (1993), Vapour Pressure of Water + Lithium Chloride + Lithium Nitrate System, J. Chem. Thermodynamics, 25, 569-577.

K

Karimi, A., (1977), Laminar Film Condensation on Helical Reflux Condensers and Related Configurations, Int. J. Heat Mass Transfer, vol. 20, pp. 1137-1144.

Kim, J.-S., Lee, H. and Won, S.-H., (1995), Vapour Pressure of Water + Lithium Chloride + Ethylene Glycol and Water + Lithium Chloride + Lithium Bromide + Ethylene Glycol, J. Eng. Data, 40, 496-498.

Kuhlenschmidt, D., (1973), Absorption Refrigeration System with Multiple Generator Stages, U.S. Patent No. 3717007.

L

Lange, CA.G.M, Oving, G J., (1999), Water-Lithium Chlorate (LiCI03) - Evaluation of a Working Pair for Absorption Heat Pumps, Munich: Proceeding of the Intemational Sorption Heat Pump Conference, March 24-26,pp.l93-195.

Lee, R. J., DiGulio, R. M., Jeter, S. M., Teja, A. S., (1990), Properties of Lithium Bromide - Water Solutions at High Temperatures and Concentrations - II: Density and Viscosity, pp. 709 - 713, Symposium papers, ASHRAE winter meeting, 10 - 14 Feb., Atlanta, Georgia.

Lienhard, J. H., (1987), A Heat Transfer Textbook, 2nd, Prentice-Hall, Inc., ISBN 0-13-385089-7 025.

M

Morawetz, E., (1989), Sorption-Compression Heat Pump, Int. J. Energy Research, Vol. 13, pp. 83-102

Munson, B., Young, D., T. Okiishi, (1989), Fundamentals of Fluid Mechanics, John Wiley & Sons, Inc.

P

Patterson, M. R., Perez-Bianco, H., (1988), Numerical Fits of the Properties of Lithium-Bromide Water solutions, ASHRAE Transaction, Vol. 94, 2, 2059-2077.

R

Rane, M. V., Erickson, D. C, (1994), Advanced Absorption Cycle: Vapour Exchanger GAX, New Orleans: Proceedings of the Intemational Absorption Heat Pump Conference, ASME AES-Vol. 31 January 19-21, pp. 25-32.

Riffat, S.B., Shankland, N J. and Wong, C.W., (1994), Rotary Absorption - Recompression Heat Pump, Building Serv. Eng. Res. Techol. 15(1) 27-30.

Riffat, S.B., Webb, R. A., Afonso, A., Oliveira, A. Siren, K. E. and Karola, A., (1996), An Efficient Rotary Absorption/Recompression Heat Pump for Air-Conditioning, Proceedings of Ab-Sorption 96, Vol. 1, pp.143-151, Sept. 17-20.

Rohsenow, W. M., and Hartnett, J. P. and Ganic, E. N., (1985), Handbook of Heat Transfer Applications, 2"" ed. New York: McGraw-Hill.

S

Saravanan, R. and Maiya, M.P., (1998), Thermodynamic Comparison of Water-Based Working Fluid Combinations for a Vapour Absorption Refrigeration System, Thermal Engineering, Vol. 18, No. 7, pp. 553-568.

Slooff, R., Mcmichael, A.J. and Kjellstrom, T., (1995), Global Warming and Stratospheric Ozone Depletion: Two Source of Risk to Human Health in the Built Environment, Proceedings of the Medical & Public Health Sessions of the Asia-Pacific Conference on the Built Environment, Vol. 2, pp. 13-24, Singapore, June 1-3, ISBN 981-00-6652-X (Vol. 2).

Stoecker, W. F., Jones, J. W., (1982), Refrigeration and Air Conditioning, McGraw - Hill Intemational Editions 2nd, ISBN 0-07-066591-5.

Sun, D. and Eames, I.W. Aphomratana, S., (1996), Evaluation of a Novel Combined Ejector-Absorption Refrigeration Cycle – I: Computer Simulation, Int. J. Refrig. Vol. 19, No. 3 pp. 172-180

T

Treybal, R. E., (1986), Mass-Transfer Operation, 3rd, Mcgraw-Hill Book Company, ISBN0-07-065176-0.

Z

Zaltash, A. and Grossman, G., (1996), Simulation and Performance Analysis of Basic GAX and Advanced GAX Cycles with AmmoniaAVater and AmmoniaAVater/LiBr Absorption Fluids, Ab-Sorption 96, Vol. II. Pp. 445-452, September 17-20, Canada, ISBN No. 0-660-16599-6.

Ziegler, F., (1985), Advanced Absorption Cycles, Proc. Int. Workshop on Heat Transformation and Storage, 9-11 Oct., Ispra, Italy. Rep. No. S A./I.04.D2. 8535., CEC, Joint Research Center, Ispra Establishment.

Ziegler, F. and Alefeld, G., (1993), Comparison of Multi-Effect Absorption Cycles, Intemational Absorption Heat Pump Conference, ASME, Vol.31, pp.257-264.

APPENDIX A

Referring to Figure A1, the thermodynamic property relationships for an ideal gas across a normal shock wave are as follows, (Hodge and Koenig 1995).

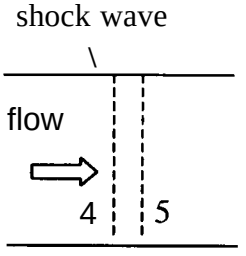

Figure A1

Static pressure ratio;
$$\frac{P_5}{P_4} = \frac{2\gamma M_{n4}^2}{\gamma+1} \frac{\gamma-1}{\gamma+1}$$

Static temperature ratio;
$$\frac{T_5}{T_4} = \frac{\left(1+\frac{\gamma-1}{2}M_{n4}^2\right)\left(\frac{2\gamma}{\gamma-1}M_{n4}^2-1\right)}{M_{n4}^2\left(\frac{2\gamma}{\gamma-1}+\frac{\gamma-1}{2}\right)}$$

Density ratio;
$$\frac{\rho_5}{\rho_4} = \frac{v_4}{v_5} = \frac{(\gamma+1)M_{n4}^2}{(\gamma-1)M_{n4}^2+2}$$

Mach Number;
$$M_{n5}^2 = \frac{M_{n4}^2(\gamma-1)+2}{2\gamma M_{n4}^2-(\gamma-1)}$$

Total temperature ratio;
$$\frac{T_{t5}}{T_{t4}} = 1$$

Total pressure ratio;
$$\frac{P_{(5}}{P_{(4}} = \left(\frac{\frac{1}{2}(\gamma+1)M_{n4}^2}{1+\frac{1}{2}(\gamma-1)M_{n4}^2}\right)^{\frac{\gamma}{\gamma-1}}\left(\frac{1}{\frac{2\gamma}{\gamma+1}M_{.4}^2-\frac{\gamma-1}{\gamma+1}}\right)^{\frac{1}{\gamma-1}}$$

APPENDIX B

Calibration of the vessels

The condenser, evaporator and measuring vessels were used to measure the flow rates for calculation of the power input, cooling capacity, ejector entrainment ratio and total vapour flow rate evolved from the solution. These were calibrated and shown as in Figures A1, A2 and A3. The temperature under which the calibrations were carried out was 20°C and the formulas were produced by Microsoft Excel. It should be noted that quadratic relationships were results from the heat elements or the cooling coils inside vessels.

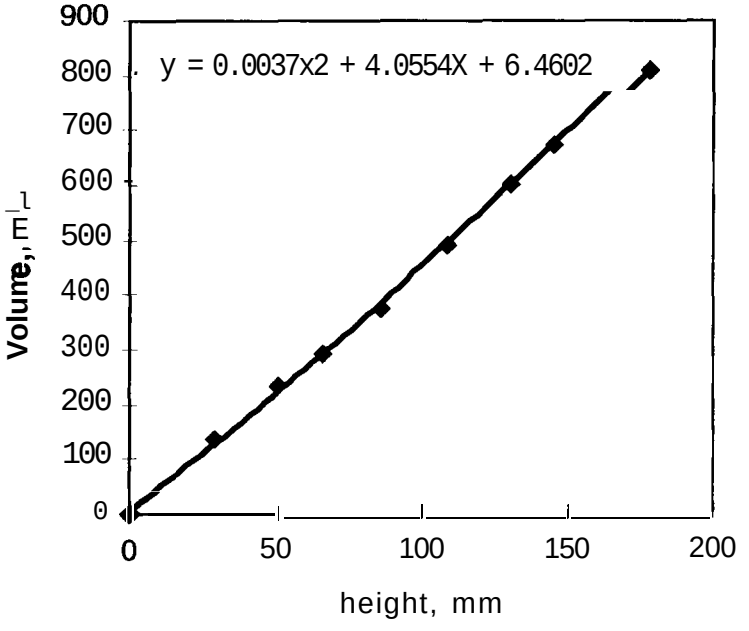

Figure Bl Evaporator volume vs. height

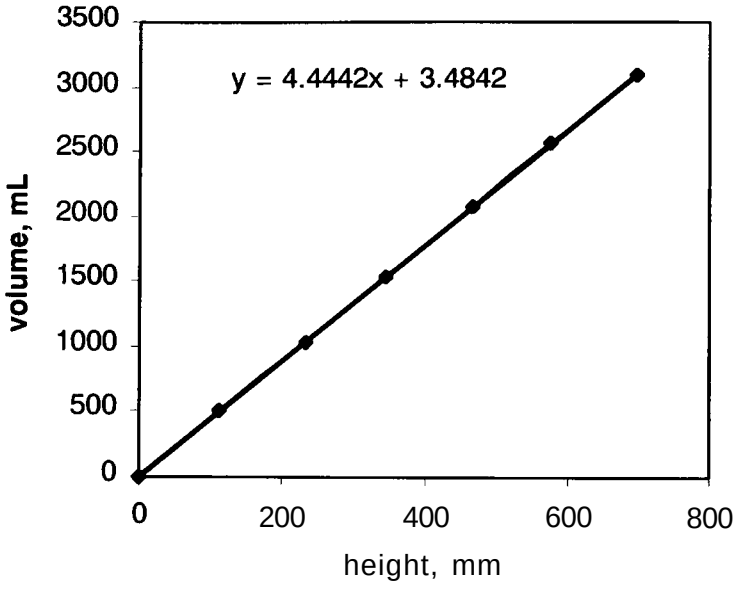

Figure B2 Measuring vessel volume vs. height

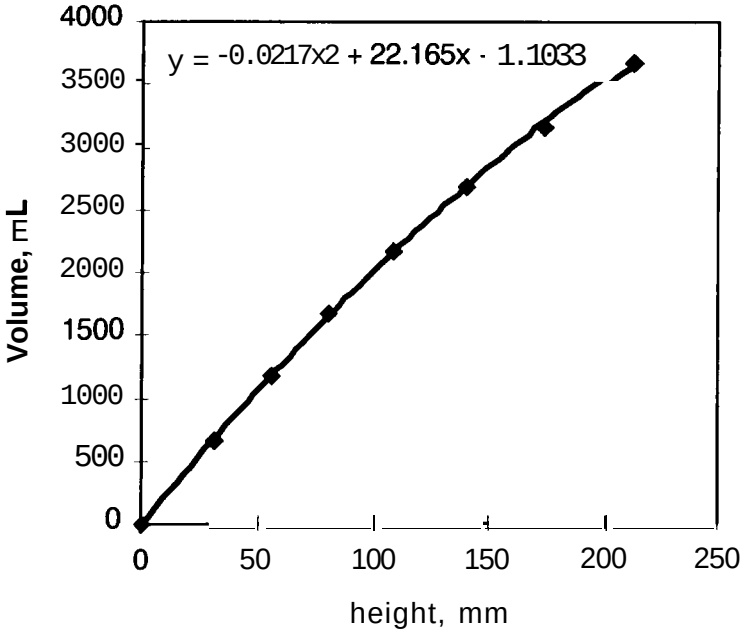

Figure B3 Condenser volume vs. height

APPENDIX C

ACCESSORIES USED IN THE EXPERIMENTAL RIG

1. Pumps:

Circulation pump for absorber

Manufacturer	Totton Pump
Model	NEMP 160/9 Polyproylene parts
Type	Centrifugal
Max flow rate	160L/min.
Max head	9m water
Power	0.18 kW

Water feed back pump

Manufacturer	Grosvenor Pump
Model	
Type	Plunger pump
Max flow rate	23L/hr.
Max head	30 bar
Power	0.18 kW 3PH

Evaporator circulation pump

Manufacturer	Totton Pump
Model	EMP 40/4
Type	Centrifugal
Max flow rate	40L/min.
Max head	4m water
Power	240V 0.35A 1HP

Concentrator circulation pump

Manufacturer	Totton Pump
Model	NEMP 40/6
Type	Centrifugal

Max flow rate	40L/min.
Max head	6m water
Power	240V 0.45A

Hot water circulation pump

Manufacturer	Totton Pump
Model	ND 25L/2
Type	Centrifugal
Max flow rate	25L/min.
Max head	2m water
Power	

2. Pressure transmitter

Manufacturer	Rosemount Limited
Model	2088 Absolute pressure transmitter
Calibrated range	0 - 1 PSI X 2
	0 - 2 0 bar
Output	4 – 20 mA or 0 – 5 V

3. Data logger

Manufacturer	Data Electronics (Aust.) Pty. Ltd.
Model	Datataker 505 Series 2
Input channels	Analogue, 10 in differential or 30 in single end
Digital charmels	4 digital input/output charmels

4. Solution flow meter

Manufacturer	Platen
Scale	0 - 2.8 $L \cdot min.^{-1}$, (calibrated at 40℃)